Modeling and Control of Subsea Installation

How Voon Ee

NATIONAL UNIVERSITY OF SINGAPORE
2009

NUS
National University
of Singapore

Modeling and Control of Subsea Installation

How Voon Ee
(*B.Eng, NATIONAL UNIVERSITY OF SINGAPORE*)

A THESIS SUBMITTED
FOR THE DEGREE OF DOCTOR OF PHILOSOPHY
DEPARTMENT OF ELECTRICAL AND COMPUTER ENGINEERING
NATIONAL UNIVERSITY OF SINGAPORE
2009

Acknowledgement

The research work reported in this thesis has been carried out at the Department of Electrical and Computer Engineering, National University of Singapore (NUS). It is my utmost honor and good fortune to work under the mentorship of two distinguished giants, Professor Shuzhi Sam Ge and Professor Choo Yoo Sang.

I want to express my deepest gratitude to my main thesis supervisor Prof. Ge who convinced me to take up this arduous but enriching and rewarding journey. Prof. Ge's fatherly teachings, strict guidance and near instant feedbacks changed my habits for the better and built my technical competencies. I salute Prof. Ge's devotion and sense of responsibility towards educating his students and for always making himself available, including the sacrifice of his personal time during late nights and weekends.

My deepest gratitude also goes to my thesis co-supervisor Prof. Choo, who gave the opportunity to work as a Research Engineer with the Centre for Offshore Research and Engineering (CORE), NUS. This provided the avenue and funding to pursue my postgraduate studies. Prof. Choo's sharing of experiences, kind guidance and emphasis on the fundamental physics provided insights and the impetus for my research direction. I toast to Prof. Choo for his exemplary efforts in building relationships with both academia and industry and dedication to the Marine and Offshore industry.

Jointly, I thank Prof. Ge and Prof. Choo, for the opportunity to participate in the idea conceptualization, grant proposal writing, project planning and management, manpower recruitment, documentation and hard work in meeting deliverables of two research projects: *Modelling and Control of Subsea Installation*, funded by Lloyds Register Education Trust, United Kingdom, and *Intelligent Deepwater Mooring System*, funded by Agency for Science,

Technology and Research (A*STAR), Singapore. Special thanks to my teammates, Dr. Chen Mou, Dr. Cui Rongxin, Dr. Ren Beibei and He Wei for their input, contributions and comradeship.

I am thankful to the Department of Civil Engineering, NUS, for the support of my continued employment as a Research Engineer throughout the duration of the candidature. Sincere appreciation to the Economic Development Board (EDB) of Singapore for funding my employment in part through the Training Attachment Program.

My gratitude goes to Dr. Tee Keng Peng and Dr. Tao Pey Yuan for their help and technical troubleshooting during the initial phases, and later comradeship. Sincere thanks goes to the many colleagues and friends in the Infrastructure Group Laboratory, Control and Simulations Laboratory, Social Robotics Laboratory, Hydrodynamics Laboratory and CORE Research Staff Office, with special mention of Dr. Wang Zhen, Yeoh Ker Wei, Wah Yi Feng, Yap Kim Thow, Cheng Jianghang and Qi Jin for the lively discussion sessions, sharing of ideas and happiness along the journey. Also, my sincere thanks to all who have helped in one way or another in the completion of this thesis.

Finally, my very special thanks and appreciation goes to my parents How Kok Wui, Leong Yin Meng, and lovely wife Vicky Tang Wai Ki, whose relentless support, love and encouragement is a great source of motivation on this journey.

Contents

Summary

The development of subsea processing equipment and the trend to go into deeper waters for untapped oil fields will result in an increased focus on offshore installation tasks and systems. The main purpose of the research in this thesis is to develop advance strategies for the control of subsea installation operations and flexible structures in the marine environment and alleviate some of the challenges.

Splash Zone Transition Control: For the subsea system to be installed on the sea bed, it first has to be lifted off a transportation barge on site using an offshore crane and placed into the water. The transition from air to water is known as splash zone transition and the vertical hydrodynamic loads on the payload can be expressed as a combination of terms from the pressure effects, slamming and viscous forces including the Froude-Kriloff forces, hydrostatic pressure and viscous drag. A simple linear in the parameter (LIP) model that is representative and captures most of the observed hydrodynamic load phenomena is presented. Model based control is designed and neural network (NN) based control is presented for the case where uncertainties exist in the system parameters.

Dynamic Positioning of Payload: When the payload is near the seabed, positioning control in the horizontal plane is investigated for the installation of subsea systems, with thrusters attached, under time-varying irrotational ocean current. Backstepping in combination with adaptive feedback approximation techniques are employed in the design of

the control, with the option of High-gain observer for output feedback control. The stability of the design is demonstrated through Lyapunov analysis where semiglobal uniform boundedness of the closed loop signals are guaranteed. The proposed adaptive neural control is able to capture the dominant dynamic behaviors without exact information on the hydrodynamic coefficients of the structure and current measurements.

Subsea Installation Control with Coupled System: Next, the coupled dynamics and control of the vessel, crane, flexible cable and payload under environmental disturbances with attached thrusters for subsea installation operations is investigated. For the practical system with physical constraints, Barrier Lyapunov Functions are employed in the design of positioning control for the flexible crane-cable-payload subsystem to ensure that the constraints are not violated. Uniform stability of the flexible subsystem is shown and asymptotic positioning of the boundaries is achieved. The scenario where nonuniformity of the cable, uncertainties and environmental disturbances exist is considered. Boundary controls are formulated using the nonlinear PDEs of the cable.

Flexible Marine Riser: Finally, active control of flexible marine riser angle and the reduction of forced vibration under a time-varying distributed load are considered using boundary control approach. A marine riser is the connection between a platform on the water surface and the installed subsea system on the sea floor. A torque actuator is introduced in the upper riser package and a boundary control law is designed to generate the required signal for riser angle control and vibration reduction with guaranteed closed-loop stability. Exponential stability can be achieved under the free vibration condition. The proposed control is simple, implementable with actual instrumentation, and is independent of system parameters, thus possessing stability robustness to variations in parameters. The design is based on the PDEs of the system, thus avoiding some drawbacks associated with the traditional truncated-model-based design approaches.

Nomenclature

$(*)'$, $(*)''$	first, second order derivative w.r.t z
$(*)'''$, $(*)''''$	third, fourth order derivative w.r.t z
$(\dot{*})$, $(\ddot{*})$	first, second order derivative of w.r.t t
x_n, y_n, ψ_n	North East Downward reference
Γ	Adaptation gain
L	length of flexible structure
t	time
m_z	uniform mass per unit length of the flexible riser
ρ_s	density of seawater
ω	frequency
E_k	kinetic energy
E_p	potential energy
W	Work done
EI	uniform flexural rigidity of beam
$f(z,t)$	time dependent distributed load
$U(t)$	velocity of ocean current
$U(z,t)$	current profile
D	external diameter
C_D	drag coefficient

C_M	inertia coefficient
δ	variation operator
c	linear structural damping coefficient
M_s	mass of surface vessel
d_s	Surface vessel motion damping
y_s, $\dot{y}_s$, $\ddot{y}_s$	surface vessel displacement
	velocity and acceleration on cable, ship and payload
$\bar{f}$, $\bar{f}_s$, $\bar{f}_L$	upper bound for disturbances
τ	control
f_s	environmental disturbance on vessel
$\rho(z),\ \rho$	mass per unit length of cable
d_c	damping coefficient for cable in fluid
$T(z,t)$	nonuniform distributed tension
$T_0(z), T_0$, P, T	tension in undisturbed flexible structure
$\theta(z)$	displaced cable weighting function
E	Young's modulus
z	axis from top boundary
A	cable cross section area
$c_1(z)$ to $c_4(z)$	cable initial conditions
$f(z,t)$	distributed disturbances
$f^*(z,t)$	transformed distributed disturbances
$y(z,t)$	transverse displacement
$w(z,t)$	transformed transverse displacement
$b_0(t)$, $b_L(t)$	boundary states at $z = 0, L$
$u_0(t)$, $u_L(t)$	control at $z = 0, L$ respectively

b_{0d}, b_{Ld}	desired position at $z = 0, L$
k_b, k_c	constrains on error signals z_3 and z_5
β, γ	constant
$\gamma(z)$	weighting function
α_1, α_2, α_3	virtual controls
z_1 to z_6	error signals
$M_0,\ M_L$	mass of crane and payload
$d_0,\ d_L$	damping coefficient at $z = 0, L$
ϕ_0 to ϕ_5	positive constants
k_{0c}, k_{Lc}	constraints on $b_0(t)$, $b_L(t)$ respectively
$\lambda,\ \lambda_1$ to λ_6	positive scalars
δ_1 to δ_5	small positive constants
f_L	disturbance on payload
$U_m, \bar{U}$	mean current
h	height of cylinder
f_v	vortex shedding frequency
S_t	Strouhal number

List of Figures

List of Tables

Chapter 1

Introduction

1.1 Background and Motivation

1.1.1 Subsea Installation

With the increased focus on subsea installation tasks to tap deep water fields, 21 companies, including 5 oil and gas operators and 6 major contractors have come together for a joint industry project named Deepwater Installation of Subsea Hardware (DISH) [2]. The objective is to investigate and develop solutions for the technical problems associated with installing subsea facilities such as templates and manifolds in very deep water ($\geq$3000m).

To carry out the installation operation, active, passive or hybrid heave compensation systems have been developed for offshore cranes or module handling systems for the installation operations. One of the most critical phases of such operations is the water entry of the hardware through the splash zone where it experiences hydrodynamic loads including slamming forces. A smooth transition through the splash zone is desirable to prevent damage to the payload.

Accurate positioning for the installation of the subsea systems onto the seabed has

also been identified as one of the problems in subsea installation operations [2]. Subsea templates, Christmas trees and manifolds have to be installed accurately in a specified spatial position and compass heading within tight limits, including rotational, vertical and lateral measurements. The tolerances for a typical subsea installation are within 2.5m of design location and within 2.5 degrees of design heading for large templates [3] and are more stringent for the installation of manifolds into the templates. With the push for using smaller installation vessels to reduce costs, the operators are concerned with the transmission of motions from the surface vessel, which are more susceptible to influences from the wave forces by virtue of their smaller build. Remote Operated Vehicles (ROVs) are also used to aid structure positioning. This can be feasible for small structures but not the large templates as a result of limited thrust available from the propulsion system. The entanglement of the umbilical of the ROV with the lifting cable and other factors such as long path lengths for round trip communication with the surface, noise, reaction delays and poor visibility may result in errors during placement [2].

1.1.2 Flexible Structures

Traditional methods in subsea installation include the use of guidelines or by a combination of ship dynamic positioning and crane manipulation to obtain the desired position and heading for the payload [2–4]. Such methods become difficult in deeper waters due to the longer cable between the surface vessel and subsea hardware when near the seabed. The longer cable increases the natural period of the cable and payload system which in turn increases the effects of pendulum-like oscillations. Time-varying distributed currents may lead to large horizontal offsets between the surface ship and the target installation site. The control for the dynamic positioning of the subsea payload is challenging due to the unpredictable exogenous disturbances such as fluctuating currents and transmission of motions from the surface vessel through the lift cable. Incorporating the flexible cable dynamics in the control design and analysis may yield better performance during installation.

Risers are the connections between a platform on the water surface and the subsea systems installed on the sea floor. A production riser is a pipe used for oil transportation, while a drilling riser is used for drilling pipe protection and transportation of the drilling mud [5]. Tension is applied at the top of the riser which allows it to resist lateral loads, and its effects on natural frequencies, mode shapes and forced vibration have been studied in [6, 7]. Both types of riser can be modeled as an extremely long and flexible tensioned prismatic tube, suspended from the ocean surface to the sea floor. In deeper waters and harsher environments, the response of the risers under various environmental conditions and sea states becomes increasingly complex. The dynamic response are nonlinear and governed by equations of motions dependent on both space and time. Idealized beam models characterized by partial differential equations (PDE) with various boundary conditions have been used to investigate and analyze the dynamic response of such structures subjected to different environmental loads [8–10]. In [11–13], the vortex induced vibrations of cables and cylinders were investigated. In [14] linear dynamics of curved tensioned elastic beams were investigated.

The riser is subjected to a time-varying distributed load due to the ocean current, resulting in undesirable transverse vibration. The vibration causes stresses in the slender body, which may result in fatigue problems from cyclic loads, damages due to wear and tear, propagation of cracks which requires inspections and costly repairs, and as a worst case, environmental pollution due to leakage from damaged areas. Another important consideration is the angle limit for the upper and lower end joints. The American Petroleum Institute requires that the mean lower and upper joint angles should be kept within two degrees while drilling and the maximum non-drilling angles should be limited to four degrees. Due to the motion of the surface vessel or the transverse vibrations of the riser, the upper or lower angle limit might be exceeded, resulting in damages to the riser end joints. For drilling and work-over operations, one objective is to minimize the bending stresses along the riser and the riser angle magnitudes at the platform and well head [15]. Hence, vibration reduction to reduce bending stresses and the control of the riser angle magnitude is desirable

for preventing damage and improving lifespan.

1.2 Previous Work

1.2.1 Adaptive and Approximation Based Control

An intuitive solution to alleviate the precision placement problem is the addition of thrusters for localized positioning when the payload is near the target site [16, 17]. The positioning control is challenging due to the unpredictable exogenous disturbances such as fluctuating currents and transmission of motions from the surface vessel through the lift cable. In [18], experiments were carried for dynamic positioning of a towed pipe. The nonlinear dynamics associated with the fluid phenomenon on the payloads, represented by a continuous infinite dimensional Navier-Stokes equation, need to be reduced to a finite dimensional approximate model which are normally experimentally determined. Due to the size, costs and the variations in design and construction, full scale experiments may not possible all structures. In most cases, the best way to determine the coefficients required are by means of model testing, where uncertainties attributed to the materials, measurement and scale effect exist.

Traditionally, such hydrodynamic loads are treated as bounded disturbances, and the standard proportional-integral-derivative (PID) algorithm is applied in motion control. The PID controller has been shown to exhibit good steady-state performance. However, its transient performance is less satisfactory, since the linear control action tends to produce large overshoots. Although the PID controller does not explicitly contain any terms from the dynamic model, the tuning of the PID gains by advanced techniques such as LQR requires knowledge of the model. Without the use of such techniques, PID tuning for the MIMO systems is generally nontrivial, and may require full-scale experiments.

In the dynamic control of offshore structures for installation, an important concern is how to deal with unknown perturbations to the nominal model, in the form of parametric

and functional uncertainties, unmodelled dynamics, and disturbances from the environment. Marine control applications are characterized by time-varying environmental disturbances and widely-changing sea conditions. In this context, stand-alone model-based controllers may not be the most ideal since they generally work best when the dynamic model is known exactly. The presence of uncertainties and disturbances could disrupt the function of the feedback controller and lead to degradation of performance. We propose to overcome this problem for the installation of subsea structures is to adopt an intelligent control strategy in the form of adaptive neural techniques to compensate for functional uncertainties in the dyanmic model and unknown disturbances from the environment. According to the Stone-Weierstrass theorem, a universal approximator, such as a neural network, can approximate any real continuous function on a compact set to an arbitrary degree of accuracy. Such approximators can utilize a standard regressor function whose structure is independent of the dynamic characteristics, thus increasing the portability of the same control algorithm on different marine systems. For systems in which the dynamic models are well-established and accurate, existing model-based schemes can be augmented by intelligent control 'modules' easily and flexibly to handle disturbances from varying weather conditions and sea states.

Direct compensation of the hydrodynamic loads is desirable but difficult to realize in practice due to the difficulty in obtaining accurate parametric coefficients. For control design, the parametric model should be simple enough for analysis, and yet be complex enough to capture the main dynamics of the system.

The approximation abilities of Artificial NNs have been proven in many research works [19–23]. The major advantages of parallel structure, learning ability, nonlinear function approximation, fault tolerance and efficient analyog VLSI implementation for real-time applications, motivate the usage of NNs in nonlinear system control and identification. NNs combined backstepping designs are reported in [24], using NN to construct observes can be found in [25,26], NN control in robot manipulators are reported in [27–30]. Adaptive neural control can overcome some limitations of model-based control which requires exact

knowledge of the system parameters [31, 32]. NNs can also be used as an alternative, to parameterize the nonlinear hydrodynamic loads and coupled with adaptive control for on-line tuning. Since NNs has also been embedded in the overall control strategy for modeling and compensation purposes in [22, 33–35]. In-depth developments in NNs for modeling and control purposes have been made in [32, 33, 35–38].

1.2.2 Control of Flexible Structures

Both the lifting cable and riser can modeled by a set of PDE which possesses infinite number of dimensions which makes it difficult to control. The control of the flexible structures and manipulators have received increasing attention in recent years [39–41]. One approach is to use an approximate finite dimensional model for control design. The approximate model can be obtained via spatial discretization to obtain a finite number of modes or by modal analysis and truncating the infinite number of modes to a finite number by neglecting the higher frequency modes. Based on a truncated model obtained from either the finite element method or galerkin method, various control approaches have been applied to improve the performance of flexible systems [42–44].

However, issues of control dimensionality and implementation may result due to the spill over effects from the control to the residual modes [45, 46]. When the control of the truncated system is restricted to a few critical modes. The control order needs to be increased with the number of flexible modes considered to achieve high accuracy of performance. The control may be difficult to implement from the engineering point of view since full states measurements or observers are often required. To avoid the problems associated with the truncated-model-based design, control methodologies such as variable structure control [47, 48], methods derived through the use of bifurcation theory and the application of Poincaré maps [49] and boundary control [50] with optimal actuator sensor placement [51] can be used.

Boundary control has been employed in a number of research fields such as vibration

control of flexible structures and fluid dynamics. Boundary Control of a nonlinear string has been investigated in [52, 53], where feedback from the velocity at the boundary of a string has been shown to stabilize the vibrations. An active boundary control system was introduced in [54] to damp undesirable vibrations in a cable. Boundary control for axially moving systems has been investigated in [55–59]. A vibration suppression scheme for an axially moving string under a spatiotemporally varying tension and an unknown boundary disturbance is investigated in [55]. In [57], the asymptotic and exponential stability of an axially moving string is proved by using a linear and nonlinear state feedback. Boundary control has been applied to beams in [60,61], where boundary feedback was used to stabilize the wave equations and design active constrained layer damping. Active boundary control of an Euler-Bernoulli beam which enables the generation of a desired boundary condition at any designators position of a beam structure has been investigated in [62]. Wave control to suppress vibration modes of flexible structure has been proposed in [63, 64]. In [50], the coupled model for longitudinal and transverse beam was derived, and the exponential stabilization of a beam in free transverse vibration, i.e. with external disturbance set to zero, via boundary control was shown with a riser example.

1.3 Thesis Objectives and Structure

The development of subsea processing equipment and the trend to go into deeper waters for untapped oil fields will result in an increased focus on offshore installation tasks and systems. The main purpose of the research in this thesis is to develop advance strategies for the control of subsea installation operations and flexible structures in the marine environment and alleviate some of the challenges.

The remainder of the thesis is organized as follows: In Chapter 2, we provide some some mathematical preliminaries which will be used throughout the thesis. A brief introduction for function approximation using NNs is given, followed by some useful technical lemmas

and definitions.

In Chapter 3, we investigate the transition of a payload from air to water, also known as splash zone transition, and the vertical hydrodynamic loads on the payload. The exogenous force during the transition can be expressed as a combination of terms from the pressure effects, slamming and viscous forces including the Froude-Kriloff forces, hydrostatic pressure and viscous drag. A simple linear in the parameter (LIP) model that is representative and captures most of the observed hydrodynamic load phenomena is presented. Model based control is designed and NN control approach is presented for the case where uncertainties exist in the system parameters.

In Chapter 4, positioning control in the horizontal plane is investigated for the installation of subsea systems near the seabed, with thrusters attached, under time-varying irrotational ocean current. Backstepping in combination with adaptive feedback approximation techniques are employed in the design of the control, with the option of High-gain observer for output feedback control. The stability of the design is demonstrated through Lyapunov analysis where semiglobal uniform boundedness of the closed loop signals are guaranteed. The proposed adaptive neural control is able to capture the dominant dynamic behaviors without exact information on the hydrodynamic coefficients of the structure and current measurements.

Next, the coupled dynamics and control of the vessel, crane, flexible cable and payload under environmental disturbances with attached thrusters for subsea installation operations is investigated in Chapter 5. For the practical system with physical constraints, Barrier Lyapunov Functions are employed in the design of positioning control for the flexible crane-cable-payload subsystem to ensure that the constraints are not violated. Uniform stability of the flexible subsystem is shown and asymptotic positioning of the boundaries is achieved. The scenario where nonuniformity of the cable, uncertainties and environmental disturbances exist is considered. Boundary controls are formulated using the nonlinear PDEs of the cable.

In Chapter 6, active control of flexible marine riser angle and the reduction of forced vibration under a time-varying distributed load are considered using boundary control approach. A marine riser is the connection between a platform on the water surface and the installed subsea system on the sea floor. A torque actuator is introduced in the upper riser package and a boundary control law is designed to generate the required signal for riser angle control and vibration reduction with guaranteed closed-loop stability. Exponential stability can be achieved under the free vibration condition. The proposed control is simple, implementable with actual instrumentation, and is independent of system parameters, thus possessing stability robustness to variations in parameters. The design is based on the PDEs of the system, thus avoiding some drawbacks associated with the traditional truncated-model-based design approaches.

Finally Chapter 7 concludes the contributions of the thesis and makes recommendation on future research works.

Chapter 2

Mathematical Preliminaries

In this chapter, we provide some mathematical preliminaries, which will be used throughout this thesis. A brief introduction for function approximation using NNs is given, followed by some useful technical lemmas and definitions.

2.1 Function Approximation

In this thesis, a class of linearly parameterized NNs with Radial Basis Functions (RBF) is used to approximate the continuous function $f_j(Z) : R^q \to R$,

$$f_{nn,j}(Z) = W_j^T S_j(Z), \tag{2.1}$$

where the input vector $Z = [Z_1, Z_2, \ldots, Z_q]^T \in \Omega_Z \subset R^q$, weight vector $W_j \in R^l$, the NN node number $l > 1$ and $S_j(Z) = [s_1, s_2, \ldots, s_l]^T \in R^l$. Universal approximation results indicate that, if l is chosen sufficiently large, $W_j^T S_j(Z)$ can approximate any continuous function, $f_j(Z)$, to any desired accuracy over a compact set $\Omega_Z \subset R^q$ to arbitrary any

accuracy. This is achieved as

$$f_j(Z) = W_j^{*T} S_j(Z) + \epsilon_j(Z), \quad \forall Z \in \Omega_z \in R^q, \tag{2.2}$$

where W_j^* is the ideal constant weight vector, and $\epsilon_j(Z)$ is the approximation error which is bounded over the compact set, i.e. $|\epsilon_j(Z)| \leq \epsilon_j^*$, $\forall Z \in \Omega_Z$ with $\epsilon_j^* > 0$ as an unknown constant. The ideal weight vector W_j^* is an "artificial" quantity required for analytical purposes. W_j^* is defined as the value of W_j that minimizes $|\epsilon_j|$ for all $Z \in \Omega_Z \subset R^q$ i.e.

$$W_j^* = \arg \min_{\mathrm{W_j} \in \mathrm{R^l}} \{ \sup_{\mathrm{Z} \in \Omega_\mathrm{Z}} |\mathrm{f_j(Z)} - \mathrm{W_j^T S_j(Z)}| \}. \tag{2.3}$$

Typical choices for $s_k(Z)$ include the sigmoid function, hyperbolic tangent function and RBF. The RBF NN is a particular network architecture which uses l Gaussian functions of the form

$$s_k(Z) = \exp\left[\frac{-(Z-\mu_k)^T(Z-\mu_k)}{\eta_k^2}\right], \quad k = 1, 2, ..., l, \tag{2.4}$$

where $\mu_k = [\mu_{k1}, \mu_{k2}, ..., \mu_{kq}]^T$ is the center of the receptive field and η_k is the width of the Gaussian function [65].

2.2 Useful Technical Lemmas and Definitions

Lemma 2.1. *[66] For bounded initial conditions, if there exists a C^1 continuous and positive definite Lyapunov function $V(x)$ satisfying $\kappa_1(\|x\|) \leq V(x) \leq \kappa_2(\|x\|)$, such that $\dot{V}(x) \leq -\rho V(x) + c$, where κ_1, $\kappa_2 : R^n \to R$ are class $\mathcal{K}$ functions and c is a positive constant, then the solution $x(t)$ is uniformly bounded.*

Lemma 2.2. *[67] Consider the basis functions of Gaussian RBF NN (2.4) with $\hat{Z}$ being the input vector, if $\hat{Z} = Z - \epsilon\bar{\psi}$, where $\bar{\psi}$ is a bounded vector and constant $\epsilon > 0$, then we*

have

$$\begin{aligned} s_i(\hat{Z}) &= \exp\Big[\frac{-(\hat{Z}-\mu_j)^T(\hat{Z}-\mu_j)}{\eta_j^2}\Big], \quad j=1,2,...,l, \\ S(\hat{Z}) &= S(Z)+\epsilon S_t, \end{aligned} \tag{2.5}$$

where S_t is a bounded vector function.

Lemma 2.3. *[68] Suppose a system output $y(t)$ and its first n derivatives are bounded such that $|y^{(k)}| < Y_K$ with positive constants Y_K, we can consider the following linear system:*

$$\begin{aligned} \varepsilon\dot{\pi}_i &= \pi_{i+1}, \quad i=1,...,n-1, \\ \varepsilon\dot{\pi}_n &= -\bar{\lambda}_1\pi_n - \bar{\lambda}_2\pi_{n-1} - ... - \bar{\lambda}_{n-1}\pi_2 - \pi_1 + \eta(t), \end{aligned} \tag{2.6}$$

where ε is any small positive constant and the parameters $\bar{\lambda}_1$ to $\bar{\lambda}_{n-1}$ are chosen such that the polynomial $s^n + \bar{\lambda}_1 s^{n-1} + ... + \bar{\lambda}_{n-1}s + 1$ is Hurwitz. Then, the follow property holds:

$$\xi_k = \frac{\pi_k}{\varepsilon^{k-1}} - \eta^{(k-1)} = -\varepsilon\psi^{(k)}, \quad k=1,...,n-1, \tag{2.7}$$

where $\psi = \pi_n + \bar{\lambda}_1\pi_{n-1} + ... + \bar{\lambda}_{n-1}\pi_1$ with $\psi^{(k)}$ denoting the k^{th} derivative of ψ. Also, there exist positive constants t^* and h_k such that $\forall t > t^*$, we have $||\xi_k|| \leq \varepsilon h_k$, $k=1,2,3,...,n$.

Lemma 2.4. *[69]: For any positive constants k_b, let $\mathcal{Z}_1 := \{z_3 \in R : -k_b < z_3 < k_b\} \subset R$ and $\mathcal{N} := \mathcal{R}^l \times \mathcal{Z}_1 \subset R^{l+1}$ be open sets. Consider the system*

$$\dot{\eta} = h(t,\eta) \tag{2.8}$$

where $\eta = [w, z_1]^T \in \mathcal{N}$ and $h : \mathcal{R}_+ \times \mathcal{N} \to R^{l+1}$ is piecewise continuous in t and locally Lipschitz in z, uniformly in t, on $\mathcal{R}_+ \times \mathcal{N}$. Suppose that there exist functions $U : \mathcal{R}^l \to \mathcal{R}_+$ and $V_3 : \mathcal{Z}_1 \to R_+$, continuously differentiable and positive definite in their respective

domains, such that

$$V_3(z_3) \to \infty \quad as \quad z_3 \to -k_b \quad or \quad z_3 \to k_b \tag{2.9}$$

$$\gamma_1(||w||) \leq U(w) \leq \gamma_2(||w||) \tag{2.10}$$

where γ_1 *and* γ_2 *are class* K_∞ *functions. Let* $V(\eta) := V_1(z_3) + U(w)$*, and* $z_3(0)$ *belong to the set* $z_3 \in (-k_b, k_b)$*. If the inequality holds:*

$$\dot{V} = \frac{\partial V}{\partial \eta} h \leq 0 \tag{2.11}$$

then $z_3(t)$ *remain in the open set* $z_3 \in (-k_b, k_b) \forall t \in [0.\infty)$

Definition 2.1. ***Barrier Lyapunov Function*** *[69] A BLF is a scalar function* $V(x)$ *defined with respect to the system* $\dot{x} = f(x)$ *on an open region* $\mathcal{D}$ *containing the origin, that is continuous, positive definite, has continuous first-order partial derivatives at every point of* $\mathcal{D}$*, has the property* $V(x) \to \infty$ *as* x *approaches the boundary of* $\mathcal{D}$*, and satisfies* $V(x(t)) \leq b,\ \forall t \geq 0$ *along the solution of* $\dot{x} = f(x)$ *for* $x(0) \in \mathcal{D}$ *and some constant* b*.*

As discussed in [69], there are many functions $V_1(z_1)$ *satisfying Definition 2.1, which may be symmetric or asymmetric. Asymmetric barrier functions are more general than their counterparts, and thus can offer more flexibility for control design to obtain better performance. However they are considerably more difficult to construct analytically, and to employ for control design. For clarity, the following symmetric* BLF *candidate considered in [1, 69] is used in this thesis:*

$$V_1 = \frac{1}{2} \log \frac{k_{b1}^2}{k_{b1}^2 - z_1^3} \tag{2.12}$$

where $\log(\cdot)$ *denotes the natural logarithm of* $(\cdot)$*, and* k_b *the constraint on* z_1*. The* BLF *escapes to infinity at* $z_1 = k_b$*. It can be shown that* V_1 *positive definite and* C^1 *continuous in the set* $z_1 < k_{b1}$*. The control design and results in this thesis can be extended to the*

asymmetric BLF case.

Definition 2.2. ***(SGUUB)*** *[70] The solution $X(t)$ of a system is semi-globally uniformly ultimately bounded (SGUUB) if, for any compact set Ω_0 and all $X(t_0) \in \Omega_0$, there exists an $\mu > 0$ and $T(\mu, X(t_0))$ such that $\|X(t)\| \leq \mu$ for all $t \geq t_0 + T$*

Chapter 3

Splash Zone Transition Control

In this chapter, a detailed model of the vertical hydrodynamic loads on a payload going through the splash zone is presented. The load can be expressed as a combination of terms from the pressure effects, slamming and viscous forces including the Froude-Kriloff forces, hydrostatic pressure and viscous drag in [71, 72]. It is a challenge to determine parameters such as viscous drag. In most cases, the best way to determine the hydrodynamic coefficients are by means of model testing [73]. However, uncertainties related to the model, measurement and scale effect still exist.

Adaptive control schemes have been proposed for continuous time systems to address parametrization in a variety of mechanism [22, 74, 75]. NNs have been found to be able to approximate any continuous nonlinear function to any desired accuracy over a compact set. Adaptive neural control can be formulated with as an alternative to model based control design due to parametric uncertainties.

The organization of this chapter is as follows: The problem formulation is given in Section 3.1. In Section 3.2, model-based and non-model-based (NN) control are developed for the system transiting through the splash zone and the closed loop system is analyzed via Lyapunov synthesis. Simulation studies are presented to show the effectiveness of the

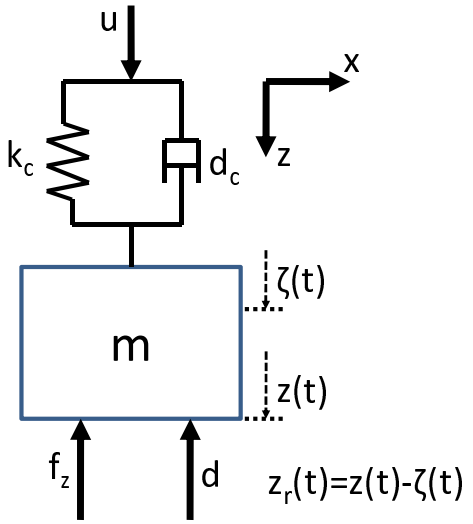

Fig. 3.1: Schematic illustration of dynamic system in splash zone

proposed controls in Section 3.3.

3.1 Problem Formulation

In this chapter, only the vertical motion of the payload moving through the splash zone will be considered. The effects from the vessel's roll and pitch motions are neglected as heave compensators only work in one degree of freedom (DOF). The reference coordinates are fixed on the crane vessel with positive z axis pointing downwards with the origin fixed on the deck of the vessel.

3.1.1 Dynamic Modeling

A large class of heave compensation cranes can be represented by the combination of a passive spring damper system and an actively control winch system. The passive component can be modelled with stiffness k_c and damping coefficient d_c. The dynamics of the system

is shown in Fig. 2.1 and can be represented by

$$m\ddot{z} + d_c\dot{z} + k_c z + d(t) \quad = \quad mg + f_z + u \tag{3.1}$$

where m and g represents the mass and gravitational constant of 9.81 ms^{-2}, z, $\dot{z}$, $\ddot{z}$ are the displacement, velocity, acceleration of the payload in the downward z-direction respectively, u is the active control force, f_z is the hydrodynamic load and *d(t)* is the disturbance, assumed to be bounded by $b_d > 0$ as $\mid d(t) \mid \leq b_d$.

3.1.2 Hydrodynamic Load Models

The hydrodynamics in this section is based on [71, 72, 76]. The vertical hydrodynamic load on a body entering the water can be expressed as a combination of forces from the pressure effects, slamming and viscous forces.

Pressure effects and slamming forces

In [71], the hydrodynamic loads are derived by the use of momentum theory. When there are no incident wave effects, the vertical hydrodynamic force on a body with uniform cross section penetrating the free-surface can be written as

$$f_{ps} \quad = \quad -\rho_s g A_z z_r - Z_{\ddot{z}_r}(z_r)\ddot{z}_r - \frac{\partial Z_{\ddot{z}_r}(z_r)}{\partial z_r}\dot{z}_r^2$$

where the states z_r, $\dot{z}_r$, $\ddot{z}_r$ denotes the position, velocity and acceleration of the payload relative to the wave elevation $\zeta(t)$, with $z_r = z - \zeta(t)$, A_z the cross sectional area, and $Z_{\ddot{z}_r}(z_r)$ the added mass of the payload in the z-direction relative to the wave respectively, ρ_s is the density of water and ϕ is the potential for the incident wave. The first term on the right represents the hydrostatic pressure on the object and the second and third terms represent the effect of the added mass and the slamming forces respectively. In practice, the

water elevation $\zeta(t)$ can be measured using a wave meter and the position of the payload z can be measured from the length of wire pay out from the crane. Hence, we can obtain $z_r = z - \zeta(t)$.

The slamming parameter $(\partial Z_{\ddot{z}_r}/\partial z_r)$ is often written as $(1/2)\rho_s A_s C_s$, where A_s and C_s is denoted efficient slamming area and slamming coefficient [77]. Hence, (3.2) becomes

$$f_{ps} = -\rho_s g A_z z_r - Z_{\ddot{z}_r}(z_r)\ddot{z}_r - \frac{1}{2}\rho_s A_s C_s \dot{z}_r^2. \tag{3.2}$$

Another component to be included is the Froude-Kriloff pressure forces, dependant on the velocity of the water particles and computed by an area pressure method:

$$\begin{aligned} f_{fk} &= -\rho_s g A_z z_r \frac{d}{dt}\frac{\partial \phi}{\partial z}\Big|_{z=z_r} \\ &= -\rho_s g A_z z_r \ddot{z}. \end{aligned} \tag{3.3}$$

Viscous Drag

Drag load caused by resistance to a partially or fully submerged body moving through a viscous fluid can be described by

$$f_{zv} = -\frac{1}{2}\rho_s C_D A_{pz} \dot{z}_r |\dot{z}_r| \tag{3.4}$$

where C_D is the drag coefficient and A_{pz} is the projected efficient drag area in the vertical direction.

Remark 3.1. *Based on the above discussion, a more complete model may consist of the following components as a sum of forces from the pressure effects, slamming and viscous forces, $f_z = f_{ps} + f_{fk} + f_{zv}$. The more complete model becomes*

$$f_z = -\rho_s g A_z z_r - \rho_s A_z z_r \ddot{z} - Z_{\ddot{z}_r}(z)\ddot{z}_r - \frac{1}{2}\rho_s A_s C_s \dot{z}_r^2 - \frac{1}{2}\rho_s C_D A_{pz} \dot{z}_r |\dot{z}_r|. \tag{3.5}$$

Equation (3.5) can be expressed in the LIP form as

$$f_z(\xi) \quad = \quad \psi^T(\xi)\theta^*, \tag{3.6}$$

where

$$\psi(\xi) \quad = \quad [z_r, z_r\ddot{z}, \ddot{z}_r, \dot{z}_r^2, \dot{z}_r|\dot{z}_r|]^T, \tag{3.7}$$

$$\theta^* \quad = \quad [-\rho_s g A_z, -\rho_s A_z, -Z_{\ddot{z}_r}(z), -\frac{1}{2}\rho_s A_s C_s, -\frac{1}{2}\rho_s C_D A_{pz}]^T, \tag{3.8}$$

where $\psi(\xi)$ a vector of known variables, $\xi = [\ddot{z}, z_r, \dot{z}_r, \ddot{z}_r]$ is the input variables and θ^* the actual parameters. Although the LIP form is very desirable for control design it is in no sense complete but a more complete representation.

3.2 Control Design and Stability Analysis

A state of the art heave compensation system combines a passive spring-damper mechanism together with position control of the crane hook [72]. The control objective is to lower the crane hook following a desired trajectory in the z axis.

Let $z_d(t), \dot{z}_d(t)$ and $\ddot{z}_d(t)$ be the position, velocity and acceleration respectively of the desired trajectory. We define the tracking errors as

$$e = z_d - z, \qquad r = \dot{e} + \lambda e \tag{3.9}$$

where $\lambda > 0$. The velocity and acceleration signals are defined as

$$\dot{z}_{ref} = \dot{z}_d + \lambda e, \qquad \ddot{z}_{ref} = \ddot{z}_d + \lambda \dot{e}. \tag{3.10}$$

Due to the uncertainties in the parameters (3.8), we first design a model based adaptive control. Let $(\hat{*})$ be the estimate of $(*)$ and $(\tilde{*}) = (*) - (\hat{*})$. We have $\hat{f}_z = \psi^T\hat{\theta}$, $\tilde{f}_z = \psi^T\tilde{\theta}$.

Design the control as

$$\begin{aligned} u_{mb} &= \hat{m}\ddot{z}_{ref} - \hat{m}g + \hat{d}_c\dot{z} + \hat{k}_c z + \hat{f}_z + u_r + u_d \\ &= \hat{W}^T S(Z) + u_r + u_d \end{aligned} \tag{3.11}$$

where $S(Z) = [\ddot{z}_{ref}, g, \dot{z}, z, \psi^T]^T$, $\hat{W}$ is the approximation weights, u_d is a standard PID type control, $u_d = k_1 r + k_i \int_0^t r d\tau$, $k_1 > 0$ and u_r is a robust control term for suppressing any modeling uncertainty, $u_r = k_2 \text{sgn}(r)$. The closed-loop system is then given by

$$m\dot{r} + u_r + u_d = d + \epsilon + \tilde{W}^T S(Z), \tag{3.12}$$

where ϵ is the approximation error and $\tilde{W} = [\tilde{m}, \tilde{m}, \tilde{d_c}, \tilde{k_c}, \tilde{\theta}^T]^T$.

Theorem 3.1. *Consider the system (3.1) with control* (3.11)*, there exist compact sets* Ω_r*,* Ω_w *and* Ω_β *and positive constants* β*,* σ*,* c_W *and* k_1 *such that all signals in the closed loop system (3.12) are bounded and stable if the parameters are updated according to*

$$\dot{\hat{W}} = \Gamma\Big[S(Z)r + \sigma\hat{W}\Big], \qquad \sigma > 0. \tag{3.13}$$

Proof: Consider the positive Lyapunov function candidate

$$V = \frac{1}{2}\Big[mr^2 + \tilde{W}^T\Gamma^{-1}\tilde{W} + k_i\Big(\int_0^t r \ d\tau\Big)^2\Big]$$

with the time derivative of V given by

$$\dot{V} = mr\dot{r} + \tilde{W}^T\Gamma^{-1}\dot{\tilde{W}} + rk_i\int_0^t r \ d\tau. \tag{3.14}$$

Substituting (3.12) into (3.14) leads to

$$\begin{aligned} \dot{V} &= r(\tilde{W}^T S(Z) + d + \epsilon - k_1 r - u_r) + \tilde{W}^T \Gamma^{-1} \dot{\tilde{W}} \\ &= -k_1 r^2 + r(d + \epsilon - u_r) + r\tilde{W}^T S(Z) + \tilde{W}^T \Gamma^{-1} \dot{\tilde{W}} \end{aligned} \tag{3.15}$$

Noting the adaptive law (3.13),

$$\dot{\tilde{W}} = -\Gamma\Big[S(Z)r + \sigma\hat{W}\Big], \quad \Gamma^T = \Gamma > 0 \tag{3.16}$$

$$\dot{V} = -k_1 r^2 + r\upsilon - \sigma\tilde{W}^T\hat{W} \tag{3.17}$$

where $\upsilon = d + \epsilon - u_r$. By completing the squares and using the following inequalities,

$$\begin{aligned} 2\tilde{W}^T\hat{W} &= \parallel \tilde{W} \parallel^2 + \parallel \hat{W} \parallel^2 - \parallel W^* \parallel^2 \\ &\geq \parallel \tilde{W} \parallel^2 - \parallel W^* \parallel^2, \end{aligned} \tag{3.18}$$

$$\begin{aligned} -r^2 + \mid r \mid \frac{\upsilon}{k_1} &\leq -\frac{r^2}{2} - \frac{1}{2}(r - \frac{\upsilon}{k_1})^2 + \frac{\upsilon^2}{2{k_1}^2} \\ &\leq -\frac{r^2}{2} + \frac{\upsilon^2}{2}, \end{aligned} \tag{3.19}$$

we obtain

$$\dot{V} \leq -\frac{k_1}{2}r^2 + \frac{\upsilon^2}{2} - \frac{\sigma \parallel \tilde{W} \parallel^2}{2} + \frac{\sigma \parallel W^* \parallel^2}{2}.$$

Considering $\parallel W^* \parallel \leq c_W$, $\varepsilon_s = (1/2)(\upsilon^2 + c_W^2)$,

$$\dot{V} \leq -\frac{k_1}{2}r^2 - \frac{\sigma}{2} \parallel \tilde{W} \parallel^2 + \varepsilon_s, \tag{3.20}$$

we define

$$\Omega_r = \Big\{ r \Big| \mid r \mid^2 \leq \frac{2\varepsilon_s}{k_1} \Big\}, \tag{3.21}$$

$$\Omega_w = \Big\{ \tilde{W} \Big| \parallel \tilde{W} \parallel^2 \leq \frac{2\varepsilon_s}{\sigma} \Big\} \tag{3.22}$$

$$\Omega_{\varepsilon_s} = \Big\{ \Big(r, \tilde{W} \Big) \Big| \frac{k_1}{2} r^2 + \frac{\sigma}{2} \parallel \tilde{W} \parallel^2 \leq \varepsilon_s \Big\}. \tag{3.23}$$

Since ε_s, σ, c_W and k_1 are positive constants, we know that Ω_r, Ω_w and Ω_{ε_s} are compact sets. From (3.20) it is shown the $\dot{V} \leq 0$ once the errors are outside the compact set Ω_{ε_s}. It can also be seen that $\dot{V}$ is strictly negative as long as r is outside the compact set Ω_r. It follows that $0 \leq V(t) \leq V(0)$, $\forall t \geq 0$. Hence $V(t) \in L_\infty$, which implies that $\tilde{W}$ is bounded and hence $\hat{W}$ is bounded. Since $r \in L_2^n$, $e \in L_2^n \cap L_\infty^n$, e is continuous and $e \to 0$ as $t \to \infty$, and $\dot{e} \in L_2^n$. By noting that $r \in L_2^n$, $x_d, \dot{x}_d, \ddot{x}_d \in L_\infty^n$, and S is of bounded functions, it is concluded that $\dot{r} \in L_\infty^n$. Using the fact that $r \in L_\infty^2$ and $\dot{r} \in L_\infty^n$, thus $r \to 0$ as $t \to \infty$. Hence $\dot{e} \to 0$ as $t \to \infty$.

3.2.1 NN Control

Due to the complexity and difficulty in modeling the hydrodynamic loads, NN may be used to generate input-output maps for a non-model-based approach. The Gaussian radial basis functions (RBF) NN is a particular network architecture which uses l Gaussian functions of the form in (2.4). We design the NN control similiar to (3.11) with

$$u_{NN} = \hat{W}^T S_{NN}(Z) + m\ddot{z}_{ref} - mg + d_c\dot{z} + k_c z + u_r + u_d \tag{3.24}$$

where $Z = [\ddot{z}, z_r, \dot{z}_r, \ddot{z}_r]^T$, weight vector $\hat{W} \in R^l$, the NN node number $l > 1$ and $S(Z) = [s_1, s_2, \ldots, s_l]^T \in R^l$ with s_i defined in (2.4).

Theorem 3.2. *Consider the system (3.1) with control* (3.24)*, there exist compact sets* Ω_r*,* Ω_w *and* Ω_β *and positive constants* β*,* σ*,* c_W *and* k_1 *such that all signals in the closed loop*

system (3.12) are bounded and stable if the parameters are updated according to

$$\dot{\hat{W}} = \Gamma\Big[S(Z)r + \sigma\hat{W}\Big], \qquad \sigma > 0. \tag{3.25}$$

Proof: The proof is similar to that in Theorem 3.2 and is omitted for conciseness.

Corollary 3.1. *The closed loop system (3.12) is asymptotically stable if the parameters are updated with*

$$\dot{\hat{W}} = \Gamma S(Z)r, \qquad \Gamma^T = \Gamma > 0 \tag{3.26}$$

and the gain of the sliding mode control $k_2 \geq \mid d + \epsilon \mid$.

Proof: Noting the adaptive law (3.26), we have

$$\dot{\tilde{W}} = -\Gamma S(Z)r, \qquad \Gamma^T = \Gamma > 0 \tag{3.27}$$

Combining (3.17) and (3.27),

$$\dot{V} \;\; = \;\; -k_1 r^2 + r(d + \epsilon - u_r). \tag{3.28}$$

Since $u_r = k_2 \mathrm{sgn}(r)$ and $k_2 \geq \mid d + \epsilon \mid$, We have $\dot{V} = -k_1 r^2 \leq 0$. According to the standard Lyapunov theorem as above, we conclude that $\dot{e}$, $\tilde{W}$, r, e, S and $\dot{r}$ are bounded. The application of the Lyapunov stability theory guarantees a level of performance for the system. With regards to implementation issues, we make the following remarks:

Remark 3.2. *It is undesirable to directly implement the sliding control term to cancel the effect of the approximation errors due to the chattering which may excite mechanical resonance. To alleviate this problem, many approximation mechanisms have been used, such as introducing a boundary layer, saturation functions [78], and a hyperbolic tangent function*

tanh(.), which has the following nice property [79],

$$0 \leq \mid \alpha \mid -\alpha \tanh(\frac{\alpha}{\epsilon}) \leq 0.2785\epsilon, \quad \forall \alpha \in R. \tag{3.29}$$

By smoothing the sgn(.) function, the closed loop system is still stable with a small residual error although asymptotic stability can no longer be guaranteed.

For example, let $u_r = k_2 \tanh(r/\epsilon_r)$, where $\epsilon_r \geq 0$ is a constant, and $k_2 \geq \mid d + \epsilon \mid$, then (3.28) becomes

$$\begin{aligned} \dot{V} &= -k_1 r^2 + r(d + \epsilon - u_r) \\ &\leq -k_1 r^2 + \mid r \mid\mid d + \epsilon \mid -rk_2 \tanh(\frac{r}{\epsilon_r}) \\ &\leq -k_1 r^2 + \mid r \mid k_2 - rk_2 \tanh(\frac{r}{\epsilon_r}). \end{aligned} \tag{3.30}$$

Using (3.29), (3.30) can be further simplified as

$$\dot{V} \leq -k_1 r^2 + 0.2785\epsilon_r k_2. \tag{3.31}$$

Obviously, $\dot{V} \leq 0$ whenever r is outside the compact set

$$\Omega_D = \left\{ r \middle| r^2 \leq \frac{0.2785\epsilon_r k_2}{k_1} \right\}. \tag{3.32}$$

Thus, we can conclude that the closed-loop system is stable and the tracking error will converge to a small neighbourhood of zero, whose size is adjustable by the design parameters k_1 and ϵ_r. It should be mentioned that these modification may cause the estimated parameters to grow unboundedly because asymptotic tracking cannot be guaranteed unless the robust control term in Theorem 3.1 is introduced.

Remark 3.3. *In the presence of approximation errors, the σ modification scheme or e*

modification [80] among others can be used to modify the adaptive laws to guarantee the robustness of the closed-loop system. In Theorem 3.1, the additional σ term in (3.13) ensures the boundedness of $\hat{W}$ when the system is subject to bounded disturbance without additional prior information about the plant. The drawback of the robust modification method introduced here is that the tracking errors may only be made arbitrarily small rather than zero.

3.3 Simulations

In this section, the control and model presented is simulated using the same full scale parameters in [72]. The payload is assumed to be launched into the water through a moonpool, rigidly attached to an actively controlled crane boom. The vessel is kept heading relative towards incoming waves, in a mean fixed position and is moving only due to first order waves. The dynamics of the system are given by

$$m\ddot{z} + d_c\dot{z} + k_c z \quad = \quad f_z + u \tag{3.33}$$

where f_z is expressed in (3.5). The following parameters are being used in the simulations. Mass, $m = 15500kg$, payload height $h = 3m$, $A_{pz} = 6.25m^2$, $r = 1.5m$, $Z_{\ddot{z}_r}(z = h) = 6$ and $C_D = 3.0$. The water elevation is modelled as a sinusoid wave with period and wave height $T = 6.0s$ and $\zeta = 1.0m$. This is used instead of the normal statistical method because the penetration of the water surface normally has a duration of one to three wave periods. Thus a worst case wave period is used that matches the resonance frequency of the moonpool. The nondimensional coefficients C_s, $\Omega(z_r) = A_z z_r$ and $Z_{\ddot{z}_r}(z)$ used in the simulations are shown in Fig. 2.2 as a function of normalized depth with respect to height

The desired trajectory is generated by:

$$\frac{x_d(s)}{x_{ref}(s)} \quad = \quad \frac{\omega_r^2}{s^2 + 2\lambda_r\omega_r s + \omega_r^2} \tag{3.34}$$

where $x_{ref} = 2h$, $\omega_r = 0.7rads^{-1}$, $\lambda_r = 1.0$ and the control parameters are chosen as $\lambda = 50$, $k_i = 0$, $k_2 = 0$ and $\hat{m}(0) = 15500kg$. The crane stiffness k_c and the damping constant d_c are calibrated and tested according to rules and regulations set by classification societies before each operation and are assumed to be perfectly known. The estimation errors of these two terms are at least one order of magnitude less than the slamming forces and are neglected in the simulations. It is assumed that no other knowledge of the system is known except for m.

3.3.1 Conventional PID Control

For the purpose of comparison, consider first the control performance when adaptation law is not activated by setting the adaptation gain $\Gamma = 0$. In this case, the resulting control action is effectively a conventional PID-type control as follows

$$u = k_1 r + k_i \int_0^t r d\tau. \tag{3.35}$$

Three sets of PID gains were designed based on the LQR method with Q, R and respective control gains as follows:

- PID1: $\{Q = 1e10,\ R = 1,\ k_p = 1.6931 \times 10^6,\ k_d = 1.0155 \times 10^6,\ k_i = 1.0000 \times 10^6\}$
- PID2: $\{Q = 1e11,\ R = 1,\ k_p = 3.2995 \times 10^5,\ k_d = 5.0941 \times 10^5,\ k_i = 3.1623 \times 10^5\}$
- PID3: $\{Q = 1e12,\ R = 1,\ k_p = 1.3752 \times 10^5,\ k_d = 1.0940 \times 10^5,\ k_i = 1.0000 \times 10^5\}$

where $k_1 = k_d$ and $\lambda = k_d/k_p$. A high Q and low R is chosen for the LQR design to place more weighting to the states of the system.

The tracking trajectory is shown in Fig. 3.3, the tracking errors and control signals under the PID control are shown in Fig. 3.4. It can be observed from these results that the lower gain PID control in PID1 cannot control the system satisfactorily. A higher gain PID control is able to reduce the tracking error significantly.

3.3.2 Model-Based Adaptive Control

We explore the model based adaptive control to augment the PID control when some knowledge of the parameters or structure of the hydrodynamics disturbances affecting the system is known. Control (3.11) is simulated with updating law (3.13) with different learning rate i.e. $\Gamma = 1, 10, 100$, control gains for u_d {PID2: $k_p = 3.2995 \times 10^5$, $k_d = 5.0941 \times 10^5$, $k_i = 3.1623 \times 10^5$}, $w_i = 0$, for $i = 1$ to 9, $\sigma = 0$. The tracking errors, control signal the norm of the adaptive weights under the model-based adaptive control are shown in Fig. 3.5.

It is observed that for the same parameters in PID2, the model-based adaptive control is able to reduce the tracking error further. This means that the 'model-based adaptive control is able to successfully compensate for the hydrodynamic forces. It is also observed that a higher adaptation gain Γ produces better tracking results. Care is required in implementation and design of the gains as system may become unstable if the adaptation gain chosen is too high.

3.3.3 Non-Model-Based (NN) Control

In the last subsection, the model based adaptive control was explored when knowledge of the parameters affecting the system is known. In the case where the knowledge of the parameters affecting the system is not known, we investigate the use of a non-model based approach, i.e. adaptive NN method to learn about the system and compensate for the system. Control (3.24) is simulated with updating law (3.25) with different learning rate i.e. $\Gamma = 10, 50, 100$, control gains for u_d {PID2: $k_p = 3.2995 \times 10^5$, $k_d = 5.0941 \times 10^5$, $k_i = 3.1623 \times 10^5$}, $w_i = 0$, for $i = 1$ to 9, $\sigma = 0$ similar to above. For the NN, we use RBF in (2.4), where $l = 81$, $S(\ddot{z}, z_r, \dot{z}_r, \ddot{z}_r)$ and RBF centers chosen as $\mu_1 = [-1.0, 0.0, -0.5, -1.0]$, $\mu_2 = [0.0, 3.0, 0.0, 0.0]$ and $\mu_3 = [1.0, 6.0, 0.5, 1.0]$.

The tracking errors, control signal the norm of the adaptive weights under the adaptive NN control are shown in Fig. 3.6. It can be seen that the NN adaptive control can improve

on the performance of the PID control u_d. Increasing Γ is observed to improve the tracking performance. The effectiveness of the NN appeared to improve only marginally when increasing the number of NN nodes any further. The performance was deemed satisfactory for this number of nodes and can demonstrate good tracking ability.

The tracking errors and control signals of PID3, model-based adaptive control with $\Gamma = 100$ and adaptive NN control with $\Gamma = 100$ is shown in Fig. 3.7. It is observed that the model-based adaptive control and the adaptive NN control can improve on the tracking performance of the pure PID control.

3.4 Conclusion

In this chapter, adaptive control for a payload transiting through the splash zone has been investigated using both model and non-model-based (NN) parametrization techniques. A detailed mathematical model for hydrodynamics loads during water entry has been presented. Model-based and non-model-based robust adaptive controls have been developed with closed loop stability. Extensive simulations have been carried out to show the effectiveness of the proposed control techniques.

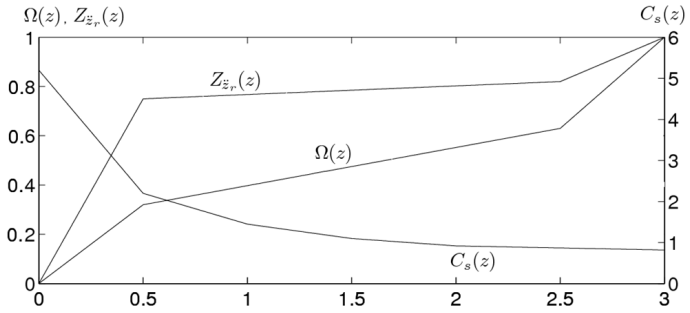

Fig. 3.2: Non-dimensional coefficients used in splash zone simulations

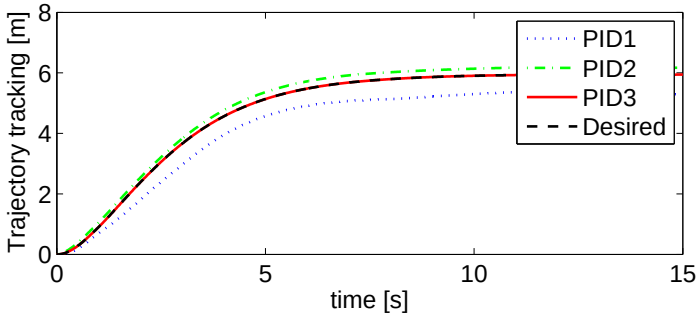

Fig. 3.3: Trajectory of payload trhough splash zone under PID control with different gains

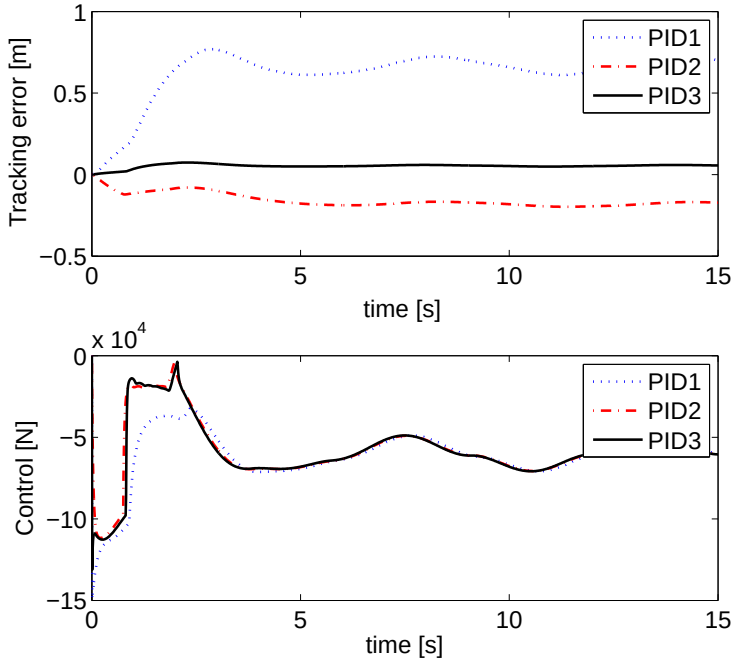

Fig. 3.4: (Top): Tracking errors and (Bottom): control signals under PID control for system transition through splash zone

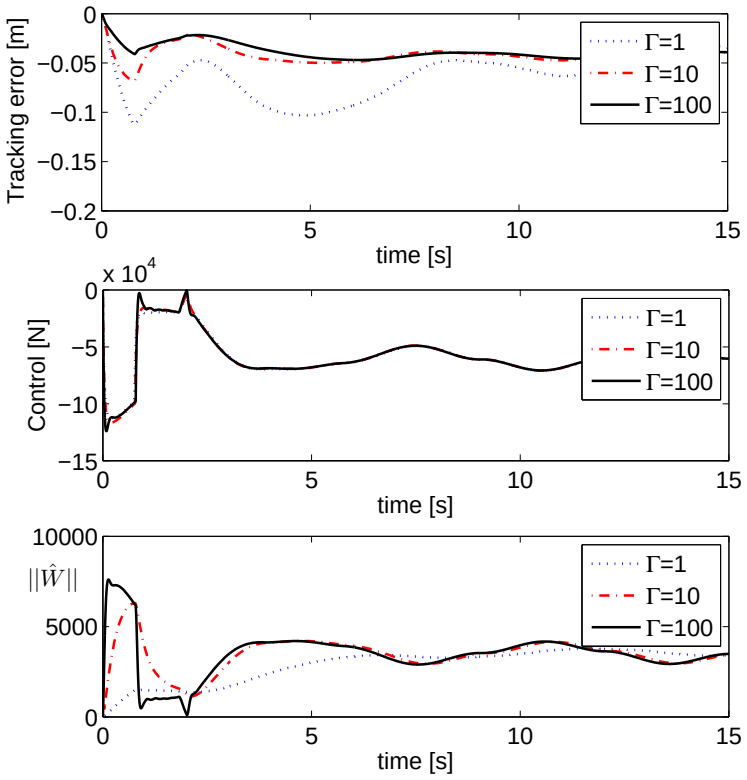

Fig. 3.5: (Top): Tracking errors, (Center): control signals and (Bottom): norm of adaptation weights $||\hat{W}||$ under model-based adaptive control with different Γ for system transition through splash zone

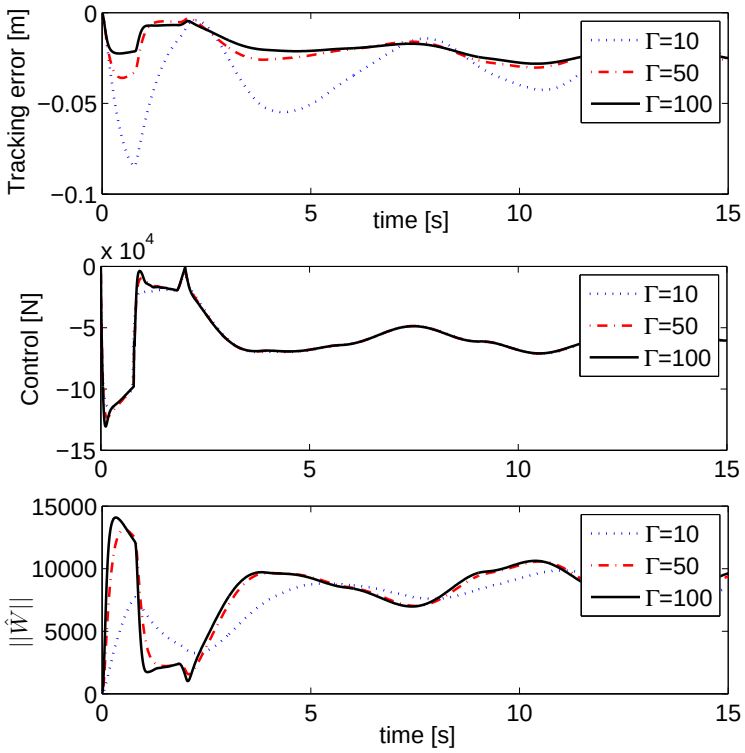

Fig. 3.6: (Top): Tracking errors, (Center): control signals and (Bottom): norm of adaptation weights $||\hat{W}||$ under adaptive NN control with different Γ for system transition through splash zone

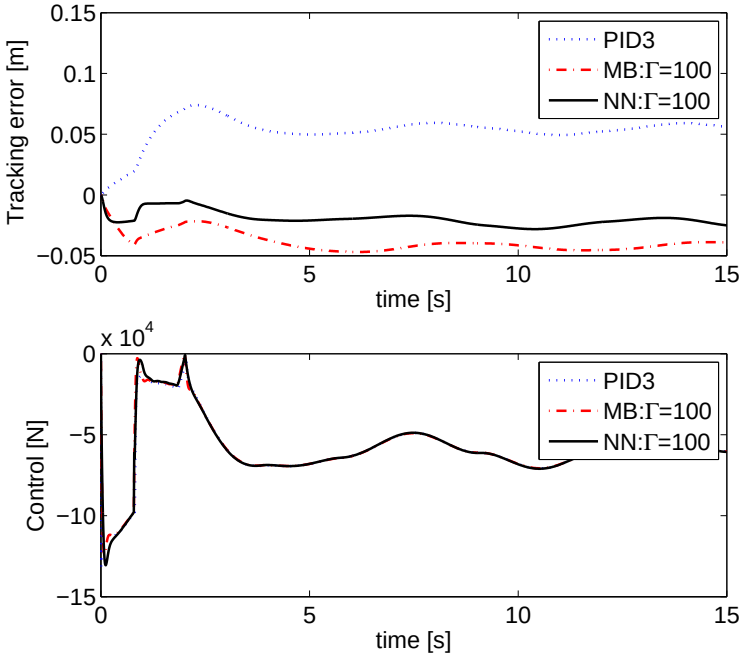

Fig. 3.7: Comparisions of (Top): tracking errors and (Bottom): control signals for PID, model-based adaptive and adaptive NN control for system transition through splash zone

Chapter 4

Dynamic Load Positioning

Near the seabed, the subsea templates, Christmas trees and manifolds have to be installed accurately in a specified spatial position and compass heading within tight limits, including rotational, vertical and lateral measurements. The tolerances for a typical subsea installation are within 2.5m of design location and within 2.5 degrees of design heading for large templates [3] and are more stringent for the installation of manifolds into the templates. Accurate positioning on the seabed has been identified as one of the problems in subsea installation operations.

An intuitive solution to alleviate the precision placement problem is the addition of thrusters for localized positioning when the payload is near the target site [16, 17]. The positioning control is challenging due to the unpredictable exogenous disturbances such as fluctuating currents and transmission of motions from the surface vessel through the lift cable. The nonlinear dynamics associated with the fluid phenomenon on the payloads, represented by a continuous infinite dimensional Navier-Stokes equation, need to be reduced to a finite dimensional approximate model which are normally experimentally determined. Due to the size, costs and the variations in design and construction, full scale experiments may not possible all structures. In most cases, the best way to determine the coefficients required are by means of model testing, where uncertainties attributed to the materials,

measurement and scale effect exist. To overcome the limitations of model-based adaptive controllers, we adopt adaptive neural control techniques to compensate for functional uncertainties and unknown disturbances from the environment through online tuning of the NN weights [81].

In this chapter, positioning control is investigated for the installation of subsea systems, with thrusters attached, under time-varying irrotational ocean current. The dynamic model and the effects of the current disturbance are presented in Section 4.1. In Section 4.2, backstepping in combination with adaptive feedback approximation techniques are employed in the design of the control, with the option of High-gain observer for output feedback control. The stability of the design is demonstrated through Lyapunov analysis where semiglobal uniform boundedness of the closed loop signals are guaranteed. The proposed adaptive neural control is able to capture the dominant dynamic behaviors without exact information on the hydrodynamic coefficients of the structure and current measurements. Comparative simulations with linear PID, PD with adaptive term and model-based controls are carried out in Section 4.3.

4.1 Problem Formulation and Preliminaries

4.1.1 Dynamic Modeling

We consider the horizontal planar dynamics for surge, sway and yaw motions of the subsea payload. The geographic reference frame, North-East-Down (n-frame) is chosen, defined relative to the Earth's reference ellipsoid, with the x_n, y_n and z_n axis directed towards the North, East and Downward normal to the Earth's surface respectively and chosen such that the target installation location is at the origin. The configuration in the n-frame is $\eta = [x_n, y_n, \psi_n]^T$, where x_n, y_n describes the distance from the target location and ψ_n denotes the rotation about the z_n axis. The body-fixed reference frame (b-frame) is a moving coordinate frame with the origin attached to the Center of Gravity and axes corresponding

to the principle axis of inertia. The frames assigned are represented in Fig. 4.1 with the payload velocity defined in the b-frame as $\nu = [u_b, v_b, r_b]^T$, where u_b, $v_b \in R$, are components of the absolute velocity in the x_b and y_b directions, $r_b \in R$ describes the angular velocity about the z_b axis, and vectors η and ν are related by the transformation,

$$\dot{\eta} = J(\eta)\nu, \tag{4.1}$$

where

$$J(\eta) = \begin{bmatrix} \cos\psi_n & -\sin\psi_n & 0 \\ \sin\psi_n & \cos\psi_n & 0 \\ 0 & 0 & 1 \end{bmatrix}. \tag{4.2}$$

Taking into account the inertial generalized forces, the hydrodynamic effects, the gravity and buoyancy contribution and the thrusters, the dynamics for low speed underwater positioning of the structure can be expressed in the canonical form for robotics [82],

$$M\dot{\nu} + C(\nu)\nu + D(\nu)\nu + g(\eta) = \tau, \tag{4.3}$$

where $M \in R^{3\times3}$ is the system inertia matrix, $C(\nu) \in R^{3\times3}$ the coriolis-centripetal matrix, $D(\nu) \in R^{3\times3}$ the damping matrix, $g(\eta) \in R^3$ the vector of gravitational and buoyancy forces and $\tau \in R^3$ the control input.

4.1.2 Effects of Time Varying Current and Disturbances

The effects of ocean current on positioning control of underwater structures are significant. The current is normally assumed to be constant and irrotational for subsea operations planning or control systems design [83]. That is, the current velocity is $v_c = [v_{c,x}, v_{c,y}, 0]^T\ ms^{-1}$ with $\dot{v}_c = 0$. However, this assumption is not strictly true and can adversely affect the performance of the control.

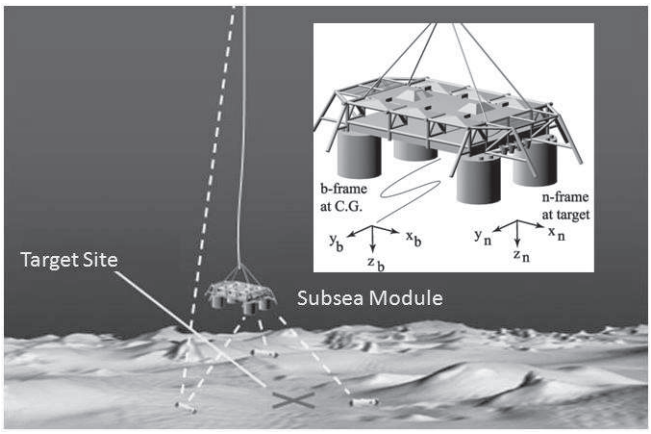

Fig. 4.1: Subsea template with relevant frames

In this chapter, we extend the investigation to include the effects of a time varying irrotational current, $v_c(t) = [v_{c,x}(t), v_{c,y}(t), 0]^T$. The magnitude $V_c(t)$ is treated as a 1st order Gauss-Markov process,

$$\dot{V}_c(t) + \mu V_c(t) = \omega, \tag{4.4}$$

$$V_{\min} \leq V_c(t) \leq V_{\max}, \tag{4.5}$$

where ω is Gaussian white noise, $\mu \geq 0$ is a constant and $V_{\min}$, $V_{\max}$ are minimum and maximum magnitude of the current speed respectively, projected based on hydrographic surveys done on site. In the horizontal plane, the current velocity can be decomposed to the b-frame via $v_{c,x}(t) = V_c(t)\cos\beta_c$ and $v_{c,y}(t) = V_c(t)\sin\beta_c$, where β_c is the sideslip angle. The disturbance from the ocean current, $\tau_c(t)$, is obtained by applying Morrison's equation for cylindrical members or other appropriate empirical formulas dependant upon the geometry of the module [84]. From (4.3), we obtain

$$M\dot{\nu} + C(\nu)\nu + D(\nu)\nu + g(\eta) = \tau + \tau_d(t), \tag{4.6}$$

where $\tau_d(t) = \tau_c(t) + \tau_l(t)$, $\tau_d \in R^3$ represents the lumped disturbance τ_c resulting from

ocean current and the unknown disturbance, τ_l, from the lift cable.

Assumption 4.1. *For time dependent function* $\tau_d(t)$, $i = 1, 2, 3$, *there exist constants* $\bar{\tau}_{d,i} \in R^+$ *where* $\|\tau_{d,i}(t)\| \leq \bar{\tau}_{d,i}$.

Remark 4.1. *The subsea payloads are rigged according to rules and regulations set by the classification societies. The dynamics in the roll and pitch are assumed to be accounted for in the rigging configuration and the heave motion due to the wave, structure weight and the upward tension of the cable, is to be controlled by a separate heave-compensated system.*

Remark 4.2. *Assumption 1 is reasonable as the effects of the disturbances are largely attributed to the exogenous effects from the environment, which are finite and bounded. The maximum allowable loads from the environment during the installation operation needs to be determined at the operations design, planing and material selection phases. The allowable weather window and sea states for the operation is determined and the installation operation will not be carried out if the environment is too rough for safe operations. As such, the bounds on the disturbances* $\bar{\tau}_{d,i}$ *are assumed to be known.*

Remark 4.3. *The surface vessel is responsible for global positioning while the thrusters on the payload are responsible for local positioning and activated close to the target site. To improve the performance further, the effects of the lift cable and coupling with the surface vessel will be investigated in future work.*

Assumption 4.2. *The reference trajectory for the positioning of the payload,* η_r, *is a bounded* C^2 *function, sufficiently smooth to avoid sudden jumps of tracking error.*

4.2 Adaptive Neural Control Design

The control objective is to position and orientate the payload for accurate placement via attached thrusters. Tracking control is necessary when the installation is carried out in proximity to other critical equipment on the seabed via a reference trajectory $\eta_r(t) =$

$[x_{nr}(t), y_{nr}(t), \psi_{nr}(t)]^T$. We first consider the case where full state information ν and η are available. Dependency of the signals, where obvious, will be omitted.

Define a generalized tracking error as $z_1(t) = \eta(t) - \eta_r(t)$ and obtain $\dot{z}_1 = J(\eta)\nu - \dot{\eta}_r$. We introduce a virtual control α_1 and define a second error variable as $z_2(t) = \nu(t) - \alpha_1(t)$. From (4.2), $J(\eta)J^T(\eta) = I$, choose

$$\alpha_1(\eta, \dot{\eta}_r, z_2) = J^T(\eta)(\dot{\eta}_r - K_1 z_1), \tag{4.7}$$

where the gain matrix $K_1 = K_1^T > 0$, and obtain

$$\dot{z}_1 = J(\eta)(z_2 + \alpha_1) - \dot{\eta}_r. \tag{4.8}$$

Choosing a Lyapunov function candidate with quadratic z_1

$$V_1 = \frac{1}{2} z_1^T z_1, \tag{4.9}$$

and taking its time derivative along (4.8), we have

$$\dot{V}_1 = -z_1^T K_1 z_1 + z_1^T J(\eta) z_2. \tag{4.10}$$

Differentiating z_2 with respect to time,

$$\dot{z}_2 = M^{-1}\left[h(\nu, \eta) + \tau + \tau_d(t)\right] - \dot{\alpha_1}, \tag{4.11}$$

where

$$h(\nu, \eta) = -C(\nu)\nu - D(\nu)\nu - g(\eta), \tag{4.12}$$

$$\dot{\alpha_1} = \frac{\partial \alpha_1}{\partial \eta}\dot{\eta} + \frac{\partial \alpha_1}{\partial \dot{\eta}_r}\ddot{\eta}_r + \frac{\partial \alpha_1}{\partial z_1}\dot{z}_1. \tag{4.13}$$

Next, consider the Lyapunov function candidate and its time derivative

$$\begin{aligned} V_2^* &= V_1 + \frac{1}{2} z_2^T M z_2, && (4.14) \\ \dot{V}_2^* &= -z_1^T K_1 z_1 + z_1^T J(\eta) z_2 \\ &\quad + z_2^T (h(\nu, \eta) + \tau - M\dot{\alpha_1}) + z_2^T \tau_d(t). && (4.15) \end{aligned}$$

We can obtain the following,

$$\begin{aligned} \dot{V}_2^* &\leq -z_1^T K_1 z_1 + z_1^T J(\eta) z_2 + z_2^T (h(\nu, \eta) - M\dot{\alpha_1} + \tau) \\ &\quad + \sum_{i=1}^{3} |z_{2,i}| \tau_{d,i}(t)), && (4.16) \end{aligned}$$

where $z_{2,i} \in R$ for $i = 1, 2, 3$ are the elements of z_2. Consider the model-based control law,

$$\begin{aligned} \tau_{mb} &= -J^T(\eta) z_1 - K_2 z_2 - h(v, \eta) \\ &\quad + M\dot{\alpha_1} - K \text{sgn}(z_2)(\bar{\tau}_{d,i}), && (4.17) \end{aligned}$$

where $\text{sgn}(z_2) = \text{diag}[\text{sgn}(z_{2,i})]$ is a robust sliding term for $i = 1, 2, 3$, $\text{sgn}(\cdot)$ as the signum function, gain matrices, $K_2 = K_2^T > 0$ and $K = \text{diag}(k_{ii}) \in R^{3\times 3}$, $k_{ii} > 1$, $i = 1, 2, 3$. By substituting (4.17) into (4.16), we can rewrite (4.16) as

$$\dot{V}_2^* \leq -z_1^T K_1 z_1 - z_2^T K_2 z_2 \tag{4.18}$$

which is negative semi-definite. Since uncertainties exists in the parameters M , $C(v)$, $D(v)$ and $g(\eta)$, or are unknown, the model-based control law (4.17) may not be realizable. To overcome this challenge, we use NNs to approximate the uncertainties and propose the following control law and adaptation law,

$$\tau = -J^T(\eta) z_1 - K_2 z_2 - K \text{sgn}(z_2)(\bar{\tau}_{d,i}) + \hat{W}^T S(Z), \tag{4.19}$$

$$\dot{\hat{W}}_i \quad = \quad -\Gamma_i(S_i(Z)z_{2i} + \sigma_i\hat{W}_i), \tag{4.20}$$

where $\hat{W}$= blockdiag$[\hat{W}_1^T, \hat{W}_2^T, \hat{W}_3^T]$ are the NN weights, $S(Z) = [S_1^T(Z), S_2^T(Z), S_3^T(Z)]^T$ the basis functions, Γ_i constant gain matrices and $\sigma_i > 0$, $i = i, 2, 3$, are sigma modification constants which impose growth conditions on the weight vectors to improve the stability of $\hat{W}$ when the system is subjected to bounded disturbances [85]. The NN $\hat{W}^T S(Z)$ approximates $W^{*T}S(Z)$ defined by

$$W^{*T}S(Z) \quad = \quad -h(\eta, \nu) + M\dot{\alpha_1} - \epsilon(Z), \tag{4.21}$$

where $Z = [\eta^T, \nu^T, \alpha_1^T, \dot{\alpha_1}^T]^T$ are the input variables to the adaptive NN and $\epsilon(Z) \in R^3$ is the approximation error.

Remark 4.4. *In this chapter, we address a more challenging problem by treating the values of M , $C(\nu)$, $D(\nu)$, $g(\eta)$ $a_i(\eta, \nu)$ and $b(t)$, as completely unknown. If individual terms are known exactly, the terms can be excluded from the approximation in equation* (4.21) *and incorporated explicitly as part of the adaptive neural control law* (4.19)*, similar to the model-based control* (4.17)*.*

Theorem 4.1. *Consider the dynamic model (4.6), with control law (4.19) and adaptation law (4.20). Given that the full state information is available, for each compact set Ω_0 where ($\eta(0)$, $\nu(0)$, $\hat{W}_1(0)$, $\hat{W}_2(0)$, $\hat{W}_3(0)$) $\in \Omega_0$, i.e. the initial conditions are bounded, the trajectories of the closed-loop system are semiglobally uniformly bounded. The closed loop error signals, z_1, z_2 and $\tilde{W}$ will remain within the compact sets Ω_{z_1}, Ω_{z_2} and Ω_W respectively defined by*

$$\Omega_{z_1} : \quad = \quad \left\{ z_1 \in R^3 \mid \|z_1\| \leq \sqrt{D} \right\}, \tag{4.22}$$

$$\Omega_{z_2} : \quad = \quad \left\{ z_2 \in R^3 \mid \|z_2\| \leq \sqrt{\frac{D}{\lambda_{\min}(M)}} \right\}, \tag{4.23}$$

$$\Omega_W : \quad = \quad \left\{ \tilde{W} \in R^{l\times 3} \mid \|\tilde{W}\| \leq \sqrt{\frac{D}{\lambda_{\min}(\Gamma^{-1})}} \right\}, \tag{4.24}$$

where $D = 2\left(V_2(0) + C/\rho\right)$ with ρ and C as defined in (4.31) and (4.32) respectively.

Proof: Consider the augmented Lyapunov function candidate,

$$V_2 = V_1 + \frac{1}{2} z_2^T M z_2 + \frac{1}{2} \sum_{i=1}^{3} \tilde{W}_i^T \Gamma_i^{-1} \tilde{W}_i, \tag{4.25}$$

where $\tilde{W}_i = \hat{W}_i - W_i^*$ and $\tilde{W}_i$, $\hat{W}_i$, W_i^* are the NN weight error, estimate and actual value respectively. Differentiating (4.25), we obtain

$$\begin{aligned} \dot{V}_2 \quad \leq \quad & -z_1^T K_1 z_1 + z_1^T J(\eta) z_2 + z_2^T [h(\nu, \eta) - M\dot{\alpha}_1 + \tau] \\ & + \sum_{i=1}^{3} |z_{2,i}| \tau_{d,i} + \sum_{i=1}^{3} \tilde{W}_i^T \Gamma_i^{-1} \dot{\hat{W}}_i. \end{aligned} \tag{4.26}$$

Using the approximation (4.21) we obtain,

$$\begin{aligned} \dot{V}_2 \quad \leq \quad & -z_1^T K_1 z_1 + z_1^T J(\eta) z_2 + \sum_{i=1}^{3} |z_{2,i}| \tau_{d,i} \\ & + z_2^T \left[-W^{*T} S(Z) - \epsilon(Z) + \tau \right] + \sum_{i=1}^{3} \tilde{W}_i^T \Gamma_i^{-1} \dot{\hat{W}}_i. \end{aligned} \tag{4.27}$$

Substituting the control (4.19) and adaptation law (4.19) into (4.27) yields

$$\begin{aligned} \dot{V}_2 \quad \leq \quad & -z_1^T K_1 z_1 - z_2^T K_2 z_2 - \sum_{i=1}^{3} \left[\sigma_i \tilde{W}_i^T \hat{W}_i \right] \\ & + \frac{1}{2} \|\bar{\epsilon}(Z)\| + \frac{1}{2} z_2^T z_2, \end{aligned} \tag{4.28}$$

From the property

$$-\sigma_i \tilde{W}_i^T \hat{W}_i \leq -\frac{\sigma_i}{2} \|\tilde{W}_i\|^2 + \frac{\sigma_i}{2} \|W_i^*\|^2, \tag{4.29}$$

we obtain $\dot{V}_2$ and the bounds ρ and C as

$$\begin{aligned} \dot{V}_2 &\leq -\rho V_2 + C, && (4.30) \\ \rho &= \min\Big(2\lambda_{\min}(K_1), \frac{2\lambda_{\min}(K_2 - \frac{1}{2}I_{3\times 3})}{\lambda_{\max}(M)}, \\ &\quad \min_{i=1,2,3}\Big(\frac{\sigma_i}{\lambda_{\max}(\Gamma_i^{-1})}\Big)\Big), && (4.31) \\ C &= \sum_{i=1}^{3}\frac{\sigma_i}{2}\|W_i^*\|^2 + \frac{1}{2}\|\bar{\epsilon}\|^2, && (4.32) \end{aligned}$$

where $\lambda_{\min}(A)$ and $\lambda_{\max}(A)$ denote the minimum and maximum eigenvalues of matrix A, where $\lambda(A)$ are real, respectively. To ensure $\rho > 0$, the control gains K_1 and K_2 are chosen to satisfy the following conditions:

$$\lambda_{\min}(K_1) > 0, \qquad \lambda_{\min}(K_2 - \frac{1}{2}I_{3\times 3}) > 0. \tag{4.33}$$

From (4.30) and Lemma 6.1, it is straightforward to show that the signals $z_1, z_2, \tilde{W}_1, \tilde{W}_2, \tilde{W}_3$ are semiglobally uniformly bounded. From the boundedness of η_r in Assumption 1, we know that η is bounded. Since $\dot{\eta}_r$ is also bounded, it follows that α_1 is bounded and in turn ν is bounded. With W_i^* as slow time varying, we know that $\hat{W}_i$ is also bounded, for $i = 1, 2, 3$. For completeness, the details of the proof, similar to [66], are provided here. Multiplying (4.30) by $e^{\rho t}$ yields

$$\frac{d}{dt}(V_2 e^{\rho t}) \leq C e^{\rho t}. \tag{4.34}$$

Integrating the above inequality, we obtain

$$V_2 \leq \Big(V_2(0) - \frac{C}{\rho}\Big)e^{-\rho t} + \frac{C}{\rho} \leq V_2(0) + \frac{C}{\rho}. \tag{4.35}$$

Substituting (4.25) into (4.35),

$$\frac{1}{2}||z_1||^2 \leq V_2(0) + \frac{C}{\rho}. \tag{4.36}$$

Hence, z_1 converges to the compact set Ω_{zs}. Bounds of z_2, $\tilde{W}_i$ can be similarly shown and this concludes the proof. ■

Remark 4.5. *The stability result proposed is semiglobal in the sense that if the number of NN nodes l is chosen large enough such that the approximation holds on Ω_z, then the closed-loop stability can be guaranteed for bounded initial states and NN weights. The exact sizes of the compact sets Ω_{z1}, Ω_{z2} and Ω_W are not available as they depend on the unknown parameters W^* and ϵ.*

Remark 4.6. *The control design and stability analysis in this chapter assume that the thrusters are able to provide the force and torque as required. The effects of thruster dynamics such as thruster saturation are explored in [86–88]. It was found that thruster saturation can cause severe degradation in the tracking performance. This problem can be alleviated through an appropriate choice of trajectory if the task and disturbances are within the operational range of the propulsion system.*

4.2.1 High-Gain Observer

The proposed control (4.19) requires full state feedback $\eta(t)$ and $\nu(t)$ to be implemented. In the absence of velocity sensors such as the doppler velocity log, we introduce a High-gain observer design to estimate $\nu(t)$ through the certainty equivalence property and separation principle.

From Lemma 2.3, $\frac{\pi_{k+1}}{\varepsilon^k}$ converges asymptotically to $\eta^{(k)}$, the derivative of η to the kth order, i.e. ξ_k converges to zero with a small time constant (due to the high-gain $1/\varepsilon$) provided that η and its k derivatives are bounded. Hence, π_{k+1}/ε^k is suitable as an observer to estimate the output derivatives up to the nth order. The observer for system (4.6) is

designed with $n = 2$ and the estimate of the unmeasurable state vector z_2 can be defined as

$$\hat{z}_2 = J^T(\eta)(\pi_2/\varepsilon) - \alpha_1 \tag{4.37}$$

From the full state feedback case, we modify the control law (4.19) and adaptation law (4.20) to obtain the control and adaptation law for output feedback control as

$$\begin{aligned} \tau &= -J^T(\eta)z_1 - K_2\hat{z}_2 - K\text{sgn}(\hat{z}_2)(\bar{\tau}_{d,i}) + \hat{W}^T S(\hat{Z}), & (4.38)\\ \dot{\hat{W}}_i &= -\Gamma_i(S_i(\hat{Z}_1)\hat{z}_{2,i} + \sigma_i\hat{W}_i). & (4.39) \end{aligned}$$

The time derivative of the Lyapunov function candidate V_2 in (4.25) along the closed loop trajectory with (4.38) and (4.39) yields

$$\begin{aligned} \dot{V}_2 \leq\ & -z_1^T K_1 z_1 - z_2^T(K_2 - \frac{1}{2}I_{3\times 3})z_2 - z_2^T K_2 \tilde{z}_2 \\ & + \sum_{i=1}^{3} z_{2,i}[\hat{W}_i^T S_i(\hat{Z}_i) - W_i^{*T} S_i(Z_i)] \\ & - \sum_{i=1}^{3}[\tilde{W}_i^T S_i(\hat{Z}_i)\hat{z}_{2,i} + \sigma_i\tilde{W}_i^T\hat{W}_i] + \frac{1}{2}\|\bar{\epsilon}\|^2. \end{aligned} \tag{4.40}$$

From Lemma 2.2 and using the properties

$$\begin{aligned} \sigma_i\tilde{W}_i^T\hat{W}_i &\leq \frac{\sigma_i}{2}(||W_i^*||^2 - ||\tilde{W}_i||^2), & (4.41)\\ ||S_i(\hat{Z}_i)||^2 &\leq l_i, & (4.42) \end{aligned}$$

and $\tilde{z}_2 = \hat{z}_2 - z_2 = J^T(\eta)\xi_2$, denoting $\Lambda = \text{diag}[2l_i/\sigma_i]$,

$$V_{obs} = (1/2)\xi_2^T\xi_2, \tag{4.43}$$

we obtain

$$\dot{V}_2 \leq -z_1 K_1 z_1 - z_2^T \Big(K_2 - \frac{3}{2} I\Big) z_2 + \frac{1}{2}||\bar{\epsilon}||^2 - \sum_{i=1}^{3} \frac{\sigma_i}{4}||\tilde{W}_i||^2$$
$$+\lambda_{\max}(K_2^T K_2 + \Lambda) V_{obs} + \frac{1}{2}\sum_{i=1}^{3}\Big(\epsilon^2 ||S_{ti}||^2 + \sigma_i\Big)\|W_i^*\|^2,$$

which can be expressed in the form of (4.30),

$$\begin{aligned}
\dot{V}_2 &\leq -\rho V_2 + C, && (4.44)\\
\rho &= \min\Big(2\lambda_{\min}(K_1), \frac{2\lambda_{\min}(K_2 - \frac{3}{2} I_{3\times 3})}{\lambda_{\max}(M)},\\
&\quad \min_{i=1,2,3}\Big(\frac{\frac{\sigma_i}{4}||\tilde{W}_i||^2}{\lambda_{\max}(\Gamma_i^{-1})}\Big)\Big), && (4.45)\\
C &= \frac{1}{2}\sum_{i=1}^{3}\Big(\epsilon^2 ||S_{ti}||^2 + \sigma_i\Big)\|W_i^*\|^2,\\
&\quad +\lambda_{\max}(K_2^T K_2 + \Lambda) V_{obs} + \frac{1}{2}\|\bar{\epsilon}\|^2. && (4.46)
\end{aligned}$$

where the bounds on $V_{obs} \leq (1/2)\varepsilon^2(h_1^2 + h_2^2)$. To ensure that $\rho > 0$, the control gains K_1 and K_2 are chosen to satisfy the following conditions:

$$\lambda_{\min}(K_1) > 0, \quad \lambda_{\min}(K_2 - \frac{3}{2} I_{3\times 3}) > 0. \tag{4.47}$$

Theorem 4.2. *Consider the dynamic model (4.6), with output feedback control (4.38), adaptation law (4.39) and High-gain observer (2.6). For each compact set Ω_0 where ($\eta(0)$, $\nu(0)$, $\hat{W}_1(0)$, $\hat{W}_2(0)$, $\hat{W}_3(0)$) $\in \Omega_0$, i.e. if the initial conditions are bounded, the trajectories of the closed-loop system are semiglobally uniformly bounded. The tracking error z_1 converges to a compact set*

$$\Omega_{zs} = \Big\{z_1 \in R^3 \mid \|z_1\| \leq \sqrt{D}\Big\}, \tag{4.48}$$

where $D = 2(V_2(0) + C/\rho)$, ρ and C are defined in (4.45) and (4.46) respectively.

Proof: The stability proof of Theorem 4.2 along (4.44), (4.45) and (4.46) follows Theorem 4.1 and is omitted for conciseness.

Remark 4.7. *In this chapter, we assumed that the position measurements are perfect and proposed a rigorous theoretical treatment of the output feedback problem using High-gain observers corresponding to a non-model-based approach. If the output measurements are contaminated with zero mean Gaussian white noise within tolerance, careful implementation is necessary by designing ϵ to be sufficiently small. A saturation function can be used to overcome the peaking phenomenon of the high-gain observer following [89].*

Remark 4.8. *The tracking error has been shown to converge and remain within a small neighborhood of the origin. If the residual error is desired to be lower, it can be reduced such that C/ρ in both Theorem 1 and 2 decreases. The reduction is achieved by increasing k_1, k_2, the approximation accuracy of the NN, and the high-gain $1/\varepsilon$ of the state observer [67].*

4.3 Numerical Simulation

In this section, comparative studies were carried out via numerical methods on the proposed control and three different control methodologies. A wet Christmas tree is modeled as a cylinder with dimensions $r = 1.0m$, $L = 5.2m$ and $m = 32240kg$ representing the radius, length and dry mass respectively. The parameters in the dynamic equation (4.6) are $M = M_{RB} + M_A$, $M_{RB} = \text{diag}[32240, 32240, 16120]$, $M_A = \text{diag}[16728, 16728, 0]$, $C(\nu) = [0, 0, c_{13}; 0, 0, c_{23}; -c_{13}, -c_{23}, 0]$, $c_{13} = (M_{A,22} - M_{RB,22})\nu_2$, $c_{23} = -(M_{A,11} - M_{RB,11})\nu_1$ and $D(\nu) = \text{diag}[0.5\rho_w C_D \pi r^2 \nu,\ 0.5\rho_w C_D \pi r^2 \nu,\ 0]$, where M_{RB} is the rigid body inertia, M_A the added mass, C_D the drag coefficient and $\rho_w = 1024kgm^3$ the density of seawater. A cylindrical model was chosen for the analysis of the controls for its well studied hydrodynamic properties and characteristics in the literature [71]. The simulation step size is $0.001s$ with the update rate for controls and observer set as $10Hz$. The sampling period of $0.1s$ was used to investigate the effects of long sampling rate. A fourth-order Runge-Kutta-Merson

program with adaptive step size is used to numerically solve the equation of motions [78].

The control objective for the payload is to track a reference trajectory from an initial state in the n-frame to the target site designated as the origin for installation. The reference trajectory $\eta_r(t)$=$[x_{nr}(t), y_{nr}(t), \psi_{nr}(t)]^T$, is generated via a Hermite polynomial of the third degree with a general expression

$$\eta_r(t, t_r) = \eta_0 + \Big(-2.0\frac{t^3}{t_r^3} + 3.0\frac{t^2}{t_r^2}\Big)(\eta_f - \eta_0), \tag{4.49}$$

where $\eta_0 = [5.0, 2.0, 1.047]^T$ and $\eta_f = [0, 0, 0]^T$ are the payload initial and final positions respectively and $t_r = 150s$ represents the time at which the reference trajectory reaches the desired final position. The reference trajectory shown in Fig. 4.2 satisfies Assumption 1 and is continuous $\forall$ t with bounded η_r, $\dot{\eta}_r$ and $\ddot{\eta}_r$.

From Section 4.1.2, the time varying current profile shown in Fig. 4.3 was generated using Equation (4.4) with bounds $V_{\max} = 1.2ms^{-1}$, $V_{\min} = 0.8ms^{-1}$ and $\mu = 0$ was chosen to generate a more random ocean current. The current forces and the motion of a cylinder in fluid are derived from Morison's equations [84],

$$\bar{\tau}_{c,i} \quad = \quad C_D\rho_w\frac{D_c}{2}|v_{c,i}|v_{c,i} + C_m\rho_w\pi\frac{D_c^2}{4}\dot{v}_{c,i},\ i = 1, 2, 3, \tag{4.50}$$

where $C_D = 1.0$, $C_m = 1.0$ is the added mass coefficient, D_c the diameter of the cylindrical member, v_c, i and $\dot{v}_{c,i}$ are the velocity and acceleration of the current in each direction respectively. The effect of the current is not a linear force parallel to the current itself due to the coupling effects of the hydrodynamic terms. However, a reasonable hypothesis is made that the main contribution of the current to the vehicle motion is observed along the current direction [90]. The irrotational current is simulated to be 60° from the North-East which results in a constant $\beta_c = 30°$ due to the symmetry of the cylindrical payload. Fig. 4.3 shows the disturbances due to the current in the x, y direction.

4.3.1 Full State Feedback

Four different cases are considered. In the first case, we examine the common PID (proportional integral derivative) control. Second, we include an adaptive mechanism to the PD control for current compensation, Third, we evaluate the model-based control developed in (4.17) assuming that the parameters of the subsea structure are completely known. In the fourth case, we investigate the proposed adaptive neural control.

Case 1: PID Control. The PID control represents one of the most widely used controls and thus provides a baseline for the comparison of the performance of other controls. In this case, we consider a PID control of the form

$$\tau = -K_P z_1 - K_D \dot{z}_1 - K_I \int_0^t z_1(\varsigma) d\varsigma, \tag{4.51}$$

where K_P, K_I and K_D are the proportionate, integral and derivative gain matrices respectively. The closed loop analysis of the PID control law applied to underwater dynamics is similar to [88, 91] and not included here. An application of Lasalle's Invariance Theorem [92] shows that the PID control will perform set point regulation but not trajectory tracking [93]. While the PID control does not perform trajectory tracking, it is included as the control objective is to dynamically position the load at a fixed spatial position.

In this subsection, we assume that the model of the payload dynamics is completely known and use the Linear Quadratic Regulator (LQR) method to tune the PID control. The sets of parameters Q and R used in the LQR and the respective control gains generated are as follows

- PID1: $Q = 1 \times 10^6 I_{3,3}$, $R = 1$, $K_I = \{1000,1000,1000\}$. $K_P = \{7419,7419,5192\}$, $K_D = \{25412, 25412, 12977\}$
- PID2: $Q = 1 \times 10^8 I_{3,3}$, $R = 1$, $K_I = \{1000,1000,1000\}$, $K_P = \{36156,36156,26864\}$, $K_D = \{58753, 58753, 31083\}$

- PID3: $Q = 1 \times 10^1 0 I_{3,3}$, $R = 1$, $K_I = \{10000,10000,10000\}$, $K_P = \{212370,212370, 188010\}$, $K_D = \{173900, 173900, 126740\}$

Large Q matrices was chosen to place emphasis on the states of the system. Fig. 4.4 shows the norm of tracking error and the control input. The control action produced overshoots in the transient phase and the norm of the tracking error subsequently reduces to $||z_1|| \approx$ 0.1 during steady state. As the gain of K_P, K_I and K_D increases, the tracking errors are reduced. Conversely, the tracking errors increases significantly when the gains are reduced. In practice, large control gains are not recommended as they reduce robustness and cause large overshoots due to noisy measurements.

Case 2: PD Control with Adaptive Mechanism. The control adapted from [90] for an underwater vehicle combines a PD action with an adaptive compensation to provide asymptotic trajectory tracking. The control is given as

$$\tau = K_D s + K\tilde{\eta} + \Phi_T \hat{\lambda}, \tag{4.52}$$

$$\dot{\hat{\lambda}} = K_\lambda^{-1} \Phi_T^T s, \tag{4.53}$$

where $s = \tilde{\nu} + \Lambda_p \tilde{\eta}$, $\tilde{\nu} = \nu_r - \nu$, $\tilde{\eta} = \eta_r - \eta$, $\nu_r = J^T(\eta)\eta_r$, K_D, Λ_p and K are positive gain matrices, $K_\lambda^{-1} = \Gamma > 0$ is the adaptive gain matrix, $\hat{\lambda}$ is the adaptation weight and $\Phi_T^T s = J^T(\eta)s$ is a regressor. The closed loop stability analysis can be found in Ref. [90] and is not repeated here. The matrices are chosen as $K_D = 6 \times 10^5 I_{3\times3}$, $K = 6 \times 10^5 I_{3\times3}$, $\Lambda_p = I_{3\times3}$, and three cases with $\Gamma = 50 I_{3\times3}$, $\Gamma = 100 I_{3\times3}$ and $\Gamma = 200 I_{3\times3}$ are simulated. The norm of the tracking error and control input are shown in Fig. 4.5. It is observed that the transient response of the PD control with adaptive mechanism is large due to the inability of the adaptive mechanism to capture the effects of the current. However, when the parameters have converged, the norm of error produced during steady state is lower than that of the PD type control. The control effort which corroborates the overshoot in the transient region is also observed.

Case 3: Model-Based Backstepping Control. The model-based backstepping control in (4.17) without the robust signum term is investigated here as follows:

$$\begin{aligned}\tau_{mb} &= -J^T(\eta)z_1 - K_2 z_2 - h(\nu,\eta) \\ &\quad + M\dot{\alpha}(\eta_r, \dot{\eta}_r, \ddot{\eta}_r, z_1, z_2),\end{aligned} \tag{4.54}$$

assuming that the parameters of the subsea structure are completely known. The effects of the control gains are examined by varying the control gain matrix K_2. Simulations were carried out for $K_1 = k_1 I_{3\times 3}$, and $K_2 = k_2 I_{3\times 3}$, with $k_1 = 5$ and $k_2 = 10000$, 20000 and 30000. The tracking errors and control input signals are shown in Fig. 4.6. The norm of the tracking error for the model-based control without the robust term is satisfactory with $\|z_1\| < 0.1$. To achieve low tracking errors, model-based control requires exact knowledge of the system dynamics and parameters. This is difficult to achieve in practice as the geometry of the structure makes the identification of the hydrodynamic effects complex. Inaccurate parameter values can degrade the performance significantly. It is noted that the gains are significantly lower than that of the PID and PD plus adaptive mechanism controls earlier which is advantageous for robustness towards noisy measurements.

Case 4: Proposed Adaptive Neural Control. Linearly parameterized approximators are used in the control law and update law in (4.7), (4.19) and (4.20). $\hat{W}$=diag$[\hat{W}_1^T, \hat{W}_2^T, \hat{W}_3^T]$ are the approximation weights and $S(Z)$=$[S_1^T(Z), S_2^T(Z), S_3^T(Z)]^T$ are Gaussian RBF (2.4) and $Z = [\eta^T, \nu^T, \alpha_1^T, \dot{\alpha}_1^T]$ are the input variables. A total of $l = 512$ nodes are employed for each $S_j^T(Z)$ with centers chosen as combinations of $\mu_{k,1} = \mu_{k,2} = \{1.0, -1.0\}$, $\mu_{k,3} = \mu_{k,6} = \mu_{k,9} = \mu_{k,12} = 0$ and $\mu_{k,4} = \mu_{k,5} = \mu_{k,7} = \mu_{k,8} = \mu_{k,10} = \mu_{k,11} = \{0.1, -0.1\}$. The effects of varying the control gains Γ were investigated with $\Gamma = 1.0 I_{3\times 3}$, $\Gamma = 5.0 I_{3\times 3}$ and $\Gamma = 10.0 I_{3\times 3}$, $\sigma_i = 1 \times 10^{-5}$, $\eta_k^2 = 5.0$, $i = 1, 2, 3$, $K_1 = 5 I_{3\times 3}$ and $K_2 = 20000 I_{3\times 3}$, which satisfies the conditions in (4.33). From Fig. 4.7, it is observed that tracking performance of the control is satisfactory with the norm of tacking error $||z_1|| < 0.1$ and low transient overshoots for all three adaptation gains. The tracking error reduces corresponding to an

increase in Γ, the adaptation gain. Note that care must be taken in the design as a large Γ may result in numerical instability on the system. Fig. 4.8 shows the boundedness of the adaptation weights where a larger Γ is shown to improve the convergence rate. Similarly to model-based control, the gains are lower than the PID type controls which improves the robustness of the control.

4.3.2 Output Feedback

Using the certainty equivalence approach, the High-gain observer (2.7) has been designed to obtain the velocity estimates $\hat{\nu} = J^T(\eta)(\pi_2/\varepsilon)$ with $n = 2$, $\gamma_1 = 2.0$ and $\varepsilon = 0.1$. The four control types in Section 4.3.1 are simulated with the velocity estimate $\hat{\nu}$ and parameters as follows: (i) PID control: $\{K_P = 6 \times 10^5 I_{3\times3},\ K_D = 6 \times 10^5 I_{3\times3}\}$, (ii) PD plus adaptive: $\{\Gamma = 100 I_{3\times3}\}$, (iii) Model-based: $\{K_1 = 5I_{3\times3},\ K_2 = 20000 I_{3\times3}\ \}$ and (iv) Adaptive Neural: $\{\Gamma = 5I_{3\times3},\ \hat{Z} = [\eta^T, \hat{\nu}^T, \alpha_1^T, \dot{\alpha}_1^T]\}$.

The tracking errors for different controls are shown in Fig. 4.9 while the norm of tracking errors and control inputs are shown in Fig. 4.10. The proposed adaptive neural and model-based control formulated through backstepping of the system dynamics produced better transient and steady state response as compared to the PID and PD with adaptive control. The proposed adaptive neural control produced the lowest norm of error. This can be credited to the NN which is able to capture the system dynamics.

From Fig. 4.10, we can see that the low tracking errors of the proposed control is not the result of a larger control effort but attributed to a proper control action. Due to the large structural mass, the PID type controls require large control gains for accurate positioning. This is not recommended in practice due to measurement noise which can result in large overshoots. Fig. 4.11 shows the observer error for output feedback control under the adaptive neural control. The convergence of the high-gain observer estimates can be seen as the estimation errors peak around 0.3s and thereafter converge to a small neighborhood of zero.

4.3.3 Output Feedback with Noise

In this subsection, we simulate the output feedback adaptive neural control with additive white gaussian noise as shown in Fig. 4.12 applied to all measurements signal x_n, y_n and ψ_n. The high-gain observer is simulated with parameters $n = 2$, $\gamma_1 = 2.0$ and $\varepsilon = 0.1$ to obtain the velocity estimates. The adaptive neural control is simulated with $\{\Gamma = 5I_{3\times3}$, $\hat{Z} = [\eta^T, \hat{\nu}^T, \alpha_1^T, \dot{\alpha}_1^T]$ and $\sigma_i = 1 \times 10^{-5}\}$ similar to Case 4 above.

Subjected to the effects of the measurement noise, the trajectory of payload for output feedback adaptive neural control is shown in Fig. 4.13, with tracking errors shown in Fig. 4.14, norm of NN weights and control inputs in Fig. 4.15 and observer errors shown in Fig. 4.16. It is observed that the tracking error remain within a small envelop of zero with the NN weights bounded. We make the following remark with regards to the robustness of the high-gain observer.

Remark 4.9. *In this chapter, we proposed a rigorous theoretical treatment of the output feedback problem using the high-gain observer. The high-gain observer were chosen for its simplicity and that it does not require a model of the of the subsea payload, which is in line with the proposed non-model-based approach. In practice, the presence of measurement noise necessitates careful implementation, and places a lower limit on the size of ϵ with possible degradation of transient performance.*

4.4 Conclusion

In this chapter, stable adaptive neural based positioning control has been designed for installation of subsea structure with attached thrusters in the presence of time-varying environmental disturbances and parametric uncertainties. Full state feedback and output feedback cases have been considered. It has been shown that the closed loop signals under the proposed control are semiglobally uniformly bounded and converges to a compact set

which can be made arbitrarily small through appropriate choice of design parameters. Simulation results have demonstrated that the adaptive neural control is robust and effective in reducing the tracking error for the subsea installation operation.

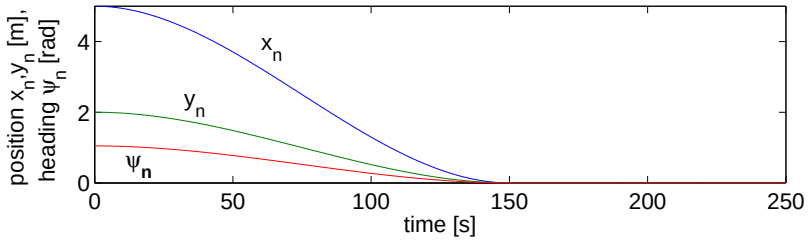

Fig. 4.2: Reference trajectory for position x_n, y_n and orientation ψ_n.

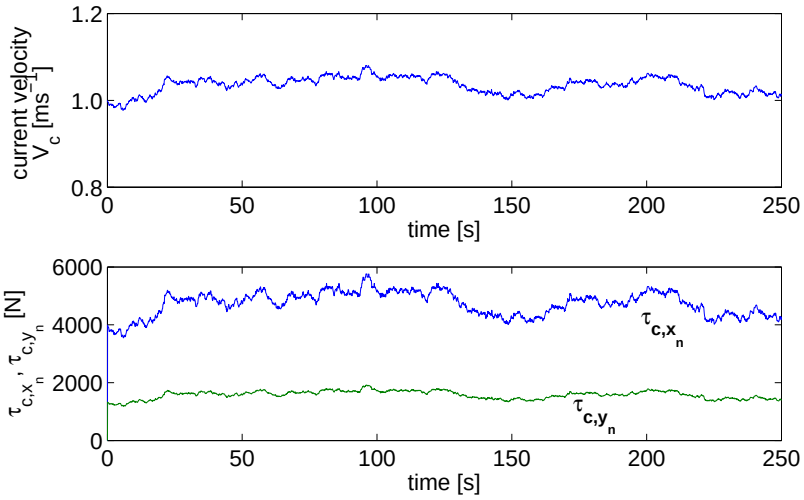

Fig. 4.3: (Top): irrotational current and (Bottom): disturbance due to current in x_n, y_n direction.

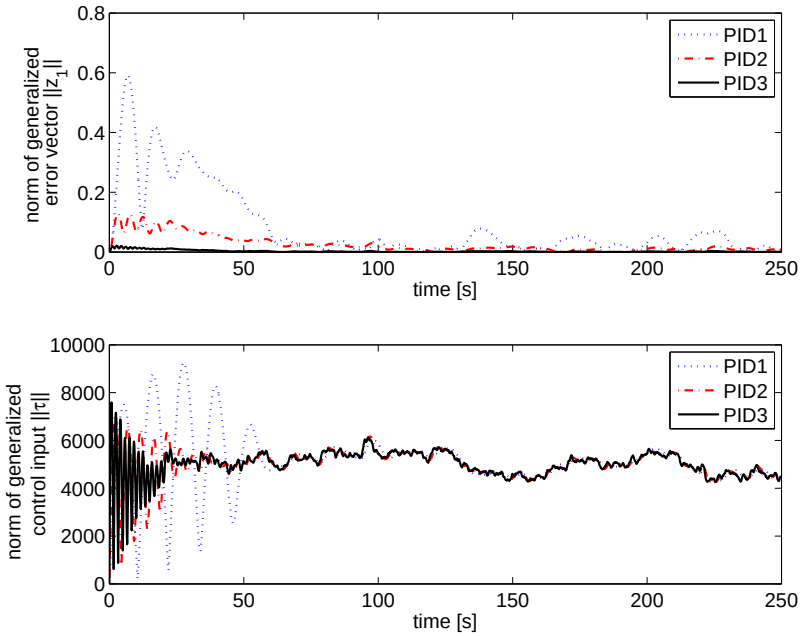

Fig. 4.4: (Top): norm of generalized error $\|z_1\|$ and (Bottom): norm of generalized control input $\|\tau\|$ for PID control

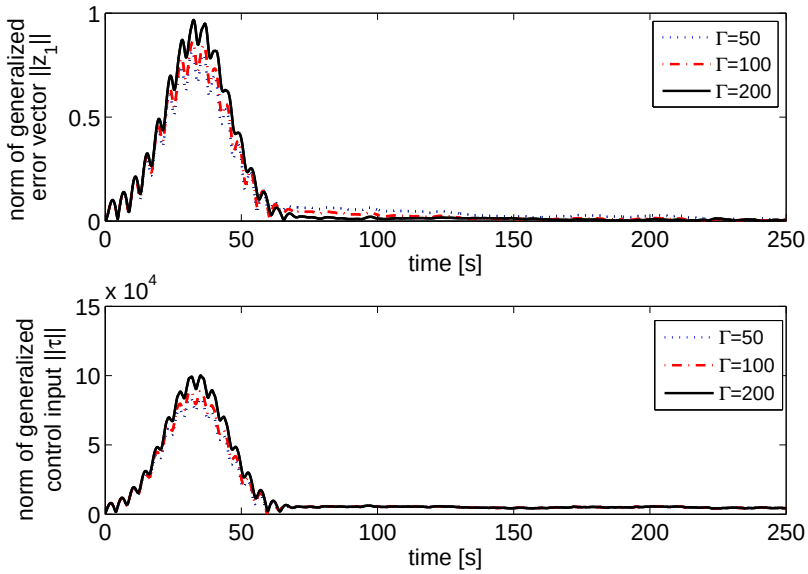

Fig. 4.5: (Top): norm of generalized error $\|z_1\|$ and (Bottom): norm of generalized control input $\|\tau\|$ for PD control with adaptive mechanism.

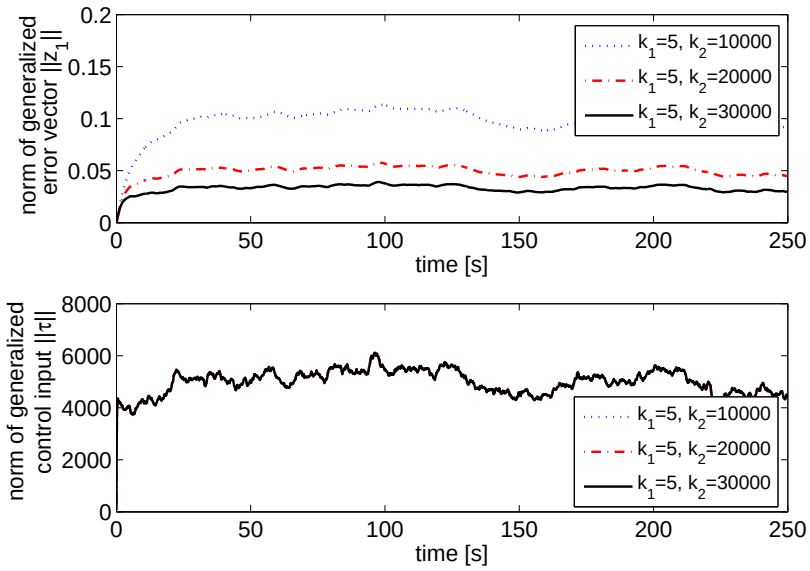

Fig. 4.6: (Top): norm of generalized error $\|z_1\|$ and (Bottom): norm of control input $\|\tau\|$ for Model Based control.

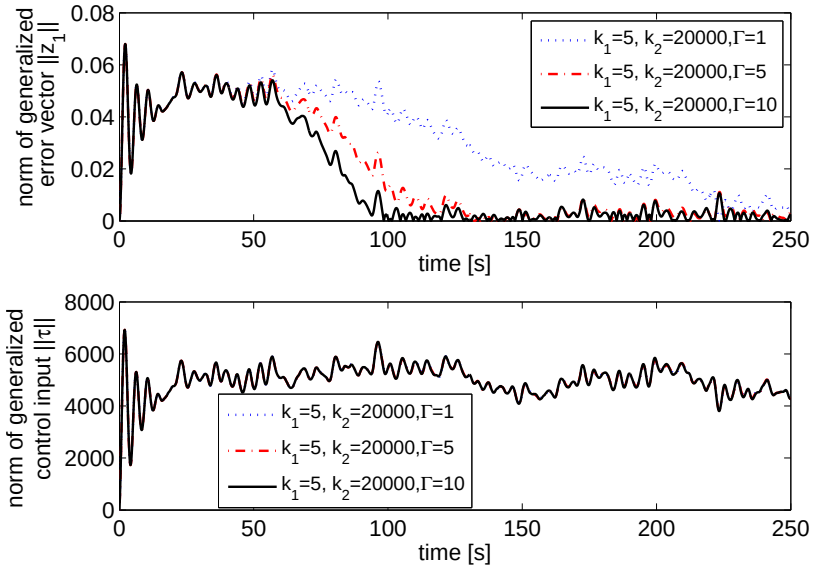

Fig. 4.7: (Top): norm of generalized error $\|z_1\|$ and (Bottom): norm of generalized control input $\|\tau\|$ for adaptive neural control with varying Γ.

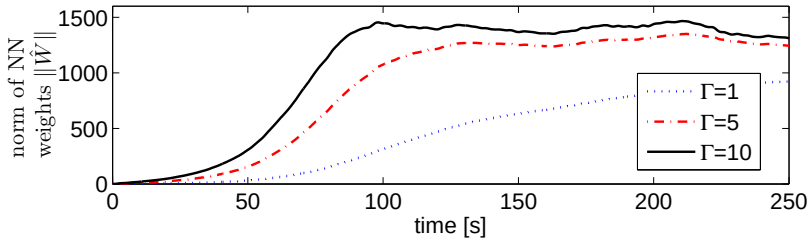

Fig. 4.8: Norm of NN weights $\|\hat{W}\|$ for adaptive neural control with varying Γ.

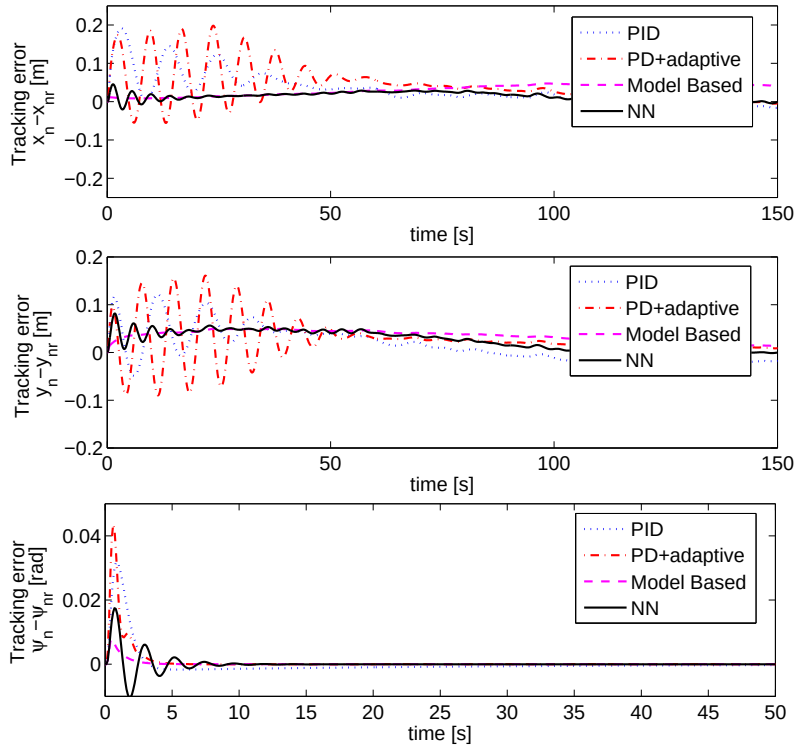

Fig. 4.9: (Top): tracking error $x_n - x_{nr}$, (Center): tracking error $y_n - y_{nr}$ and (Bottom): tracking error $\psi_n - \psi_{nr}$ for different controls using output feedback.

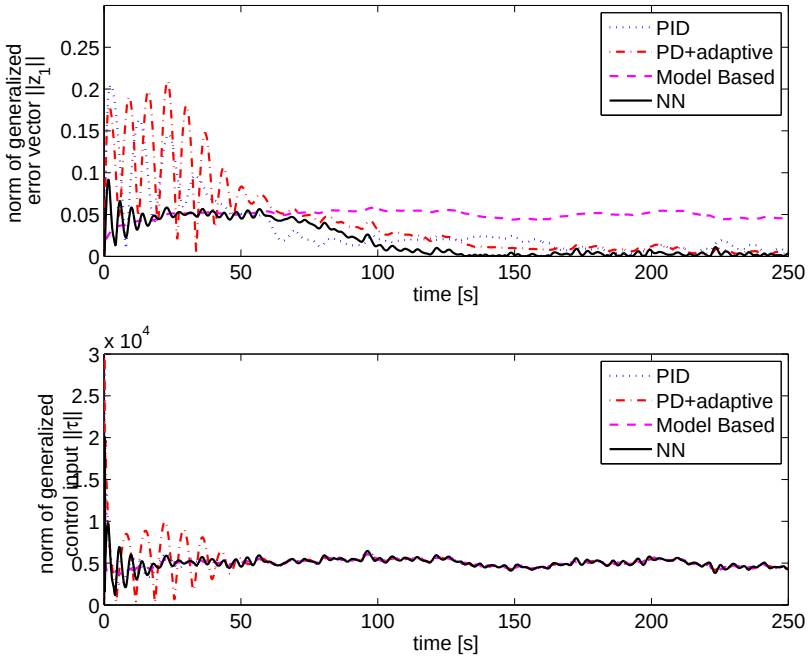

Fig. 4.10: (Top): norm of generalized error $\|z_1\|$ and (Bottom): norm of generalized control input $\|\tau\|$ for different controls using output feedback.

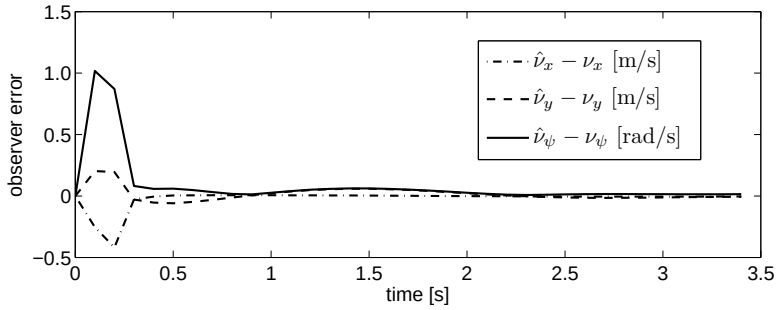

Fig. 4.11: Observer error for output feedback control using High-gain observer with adaptive neural control.

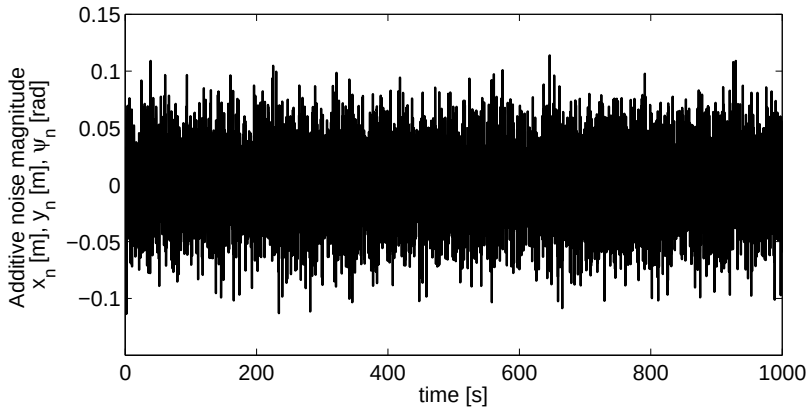

Fig. 4.12: Additive Gaussian white noise added to all measurement signals x_n, y_n and ψ_n

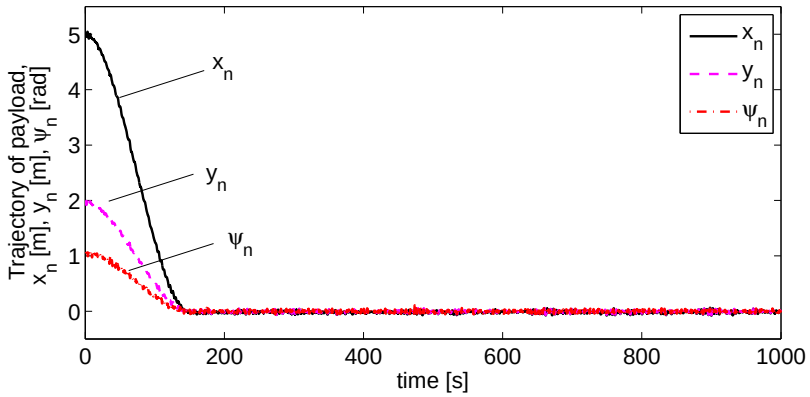

Fig. 4.13: Trajectory of payload for output feedback adaptive neural control with measurement noise

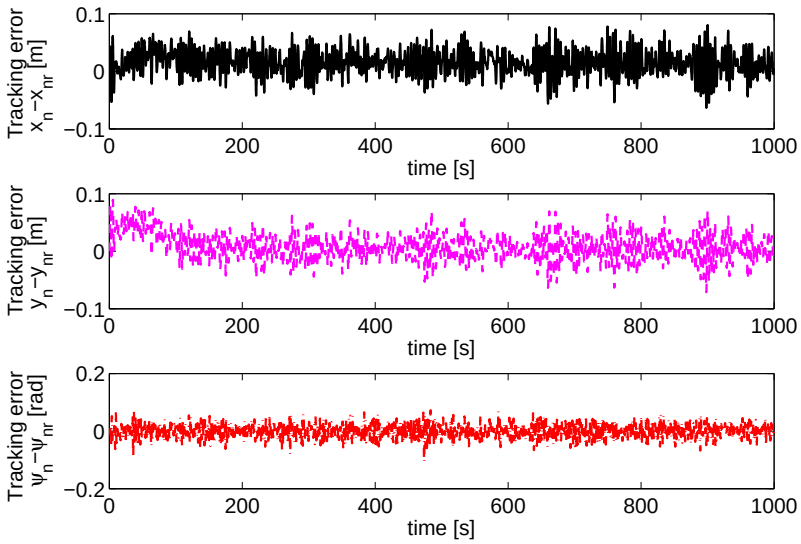

Fig. 4.14: (Top): tracking error $x_n - x_{nr}$, (Center): tracking error $y_n - y_{nr}$ and (Bottom): tracking error $\psi_n - \psi_{nr}$ for output feedback adaptive neural control with measurement noise

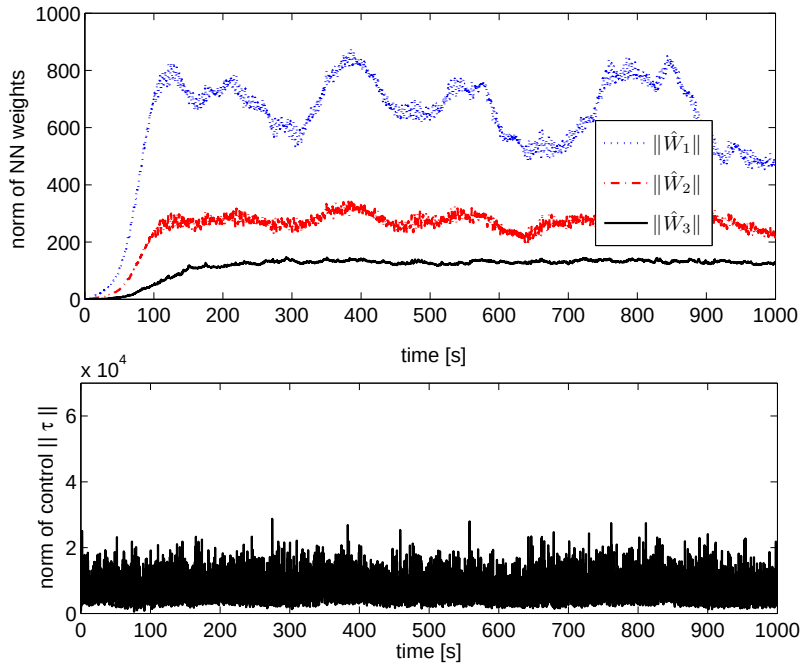

Fig. 4.15: (Top): Norm of NN weights $\|\hat{W}_i\|$, $i = 1, 2, 3$ and (Bottom): norm of generalized control input $\|\tau\|$ for output feedback adaptive neural control with measurement noise

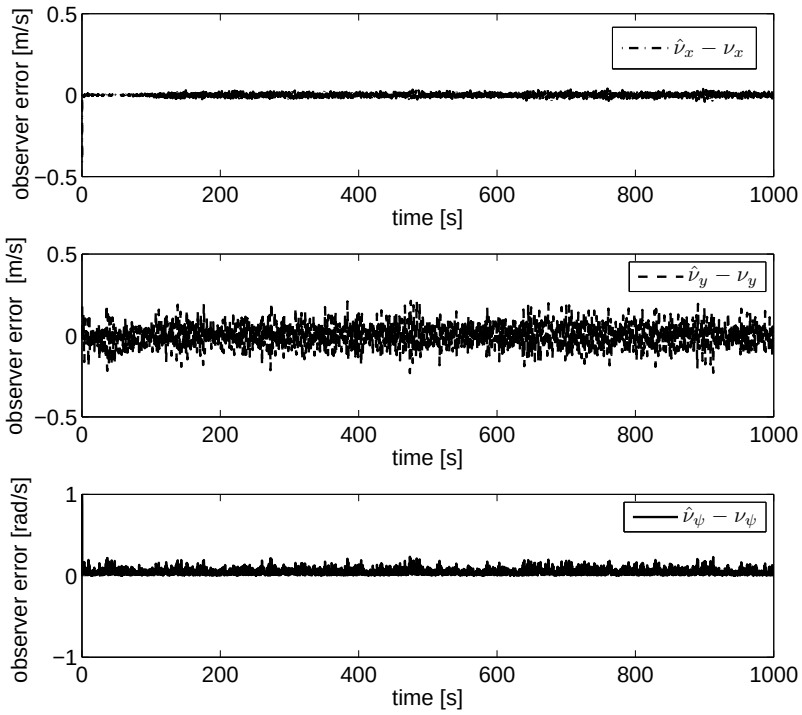

Fig. 4.16: Observer error for output feedback control using high-gain observer with adaptive neural control subjected to measurement noise.

Chapter 5

Coupled Positioning with BLF and Nonuniform Cable

In the last chapter, we proposed a tracking control for the payload using an adaptive neural technique to capture the dominant dynamic behaviors through online tuning of the NN weights. This avoided the need for exact information on the hydrodynamic coefficients of the structure and current measurements. With the trend towards installations in deeper waters, the longer cable increases the natural period of the cable and payload system which in turn increase the effects of pendulum-like oscillations. Time-varying distributed currents may lead to large horizontal offsets between the surface ship and the target installation site. An intuitive solution to alleviate the precision placement problem is the addition of thrusters for localized positioning when the payload is near the target site [16,17]. The control for the dynamic positioning of the subsea payload is challenging due to the unpredictable exogenous disturbances such as fluctuating currents and transmission of motions from the surface vessel through the lift cable.

In this chapter, we investigate the coupled dynamics of the vessel-crane-cable-payload system and design controls for positioning and stabilization. The flexible lift cable can

modeled by a set of PDE which possesses infinite number of dimensions which makes it difficult to control. To avoid the problems associated with the truncated-model-based design of finite dimensionality, we design the boundary control and perform Lyapunov analysis based on the PDE directly. We tackle the positioning problem for the system with output constraints in the form of safety specifications and operational limits. Existing methods to handle constraints include model predictive control, reference governors and the use of set invariance.

For the practical system with physical constraints, we employ Barrier Lyapunov Function [1, 69, 94, 95] in the design of positioning control for the flexible crane-cable-payload subsystem to ensure that the constraints are not violated. Uniform stability of the flexible subsystem is shown and asymptotic positioning of the boundaries is achieved. Next, we tackle the scenario where nonuniformity of the cable, uncertainties and environmental disturbances are considered. Boundary controls are formulated using the nonlinear PDE of the cable. Numerical simulations are provided to illustrate the performance of the proposed controls.

The remainder of this chapter is organized as follows: In Section 5.1, coupled dynamics of the surface vessel and the crane-cable-payload flexible subsection are presented. Following in Section 5.2, the vessel control is formulated via backstepping. Positioning controls are proposed considering a physical systems with practical constraints. Thereafter, a boundary control is derived for the case of a nonuniform cable in Section 5.3. The simulation study in Section 5.4 demonstrates the effectiveness of the proposed controls under a theoretical worst case disturbance to stress the controls and a more realistic disturbance to invetigate the performance.

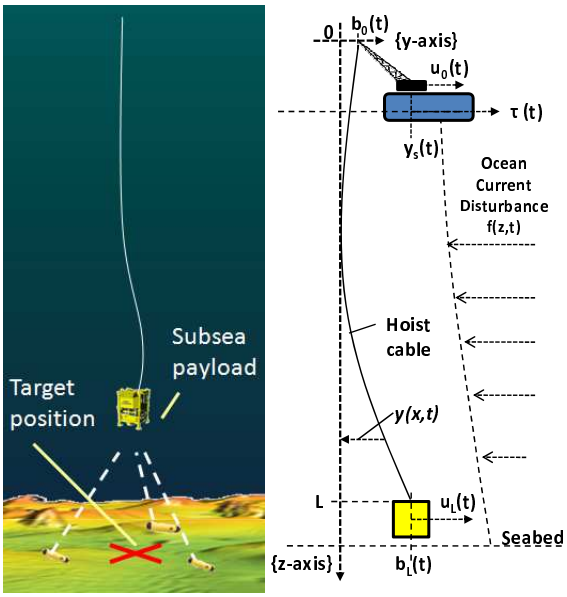

Fig. 5.1: Model of subsea installation operation and cable

5.1 Problem Formulation

5.1.1 Dynamics of Surface Vessel

In the system considered, the top end of the lifting cable is attached to a crane, onboard an ocean surface vessel and the bottom attached to a subsea module to be positioned for installation on the seafloor. The dynamics of the surface vessel can be modeled as

$$M_s\ddot{y}_s(t) + d_s\dot{y}_s(t) = \tau(t) + f_s(t) \tag{5.1}$$

where $y_s(t)$, $\dot{y}_s(t)$ and $\ddot{y}_s(t)$ are the displacement, velocity and acceleration of the surface vessel respectively, M_s the mass of the surface vessel, d_s the damping, $\tau(t)$ the control force from the vessel dynamic positioning thrusters and $f_s(t)$ the environmental disturbances. We assume that the motions of the vessel is completely determined by the waves and thruster, which is a reasonable assumption since the vessel mass, wave forces and thrust on it are

much larger than the mass of the crane and coupled forces.

5.1.2 Dynamics of the Crane-Cable-Payload Flexible Subsystem

Dynamic equations that govern the motion of the lifting cable can be derived through the extended Hamilton's principle or through discretization such as the finite element method. It has been shown in [96] that, assuming small displacements and employing first order Taylor series expansion, the equation of motion for the cable can be obtained as

$$\rho(z)\ddot{y}(z,t) + d_c\dot{y}(z,t) = \frac{\partial}{\partial z}[T(z,t)y'(z,t)] + f(z,t) \tag{5.2}$$

where $*'$ and $*''$ represent the first order and second order derivative of $*$ with respect to z respectively, $\dot{*}$ and $\ddot{*}$ the first and second order derivative of $*$ with respect to time t, $y(z,t)$ the displacement of the cable in the transverse direction, $\rho(z)$ the nonuniform mass per unit length of the cable, $T(z,t)$ the nonuniform distributed tension, d_c is the damping coefficient for the cable in fluid and $f(z,t)$ the distributed disturbance along the cable due to ocean currents. The tension in the cable can be expressed as

$$T(z,t) = T_0(z) + \theta(z)[y'(z,t)]^2 \tag{5.3}$$

where $T_0(z) > 0$ is the nonuniform tension in the undisturbed string and $\theta(z) \geq 0$ is a weighting function that accounts for strain in the displaced cable together with $[y'(z,t)]^2$. In the case where the cable is assumed to be uniform, and the tension is assumed to be independent of z, with $T_0(z) = T_0$ and $\theta(z) = 0.5EA$ as used in [97, 98]. Substituting the tension (5.3) into the dynamical model (5.2) yields the governing equation of the lifting cable

$$\begin{aligned}\rho(z)\ddot{y}(z,t) + d_c\dot{y}(z,t) &= \left[T_0(z) + 3\theta(z)[y'(z,t)]^2\right] y''(z,t) \\ &\quad + T_0'(z)y'(z,t) + \theta'(z)[y'(z,t)]^3 + f(z,t)\end{aligned} \tag{5.4}$$

with initial conditions expressed as

$$y(z,0) = c_1(z) \quad \text{and} \quad \dot{y}(z,0) = c_2(z) \tag{5.5}$$

and boundary conditions

$$y(0,t) = b_0(t) \quad \text{and} \quad y(L,t) = b_L(t) \tag{5.6}$$

where $\{c_1(z),\, c_2(z)\}$ and $\{b_0(t)\ b_L(t)\}$ are arbitrary sets of initial conditions and boundary conditions respectively. The boundary conditions for the cable can be described by the following dynamic equations

$$M_0\ddot{b}_0(t) = u_0(t) - T(0,t)y'(0,t) - d_0(t)\dot{b}_0(t) - M_0\ddot{y}_s(t) \tag{5.7}$$

$$M_L\ddot{b}_L(t) = u_L(t) + T(L,t)y'(L,t) - d_L(t)\dot{b}_L(t) + f_L(t) \tag{5.8}$$

where $u_0(t)$ and $u_L(t)$ are the control forces, $d_0(t)$ and $d_L(t)$ the damping coefficients at points $z = 0, L$ respectively, M_0 the mass of the crane on the vessel, M_L and $f_L(t)$ the mass and the environment disturbance on the subsea module attached to the bottom of the cable respectively. The effects of the vessel motion on the top boundary are coupled into the crane-cable-payload subsystem through $\ddot{y}_s(t)$ in (5.7).

5.1.3 Effects of Time-Varying Distributed Disturbances

The effects of a time-varying surface current $U(t)$ on the cable can be modeled as a distributed load on the cable [71, 99], expressed as an in-line drag force $f(z,t)$, consisting of a mean drag and an oscillating drag about the mean modeled as

$$f(z,t) = \frac{1}{2}\rho_s C_D(z)U(z,t)^2 D(z) + A_D\cos(4\pi f_v(z,t)t + \varsigma), \tag{5.9}$$

where $C_D(z)$ is the drag coefficient, $f_v(z,t)$ the shedding frequency, ρ_s the sea water density, ς the phase angle, and A_D the amplitude of the oscillatory part of the drag force, typically 20% of the first term in $f(z,t)$ [71]. The non-dimensional vortex shedding frequency can be expressed as

$$f_v(z,t) = \frac{S_t U(z,t)}{D(z)}, \tag{5.10}$$

where S_t is the Strouhal number and $D(z)$ is the cable diameter. The current profile $U(z,t)$, similar to that shown in Fig. 5.1, relates the distributed effects of the ocean surface current velocity $U(t)$ through the water column.

Assumption 5.1. *For the distributed disturbance $f(z,t)$ on the cable, we assume that there exists a constant $\bar{f} \in R^+$, such that $||f(z,t)|| \leq \bar{f}$, $\forall (z,t) \in [0,L] \times [0,\infty)$. This is a reasonable assumption as the effects of the time-varying current, $f(z,t)$, are exogenous, have finite energy and hence are bounded, i.e. $f(z,t) \in \mathcal{L}_\infty([0,L])$. For similar reasons, the environmental disturbances $f_s(t)$ and $f_L(t)$ are assumed bounded, i.e. there exists positive constants $\overline{f}_s$ and $\overline{f}_L$ such that $|f_s(t)| \leq \overline{f}_s$ and $|f_L(t)| \leq \overline{f}_L$, $\forall t \in [0,\infty)$.*

Remark 5.1. *For control design, only the assertion that there exists an upper bound on the disturbance in Assumption 1, $||f(z,t)|| < \bar{f}$, is necessary. The knowledge of the exact value for $f(z,t)$ is not required $\forall (z,t) \in [0,L] \times [0,\infty)$. As such, different disturbance models up to various levels of fidelity, such as those found in [99–103], can be applied without affecting the control design or analysis.*

Remark 5.2. *"In this chapter, we focus on the dynamics and control problem considering the coupled vessel, crane, flexible cable and payload. To present the ideas in a clear and succinct manner, we consider the case of full-state feedback without parametric uncertainties. Three disturbances have been considered in the system dynamics: (i) the disturbances on the vessel $f_s(t)$, (ii) the distributed disturbance on the flexible cable $f(z,t)$ and (iii) the disturbance on the payload near the seabed $f_L(t)$. In Assumption 6.1, all three disturbances are assumed to be bounded as follows $|f_s(t)| < \bar{f}_s$, $f(z,t) < \bar{f}$ and $f_L(t) < \bar{f}_L$. In the*

control design to be carried out, $\bar{f}_s$ and $\bar{f}_L$ are assumed to be known. This is reasonable as in practice, the operators would wait for a suitable weather window before commencing the subsea installation operation. The maximum disturbance load from the environment would be factored in the calculations of the suitable weather window.

Lemma 5.1. *[66, 104]: For bounded initial conditions, if there exists a C^1 continuous and positive definite Lyapunov function $V(x)$ satisfying $\varphi_1(\|x\|) \leq V(x) \leq \varphi_2(\|x\|)$, such that $\dot{V}(x) \leq -\lambda V(x) + \epsilon$, where φ_1, $\varphi_2 : R^n \rightarrow R$ are class $\mathcal{K}$ functions and ϵ is a positive constant, then the solution $x(t)$ is uniformly bounded.*

Lemma 5.2. *[105]: Let $y_1(z,t)$, $y_2(z,t) \in R$ with $x \in [0, L]$ and $t \in [0, \infty)$, the following inequalities hold:*

$$2y_1y_2 \leq 2|y_1y_2| \leq y_1^2 + y_2^2, \quad \forall y_1, y_2 \in \mathcal{R}. \tag{5.11}$$

From inequality (6.15)*, we can obtain,*

$$|y_1y_2| = \left|\left(\frac{1}{\sqrt{\delta}}y_1\right)\left(\sqrt{\delta}y_2\right)\right| \leq \frac{1}{\delta}y_1^2 + \delta y_2^2, \quad \forall y_1, y_2 \in \mathcal{R} \text{ and } \delta > 0. \tag{5.12}$$

Lemma 5.3. *[106, 107]: Let $y(z,t) \in R$ be a function defined on $z \in [0, L]$ and $t \in [0, \infty)$ that satisfies the boundary condition $y(0,t) = 0$, $\forall t \in [0, \infty)$, then the following inequalities hold:*

$$\int_0^L y^2(z,t)dz \leq L^2 \int_0^L [y'(z,t)]^2 dz, \tag{5.13}$$

$$y^2(z,t) \leq L^2 \int_0^L [y'(z,t)]^2 dz, \quad \forall z \in [0, L]. \tag{5.14}$$

Remark 5.3. *The effects of using cables with variation in parameters, uncertainties, disturbances and the transition between the air and water surface can be incorporated explicitly through $\rho(z)$, $T_0(z)$, $\theta(z)$ and $f(z,t)$.*

Assumption 5.2. *The values of $\rho(z)$, $T_0(z)$ and $\theta(z)$ are bounded by known constant lower*

and upper bounds $\forall x \in [0, L]$ *as follows:*

$$0 \leq \underline{\rho} \leq \rho(z) \leq \overline{\rho} \tag{5.15}$$

$$0 \leq \underline{T} \leq T_0(z) \leq \overline{T} \tag{5.16}$$

$$0 \leq \underline{\theta} \leq \theta(z) \leq \overline{\theta} \tag{5.17}$$

The partial derivatives $\rho'(z)$, $T_0'(z)$ *and* $\theta'(z)$ *are within a known range. This is reasonable as general values can be determined in the material selection and operation engineering phase.*

5.2 Control Design

As the dynamics of the surface vessel is coupled into the crane-cable-payload system, we first propose a control design for the surface vessel using the backstepping approach [108]. Next we design positioning controls $u_0(t)$, $u_L(t)$ for the crane and subsea payload, employing SBLF in view of the constraints on the physical system. In the following subsection, we examine the coupled system with a nonuniform cable and proposed a stabilizing boundary control. For conciseness, dependency of the terms will be omitted where obvious.

5.2.1 DP Control of Surface Vessel

The control design and stability analysis of the vessel with a DP system for global positioning is demonstrated through the backstepping methodology [108]. We define error variables $z_1 = y_s - y_{sd}$ and $z_2 = \dot{y}_s - \alpha_1$, where y_{sd} is the desired position for the surface vessel. Differentiating z_1 with respect to time yields $\dot{z}_1 = z_2 + \alpha_1$. Consider the Lyapunov function candidate $V_1 = (1/2)z_1^2$ and choosing the virtual control as $\alpha_1 = -k_1 z_1$, the time derivative

of V_1 yields

$$\dot{V}_1 = -k_1 z_1^2 + z_1 z_2 \tag{5.18}$$

Differentiating z_2 with respect to time yields $\dot{z}_2 = m_s^{-1}(-d_s\dot{y}_s + \tau + f_s(t)) - \dot{\alpha}_1$, where $\dot{\alpha}_1 = -k_1\dot{z}_1$. Consider the augmented Lyapunov function candidate $V_2 = V_1 + (1/2)m_s z_2^2$ and taking its time derivative, we have the following

$$\dot{V}_2 \leq -k_1(t)z_1^2(t) + z_1(t)z_2(t) + z_2(t)(-d_s\dot{y}_s(t) + \tau(t) - m_s\dot{\alpha}_1(t)) + |z_2(t)|\overline{f}_s \tag{5.19}$$

Designing the model based vessel control as

$$\tau = -z_1(t) - k_2 z_2(t) + d_s\dot{y}_s(t) + m_s\dot{\alpha}_1(t) - u_{rs} \tag{5.20}$$

where $u_{rs} = \mathrm{sgn}(z_2(t))\overline{f}_s$, we obtain

$$\dot{V}_2 \leq -k_1 z_1^2(t) - k_2 z_2^2(t) \tag{5.21}$$

Lemma 5.4. *Consider the vessel dynamics* (5.1) *with Assumption 1, under the action of full-state feedback control law* (5.20)*, the vessel position in the closed-loop system* y_s *converges to the desired position* y_{sd} *asymptotically.*

Proof: With the choice of α_1 and τ above, the time derivative of the Lyapunov function candidate V_2 is negative semidefinite. Global asymptotic stability of $z_1(t)$ and $z_2(t)$ can be concluded [108], i.e. $z_1(t)$, $z_2(t) \to 0$ and the vessel position y_s converges to the desired position y_{sd} asymptotically.

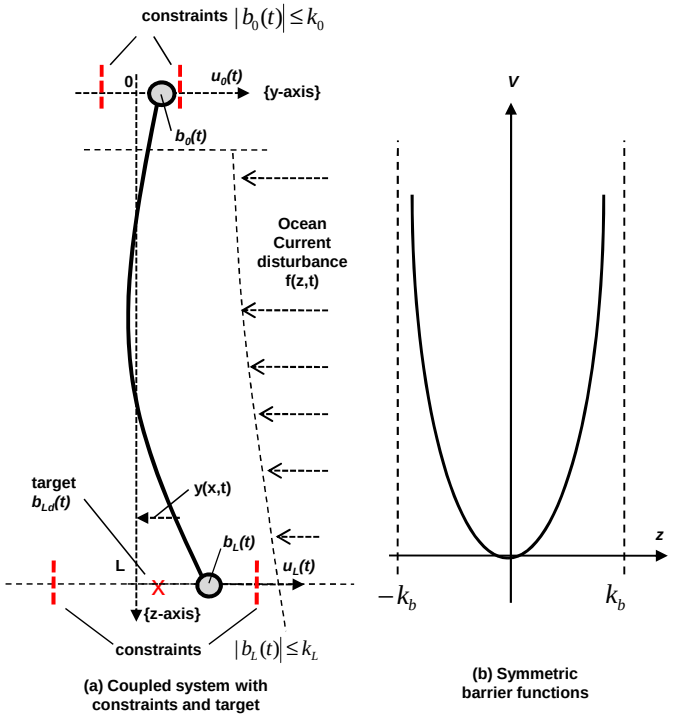

Fig. 5.2: (a) Schematic illustration of the coupled system with constraints and target and (b) Symmetric barrier functions [1]

5.2.2 Boundary Positioning Control using Barrier Lyapunov Functions

During subsea installation operations, positioning of the subsea module is desired. As the practical system is subjected to constraints on both the motion of the crane at the top boundary, and the maximum offset which the payload can deviate at the bottom boundary as shown in Fig 5.2(a), SBLF are employed in the position control design for the top crane and bottom payload. By ensuring boundedness of the SBLF [1, 69, 94] in the closed loop coupled with the dynamics of the flexible cable system, we ensure that (i) the coupled crane, cable, payload flexible system is stable, (ii) the physical limits are not transgressed and (iii) simultaneous positioning of the crane and payload for installation is achieved.

Stability of Flexible System Under Distributed Disturbance

In this subsection, we consider a simplified cable model [105] of (5.4) to illustrate the positioning control design technique using SBLF as follows

$$\rho\ddot{y}(z,t) + d_c\dot{y}(z,t) = Py''(z,t) + f(z,t) \tag{5.22}$$

where $P = T(z,t) = T(0,t) = T(L,t) > 0$ is the constant tension, with conditions $b_0(t)$ and $b_L(t)$ in (5.6), boundary dynamics (5.7) and (5.8), distributed viscous damping and disturbance $f(z,t)$ for the positioning of the subsea module. To facilitate the stability analysis, we introduce the transformation

$$w(z,t) = y(z,t) - \frac{z}{L}b_L(t) + \frac{z-L}{L}b_0(t) \tag{5.23}$$

to obtain the modified governing equation as

$$\rho\ddot{w}(z,t) + d_c\dot{w}(z,t) = Pw''(z,t) + f^*(z,t) \tag{5.24}$$

where we obtain the distributed disturbance as

$$f^*(z,t) = f(z,t) - \frac{z}{L}(\rho\ddot{b}_L(t) + d_c\dot{b}_L) + \frac{z-L}{L}(\rho\ddot{b}_0(t) + d_c\dot{b}_0) \tag{5.25}$$

with pinned conditions at the boundaries and initial conditions obtained as

$$w(0,t) = w(L,t) = 0 \tag{5.26}$$

$$w(z,0) = c_3(z),\ \dot{w}(z,0) = c_4(z) \tag{5.27}$$

For the stability analysis of the transformed flexible subsystem subjected to the distributed disturbances, we consider the following Lyapunov function candidate:

$$V_p(t) = V_a(t) + V_b(t) \tag{5.28}$$

where

$$V_a(t) = \frac{1}{2}\int_0^L \left\{\rho\dot{w}^2(z,t) + P[w'(z,t)]^2\right\} dz \tag{5.29}$$

$$V_b(t) = \int_0^L \rho\beta w(z,t)\dot{w}(z,t)dz \tag{5.30}$$

where $\beta > 0$ is a small positive weighing constant which satisfies the inequality

$$\beta < \frac{\min\{\rho,\ P\}}{2\rho\max\{1, L^2\}} \tag{5.31}$$

Lemma 5.5. *The function $V_b(t)$ in* (5.30) *with crossing term $w(z,t)\dot{w}(z,t)$ can be upper and lower bounded as*

$$0 \leq \lambda_1 V_a(t) \leq V_b(t) \leq \lambda_2 V_a(t) \tag{5.32}$$

where λ_1 and λ_2 are positive constants.

Proof: The proof of Lemma 5.5 can be found in Appendix A1.

Lemma 5.6. *The time derivative of the Lyapunov function candidate in* (5.28) *can be upper bounded with*

$$\dot{V}_p(t) \leq -\lambda_3 V_a(t) + \epsilon_p \tag{5.33}$$

where λ_3 and ϵ_p are positive constants defined as

$$\lambda_3 = \frac{\min\{\beta(P - d_c\delta_2 L^2 - \delta_3 L^2), d_c - \delta_1 - \beta\left(\rho + \frac{d_c}{\delta_2}\right)\}}{\max\{\rho, P\}} > 0 \tag{5.34}$$

$$\epsilon_p = \left(\frac{1}{\delta_1} + \frac{\beta}{\delta_3}\right) \max_{t=[0,\infty)} \int_0^L f^{*2}(z,t)dz > 0 \tag{5.35}$$

Proof: The proof of Lemma 5.6 is shown in Appendix A2.

Remark 5.4. *It is observed that under Assumption 6.1 where $f(z,t) \in L_\infty$, if boundary states b_0, $\dot{b}_0$, $\ddot{b}_0$, b_L, $\dot{b}_L$ and $\ddot{b}_L$ of the original system* (5.4) *are bounded, we obtain $\epsilon_p < \infty$. That is, if we design boundary controls that ensure the boundedness of the boundary states, then the flexible subsystem is bounded.*

Positioning Control Using Barrier Lyapunov Functions

In this subsection, we design positioning controls for the boundary crane and payload using BLF after which the main result will be formalized.

Top Boundary: Consider the crane dynamics at the top boundary for the cable in Eq. (5.4):

$$M_0\ddot{b}_0(t) = u_0(t) - T(0,t)y'(0,t) - d_0(t)\dot{b}_0(t) - M_0\ddot{y}_s(t) \tag{5.36}$$

where the system state $b_0(t)$ at the top boundary is required to satisfy $|b_0(t)| < k_{0c}$ with constrain k_{0c} being a positive constant. We define the error coordinates $z_3 = b_0 - b_{0d}$ and $z_4 = \dot{b}_0 - \alpha_2$, where α_2 is a virtual control to be designed. To design a control that does not drive b_0 out of the interval $(-k_{0c}, k_{0c})$, the following Lyapunov function candidate comprising a barrier function [94] with schematic shown in Figure 5.2(b) is proposed for

the top boundary as

$$V_3 = \frac{\phi_0}{2} \log \frac{k_b^2}{k_b^2 - z_3^2} \tag{5.37}$$

where ϕ_0 is a positive constant, $\log(*)$ the natural logarithm of $(*)$, and $k_b = k_{0c} - A_0$ the constraint on z_3, where $A_0 < k_{0c}$ is a positive constant, that is, we require $|z_3| < k_b$. It can be shown that V_3 is positive definite and C^1 continuous on the set $|z_3| < k_b$ and thus is a valid Lyapunov function candidate. The derivative of V_3 is given by

$$\dot{V}_3 = \frac{\phi_0 z_3 \dot{z}_3}{k_b^2 - z_3^2} = \frac{\phi_0 z_3 (z_4 + \alpha_2)}{k_b^2 - z_3^2} \tag{5.38}$$

for which the design of virtual control

$$\alpha_2 = -(k_b^2 - z_3^2)\phi_1 z_3 \tag{5.39}$$

where $\phi_1 > 0$ is a constant, yields

$$\dot{V}_3 = -\phi_0 \phi_1 z_3^2 + \frac{\phi_0 z_3 z_4}{k_b^2 - z_3^2} \tag{5.40}$$

In the second step, choose Lyapunov function candidate as follows:

$$V_4 = V_3 + \frac{1}{2} z_4^2 \tag{5.41}$$

which yields the derivative

$$\dot{V}_4 = -\phi_0 \phi_1 z_3^2 + \frac{\phi_0 z_3 z_4}{k_b^2 - z_3^2} + z_4 M_0^{-1}(u_0 - T(0,t)y'(0,t) - d_0 \dot{b}_0 - M_0 \ddot{y}_s - \dot{\alpha}_2) \tag{5.42}$$

where $\dot{\alpha}_2$ is given by

$$\dot{\alpha_2} = \phi_1 (3z_3^2 - k_b^2)[z_4 - (k_b^2 - z_3^2)\phi_1 z_3] \tag{5.43}$$

By designing the control as

$$u_0 = T(0,t)y'(0,t) + d_0\dot{b}_0 + M_0\ddot{y}_s + \dot{\alpha}_2 - M_0\left(\phi_2 z_4 + \frac{\phi_0 z_3}{k_b^2 - z_3^2}\right) \tag{5.44}$$

where $\phi_2 > 0$ is a constant, we have

$$\dot{V}_4 = -\phi_0\phi_1 z_3^2 - \phi_2 z_4^2 \tag{5.45}$$

Bottom Boundary: Similar to the methodology as for the top boundary, we consider payload dynamics at the bottom boundary for the crane-cable-payload in Eq. (5.4):

$$M_L\ddot{b}_L(t) \;\; = \;\; u_L(t) + T(L,t)y'(L,t) - d_L(t)\dot{b}_L(t) + f_L(t) \tag{5.46}$$

where the system state $b_L(t)$ at the bottom boundary is required to satisfy the constraint $|b_L(t)| < k_{Lc}$ with k_{Lc} being a positive constant. We define the error coordinates $z_5 = b_L - b_{Ld}$ and $z_6 = \dot{b}_L - \alpha_3$, where α_3 is a virtual control, and design the Lyapunov function candidate with a barrier function for the payload dynamics as

$$V_5 = \frac{\phi_3}{2}\log\frac{k_c^2}{k_c^2 - z_5^2} \tag{5.47}$$

where ϕ_3 is a positive constant and $k_c = k_{Lc} - A_L$ the constraint on z_5, where $A_L < k_{Lc}$ is a positive constant. The derivative of V_5 is given by

$$\dot{V}_5 = \frac{\phi_3 z_5 \dot{z}_3}{k_c^2 - z_5^2} = \frac{\phi_3 z_5(z_6 + \alpha_3)}{k_c^2 - z_5^2} \tag{5.48}$$

for which the design of virtual control

$$\alpha_3 = -(k_c^2 - z_5^2)\phi_4 z_5 \tag{5.49}$$

where $\phi_4 > 0$ is a constant, yields

$$\dot{V}_5 = -\phi_3\phi_4 z_5^2 + \frac{\phi_2 z_5 z_6}{k_c^2 - z_5^2} \tag{5.50}$$

In the second step, choose Lyapunov function candidate as follows:

$$V_6 = V_5 + \frac{1}{2}z_6^2 \tag{5.51}$$

which yields the derivative

$$\begin{aligned} \dot{V}_6 \quad \leq \quad & -\phi_3\phi_4 z_5^2 + \frac{\phi_3 z_5 z_6}{k_c^2 - z_5^2} + z_6 M_L^{-1}(u_L + T(L,t)y'(L,t) - d_L\dot{b}_L - \dot{\alpha}_3) \\ & + M_L^{-1}|z_6| f_L(t) \end{aligned} \tag{5.52}$$

where $\dot{\alpha}_3$ is given by

$$\dot{\alpha}_3 = \phi_4(3z_5^2 - k_c^2)[z_6 - (k_c^2 - z_5^2)\phi_4 z_5] \tag{5.53}$$

By designing the control as

$$u_L = -T(L,t)y'(L,t) + d_L\dot{b}_L + \dot{\alpha}_3 - u_{rblf} - M_L\left(\phi_5 z_6 + \frac{\phi_2 z_5}{k_c^2 - z_5^2}\right) \tag{5.54}$$

where $u_{rblf} = \mathrm{sgn}(z_6)\bar{f}_L$ and $\phi_5 > 0$ is a constant, we have

$$\dot{V}_6 \leq -\phi_3\phi_4 z_5^2 - \phi_5 z_6^2 \tag{5.55}$$

The following theorem presents the result on the positioning control and the stability of the system.

Theorem 5.1. *Consider the flexible cable system* (5.22) *transformed to* (5.24) *with boundary conditions* (5.26)*, initial conditions* (5.27)*, crane dynamics* (5.36) *at the top boundary, payload dynamics* (5.46) *at the bottom boundary, fullstate feedback controls* (5.44) *and*

(5.54), *Assumption 6.1 and Lemmas 5.1-5.6. If the initial boundary states* b_0, $\dot{b}_0$, $\ddot{b}_0$, b_L, $\dot{b}_L$ *and* $\ddot{b}_L$ *of the original system* (5.22) *are bounded, with initial conditions in the sets,* Ω_0, Ω_L *where* $z_3(0) \in \Omega_0 := \{|z_3| < k_b\}$ *and* $z_5(0) \in \Omega_L := \{|z_5| < k_c\}$, *then the following properties hold:*

(i) the flexible system (5.24) *subjected to distributed disturbance* $f^*(z,t)$ *under Assumption 6.1 is uniformly bounded, i.e.* $w(z,t) \in \mathcal{L}_\infty \ \forall (z,t) \in [0,L] \times [0,\infty)$, *with all closed loop signals bounded, which implies that the original system* (5.22), $y(z,t) \in \mathcal{L}_\infty \ \forall (z,t) \in [0,L] \times [0,\infty)$.

(ii) the positioning error z_3 *is asymptotically stable, i.e.* $b_0(t) \to b_{0d}(t)$ *as* $t \to \infty$ *all states bounded and the constraint* $|z_3(t)| < k_b$ *is never violated.*

(iii) the positioning error z_5 *is asymptotically stable, i.e.* $b_L(t) \to b_{Ld}(t)$ *as* $t \to \infty$ *with all states bounded and the constraint* $|z_5(t)| < k_c$ *is never violated.*

Proof: (i) Since $\dot{V}_4 \leq 0$, it can be shown that $V_4(t)$ is bounded $\forall t > 0$ provided that $V_4(0)$ is bounded and $|z_3(0)| < k_b$. From (5.41), it follows that $V_3(t)$ is bounded. According to (5.37), we know that for $V_3(t)$ to be bounded, it has to be true that $|z_3(t)| \neq k_b$. Therefore the tracking error z_3 remains in the region $|z_3(t)| < k_b$. Hence, we have $|b_0(t)| < k_{0c}$ and states $\dot{b}_0$ and $\ddot{b}_0$ at the top boundary are bounded. The boundedness of b_L, $\dot{b}_L$, $\ddot{b}_L$ can be similarly shown. Since the boundary states are bounded, Lemma 5.6 holds and $V_p(t)$ is upper bounded with Eq. (5.33). From Eqs. (5.32) and (5.33), we have

$$\dot{V}_p(t) \leq -\lambda V_p(t) + \epsilon_p \tag{5.56}$$

where $\lambda = \lambda_3/\lambda_2$. The uniform boundedness of the $w(z,t)$ can be shown by multiplying Eq. (5.56) by $e^{\lambda t}$,

$$\frac{\partial}{\partial t}(V_p e^{\lambda t}) \leq \epsilon_p e^{\lambda t} \tag{5.57}$$

Integration of the above and applying Lemma 6.1 with Eqs. (5.32) and (5.29) yields

$$\lambda_1 V_a(t) \leq V_p(t) \leq V_p(0) + \frac{\epsilon_p}{\lambda} \in \mathcal{L}_\infty \tag{5.58}$$

Since $V_a(t)$ is bounded, $\dot{w}(z,t)$ and $w'(z,t)$ are bounded $\forall (z,t) \in [0,L] \times [0,\infty)$. Using Lemma 5.3, we obtain $w(z,t) \in \mathcal{L}_\infty$ and hence $y(z,t), y'(z,t) \in \mathcal{L}_\infty$ At this point, we have shown that all signals in the positioning controls (5.44) and (5.54) are bounded. Finally using Assumption 6.1, Eqs. (5.24) to (5.27), we conclude that $\ddot{w}(z,t)$ and hence $\ddot{y}(z,t)$ are bounded $\forall (z,t) \in [0,L] \times [0,\infty)$.

Remark 5.5. *There is a concern of $u_0(t)$ or $u_L(t)$ becoming unbounded whenever $|z_3(t)| = k_b$ or $|z_5(t)| = k_c$. In Lemma 2.4, it has been established that, in the closed loop, the error signal $|z_3(t)|$ never reaches k_b. As a result, the control $u_0(t)$ will not become unbounded because of the presence of terms comprising $(k_b^2 - z_3^2(t))$ in the denominator. Since u_0 and u_L for the boundaries and all closed loop signals are bounded, the accelerations of the boundary states $\ddot{b}_0$ and $\ddot{b}_L$ are bounded.*

(ii) To show that $b_0(t) \to b_{0d}$ as $t \to \infty$, we compute $\ddot{V}_4$ as follows:

$$\ddot{V}_4 = -2\phi_0\phi_1 z_3 \dot{z}_3 - 2\phi_2 z_4 \dot{z}_4 \tag{5.59}$$

From the boundedness of the closed loop signals, we can show that $\ddot{V}_2$ is bounded and uniformly continuous. Using Barbalat's Lemma [109], $z_3(t), z_4(t) \to 0$ as $t \to \infty$. Hence, the state $b_0(t) \to b_{0d}(t)$ as $t \to \infty$.

(iii) The proof is similar to that in (i) and will be omitted for conciseness.

Remark 5.6. *In the control design, a particular choice of SBLF, e.g. $V_5 = (\phi_3/2)\log(k_c^2/(k_c^2 - z_5^2))$ was employed. We can extend the result for Asymmetric Barrier Lyapunov Functions (ABLS) or general forms of barrier functions in Lyapunov synthesis satisfying $V_5(z_5) \to \infty$ as $z_5 \to -k_b$ or $z_5 \to k_c$ following the methodology in [1], where $k_b \neq k_c > 0$*

are the barrier constraints.

Remark 5.7. *To handle unknown perturbations to the nominal model in the form of parametric uncertainties or modeling errors, adaptive model-based or approximation based control techniques can be employed following the framework set up in [1, 66, 69].*

5.3 Boundary Stabilization of Coupled System with Nonuniform Cable

In this subsection, we consider the nonuniformity of the cable and design boundary controls for stabilization of the crane and payload thruster using the PDE of the flexible subsystem subjected to a distributed disturbance via Lyapunov synthesis.

Consider the following Lyapunov function candidate:

$$V(t) = V_c(t) + V_d(t) + V_e(t) \tag{5.60}$$

where

$$V_c(t) = \frac{1}{2}\int_0^L \left\{\rho(z)\dot{y}^2(z,t) + T_0(z)[y'(z,t)]^2 + \frac{1}{2}\theta(z)[y'(z,t)]^4\right\} dz \tag{5.61}$$

$$V_d(t) = \frac{1}{L}\int_0^L \left\{\rho(z)\gamma(z)z\dot{y}(z,t)y'(z,t)\right\} dz \tag{5.62}$$

$$V_e(t) = \frac{1}{2}M_0\dot{b}_0^2(t) + \frac{1}{2}M_L\Big[\dot{y}(L,t) + \frac{3}{8}\gamma(L)y'(L,t)\Big]^2 \tag{5.63}$$

and $\gamma(z)$ is a positive scalar function which satisfies the inequality

$$0 < \int_0^L \gamma(z)dz < \frac{L\min\{\underline{\rho},\ \underline{T}, \underline{\theta}\}}{2\overline{\rho}} \tag{5.64}$$

Lemma 5.7. *The function $V_d(t)$ with crossing term $\int_0^L \dot{y}(z,t)y'(z,t)dz$ can be upper and*

lower bounded as

$$0 \leq \lambda_4 V_c(t) \leq V_d(t) \leq \lambda_5 V_c(t) \tag{5.65}$$

where λ_4 *and* λ_5 *are positive constants*

Proof: The proof of Lemma 5.7 is demonstrated in Appendix A3.

Lemma 5.8. *Designing boundary controls* $u_0(t)$ *and* $u_L(t)$ *at* $z = 0$ *and* L *respectively as*

$$u_0(t) = -k_0 \dot{y}(0,t) + 2T(0,t)y'(0,t) + d_0(t)\dot{b}_0(t) + M_0 \ddot{y}_s \tag{5.66}$$

$$\begin{aligned} u_L(t) &= -k_L \left[\dot{y}(L,t) + \frac{3}{4}\gamma(L)y'(L,t) \right] - u_{rbc} + d_L \dot{b}_L(t) \\ &\quad -2T(L,t)y'(L,t) - \frac{3}{4}M_L\gamma(L)\dot{y}'(L,t) \end{aligned} \tag{5.67}$$

where $u_{rbc} = sgn\left[\dot{y}(L,t) + \frac{3}{4}\gamma(L)y'(L,t)\right]\overline{f}_L$*, the time derivative of the Lyapunov function candidate in* (5.60) *can be upper bounded with*

$$\dot{V}(t) \leq -\lambda_6[V_c(t) + V_e(t)] + \varepsilon \tag{5.68}$$

where $\lambda_6 > 0$ *and* $\varepsilon > 0$ *are positive constants.*

Proof: The details of the proof for Lemma 5.8 can be found in Appendix A4.

From Eqs. (5.65) and (5.68), we can rewrite the time derivative of the Lyapunov function candidate into the form of Lemma 6.1 as

$$\dot{V}(t) \leq -\lambda V(t) + \varepsilon \tag{5.69}$$

where $\lambda = \lambda_6/\lambda_5$. The following theorem presents the results for the boundary for the coupled system.

Theorem 5.2. *Consider the coupled system* (5.1), (5.4), (5.7) *and* (5.8), *with initial conditions* (5.5), *boundary conditions* (5.6), *scalar function* $\gamma(z)$ *satisfying inequalities* (5.64) *and* (A.25), *Assumptions 6.1 and 5.2, fullstate feedback from the vessel, crane and payload, vessel control* (5.20), *boundary controls* (5.66) *and* (5.67), *the closed loop system subjected to the distributed disturbance* $f(z,t)$ *is uniformly bounded.*

Proof: The uniform boundedness of the deflection $y(z,t)$ can be shown by multiplying Eq. (5.69) by $e^{\lambda t}$,

$$\frac{\partial}{\partial t}(Ve^{\lambda t}) \leq \varepsilon e^{\lambda t} \tag{5.70}$$

Integration of the above and applying Lemma 6.1 yields

$$V(t) \leq \left(V(0) - \frac{\varepsilon}{\lambda}\right) e^{\lambda t} + \frac{\varepsilon}{\lambda} \leq V(0) + \frac{\varepsilon}{\lambda} \in \mathcal{L}_\infty \tag{5.71}$$

Utilizing Eqs. (5.61) and (5.65), we have

$$V_c(t) \leq \frac{1}{\lambda_4} V(t) \in \mathcal{L}_\infty \tag{5.72}$$

Since $V_c(t)$ is bounded, $\dot{y}(z,t)$ and $y'(z,t)$ are bounded $\forall (z,t) \in [0,L] \times [0,\infty)$. From Lemma 5.4, bounded $\dot{y}(z,t)$ and $y'(z,t)$, the boundary controls (5.66) and (5.67) are bounded. From the above statements and Eq. (5.4)-(5.8), we can concluded that $\ddot{y}(z,t)$ and $y(z,t) \in \mathcal{L}_\infty$.

Remark 5.8. *The challenge in addressing nonuniformities when working with boundary control lies in the determining an appropriate (nonuniform) cross term in the Lyapunov function [105]. In [110], the increasing nonuniform term in the form of* $\gamma(z) = \gamma_1 e^{\gamma_2 z}$ *with* $\gamma_1 > 0$ *being sufficiently small and* γ_2 *being large was proposed. When* $T_0(z)$ *and* $\theta(z)$ *are constants,* $\gamma(z)$ *and* $\gamma(z)\rho(z)$ *can be chosen to be nondecreasing.*

Remark 5.9. *The robust signum control terms in control* (5.20), (5.54) *and* (5.67) *may induce chattering due to the discontinuous property which result in mechanical wear and*

tear. To solve this problem, several nice smooth modifications have been investigated in the literature, such as boundary layers [111,112] and the use of a hyperbolic tangent function [79] which has the following nice property,

$$0 \leq |\chi| - \chi \tanh\left(\frac{\chi}{\varepsilon_d}\right) \leq 0.2785\varepsilon_d, \quad \forall \chi \in R \tag{5.73}$$

where $\varepsilon_d > 0$. *For example, let* $u_{rs} = k_3 \tanh(z_2/\varepsilon_d)$ *in* (5.20) *where* $k_3 \geq \bar{f}_s$. *From* (5.21) *and* (5.73), *we obtain*

$$\dot{V}_2 \leq -k_1 z_1^2 - k_2 z_2^2 + 0.2785 k_3 \varepsilon_d \tag{5.74}$$

Obviously, $\dot{V}$ *is strictly negative whenever the errors* z_1 *and* z_2 *are outside the following compact set*

$$\Omega_{c_s} \quad = \quad \left\{(z_1, z_2) \middle| \; k_1 z_1^2 + k_2 z_2^2 \leq 0.2785 k_3 \varepsilon_d \right\} \tag{5.75}$$

i.e. z_1 *will converge to a small neighborhood of zero, whose size adjustable by the design parameters* k_1 *and* k_2. *By smoothing the signum function, the closed loop system is stable with a small residual error and a reduction in chattering. Similar smoothing modifications can be applied for* u_{rblf} *and* u_{rbc} *in* (5.54) *and* (5.67) *and the analysis is omitted for conciseness.*

5.4 Numerical Simulations

5.4.1 Worst Case Harmonic Disturbances

The closed loop system (5.1) and (5.2), with boundary dynamics (5.7) and (5.8), distributed disturbance (5.9), vessel control (5.20), positioning controls (5.44) and (5.54) and stabilizing boundary controls (5.66) and (5.67) are simulated to investigate the performance of the proposed controls under theoretical worst case diturbances. A nondimensionalization and

finite difference scheme is used to numerically solve the PDE with the non-dimensionalized space interval $h = 0.02$ and time interval $t = 0.0045s$.

The vessel with $M_s = 9.6 \times 10^7 kg$, $d_s = 9.2 \times 10^7$, starts initial condition $y_s(0) = 10.0m$ with target position $y_{sd} = 0.0m$ at the origin. The crane with $M_0 = 1.0 \times 10^6 kg$, $d_0 = 8.0 \times 10^5$, cable with $T(z,t) = T_0 + 0.5EA[y'(z,t)]^2$, $T_0 = 4.0 \times 10^6 N$, $L = 1000m$, $E = 4.0 \times 10^9$, $D = 0.2m$, $\rho = 8.02 kgm^{-3}$, $d_c = 0$ and payload modeled as a cylinder with $M_L = 4 \times 10^5 kg$, $d_L = 2 \times 10^5$, height $h_c = 10.0m$, diameter $D_c = 5.0m$ starts initially at rest, is excited by a distributed transverse load. It is noted that the damping of the cable d_c and robust signum terms in all proposed controls are set to zero to demonstrated the robustness of the proposed control.

The ocean surface current velocity $U(t)$ is modeled as a mean flow with worst case sinusoid components, $\omega_i = \{2.2189, 4.4378, 6.6567, 8.8756\}$, for $i = 1$ to 4 that matches the first four natural frequency of the cable. The current $U(t)$ can be expressed as

$$U(t) = \bar{U} + U_m \sum_{i=1}^{N} \sin(\omega_i t), i = 1, 2, \ldots, N \tag{5.76}$$

where $\bar{U}$ is the mean flow current and U_m is the amplitude of the oscillating flow. The full current load is applied from $z = 0$ to $300m$, and thereafter linearly decline to an oscillating current with mean $1.0ms^{-1}$ at $z = 1000m$ to obtain a depth dependent ocean current profile $U(z,t)$. The distributed disturbance is generated using Eq. (5.9), the disturbance on the vessel is generated as

$$f_s = [3 + 0.8\sin(0.7t) + 0.2\sin(0.5t) + 0.2\sin(0.9t)] \times 10^6 \tag{5.77}$$

and the disturbance on the subsea payload modeled as a cylinder is derived from Morison's equation

$$f_L = \frac{1}{2} C_D \rho_s h D_c |U(L,t)| U(L,t) \tag{5.78}$$

where $C_D = 1.0$ is the drag coefficient.

Surface Vessel Control: The surface vessel subjected to disturbance (5.77) is simulated under the action of backstepping control (5.20) with control gains $k_1 = 1.0$ and $k_2 = 5.0 \times 10^7$. The position, control and disturbance on the surface vessel are shown in Fig. 5.10, where it can be observed that the backstepping control is able to position the vessel near its desired position at the origin.

Crane-Cable-Payload Subsystem Without Controls: Under the action of the vessel control, the dynamics of the cable is simulated without control and the 3D spatial time representation is shown in Fig. 5.11. It can be seen that at $t = 500s$, the subsea payload has deviated $150m$ from the origin under the action of the distributed disturbance on the cable and the disturbance force acting on the payload due to the current.

SBLF Positioning Controls: The positioning controls (5.44) and (5.54) developed using SBLF are simulated with crane desired position $b_{0d} = 0m$, constraints $k_{0c} = 30m$, $A_0 = 10m$, control gains $\phi_0 = \phi_1 = \phi_2 = 10$, subsea payload desired position $b_{Ld} = 10m$, constraints $k_{Lc} = 50m$, $A_L = 30m$ and control gains $\phi_3 = \phi_4 = \phi_5 = 5.0$. The 3D spatial time representation is shown in Fig. 5.12 and the position, control and tension at the top (crane) and bottom (subsea payload) boundaries are shown in Figs. 5.13 and 5.14 respectively. The designed control is able to keep the crane at the desired position and the subsea payload position converge from the origin to the desired position when the system is subjected to the environmental disturbances.

Stabilizing Boundary Control: The boundary controls (5.66) and (5.67) are simulated with $k_0 = k_L = 5 \times 10^8$ and $\gamma = 1 \times 10^{-5}$. The 3D spatial time representation for the boundary control is shown in Fig. 5.15 and the position, control and tension at the top (crane) and bottom (subsea payload) boundaries are shown in Figs. 5.16 and 5.17 respectively. From the simulations, it is observed that the proposed boundary controls can stabilize the boundary at the origin under the influence of the disturbances.

Remark 5.10. *To demonstrate the robustness of the proposed control, the damping of the cable and all robust signum terms in all proposed controls are set to zero. The ocean surface current and hence the distributed disturbance is simulated with worst case sinusoid components to excite large amplitude transverse resonance in the cable. As such, a large oscillating control signal is required to keep the payload at the target location.*

Remark 5.11. *In the simulations, the control is able to generate the adequate response for positioning the payload at the desired location within tight limits. For implementation, thruster performance needs to be included during the operation planning process such as weather window selection and safety considerations to ensure that the environmental forces are within operational limits and the required thrust is available for positioning.*

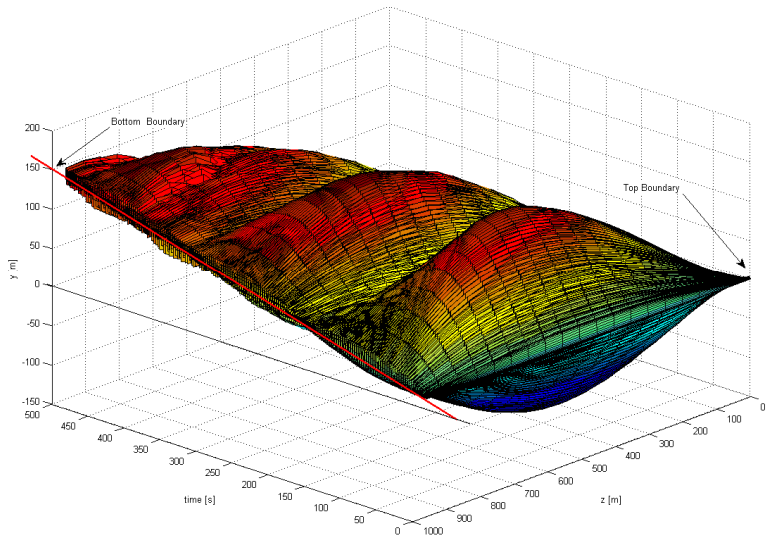

Fig. 5.3: Spatial-time representation of cable motions without control under worst case disturbances. The top boundary is at the crane and the bottom boundary at the subsea payload.

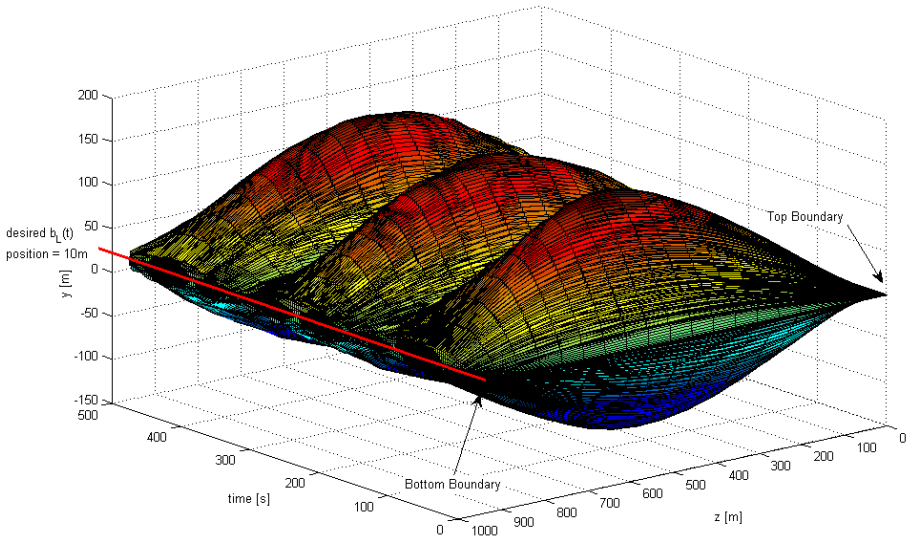

Fig. 5.4: Spatial-time representation of cable motions with positioning control under worst case disturbances. The top boundary is at the crane and the bottom boundary is at the subsea payload, maintained at desired position $b_L = 10m$.

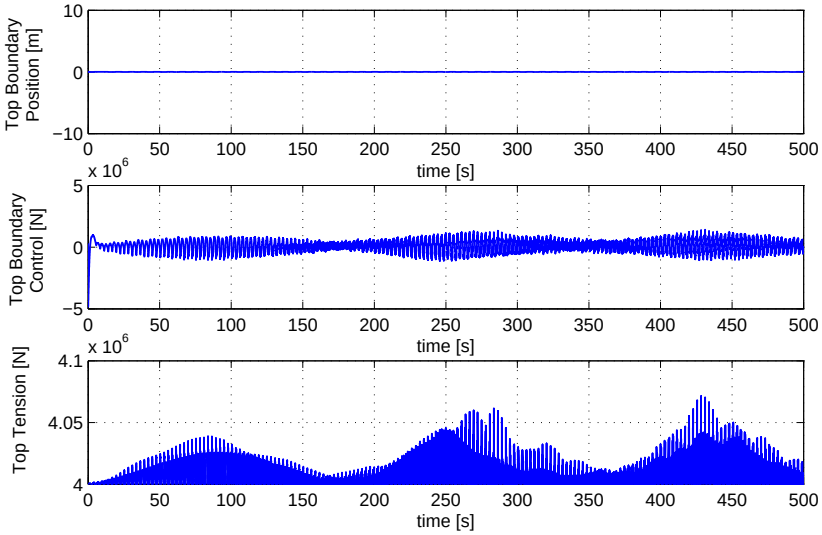

Fig. 5.5: (Top) position of the crane with desired position at origin, (center) control force on the crane and (bottom) tension at crane with position control (5.44) under worst case disturbances.

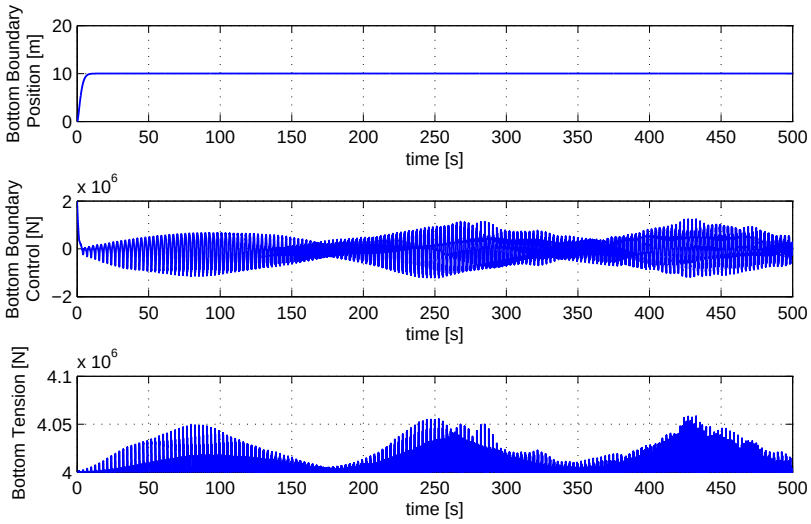

Fig. 5.6: (Top) position of the payload with desired position at $B_{LD} = 10m$, (center) control force and (bottom) cable tension at subsea payload with positioning control (5.54) under worst case disturbances.

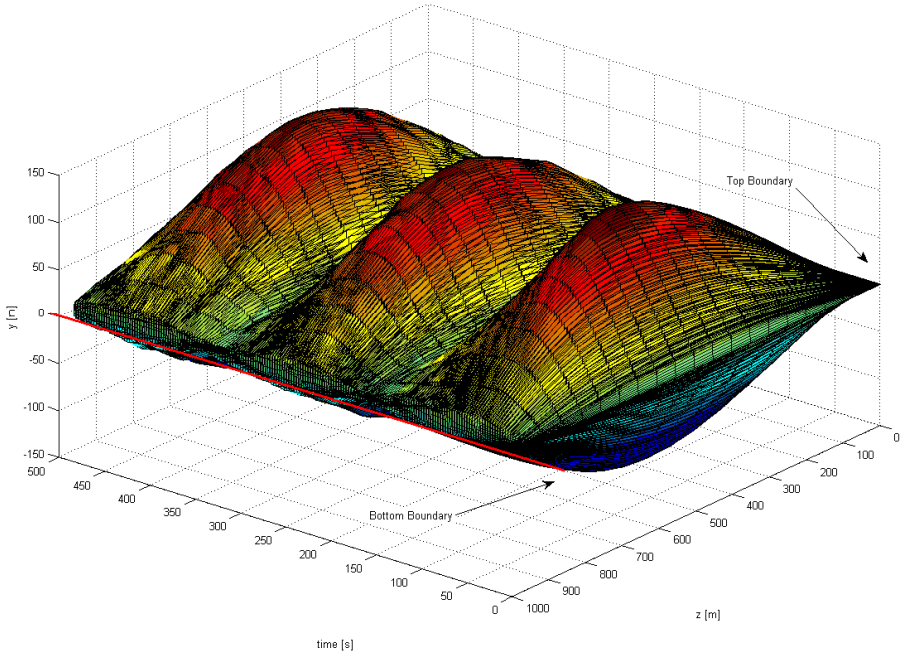

Fig. 5.7: Spatial-time representation of the cable motions control with stabilizing boundary control (5.66) and (5.67) under worst case disturbances.

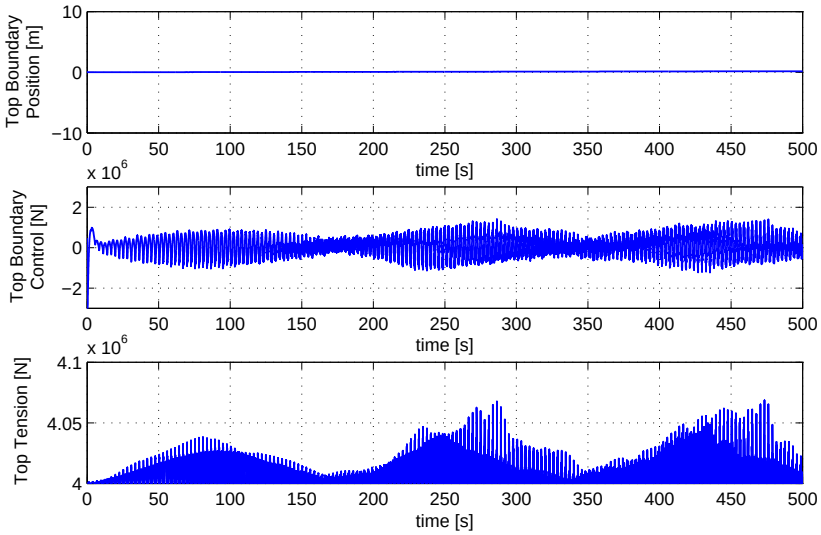

Fig. 5.8: (Top) position of the crane, (center) control force on the crane and (bottom) tension at crane with stabilizing boundary control (5.66) under worst case disturbances.

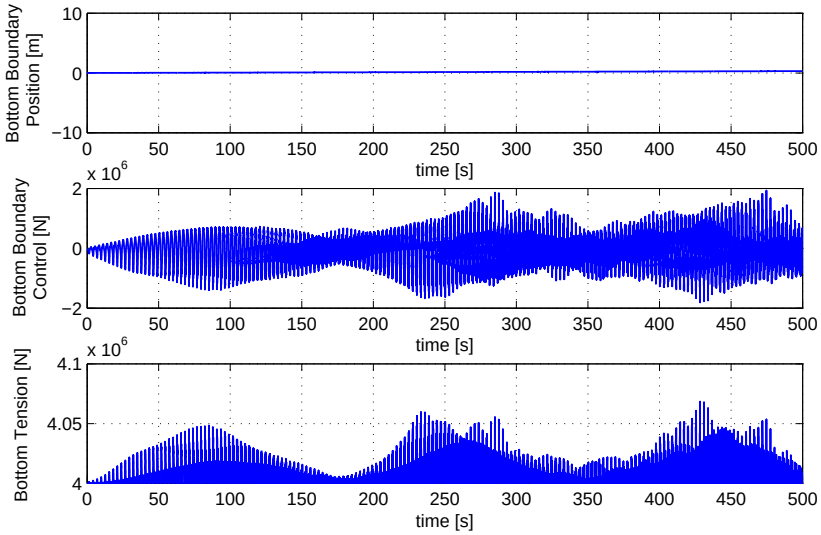

Fig. 5.9: (Top) position of the payload, (center) control force on the payload and (bottom) tension at payload with stabilizing boundary control (5.67) under worst case disturbances.

5.4.2 Practical Disturbances

To validate the proposed control under practical disturbances, hydrodynamic analysis has been carried out for the vessel to calculate the vessel disturbance f_s. The excitation forces for wave, wind and current and the Response Amplitude Operations (RAOs) of the vessel are generated using a hydrodynamic software. The underwater dimensions of the vessel are $255m$ length $\times$ $57m$ breath $\times$ $11.8m$ maximum draught. Head sea, wind and current in the same direction is simulated with JONSWAP spectrum of significant wave height, $H_s = 3.0m$ (rough sea), peak period of spectrum = $7.0s$, γ coefficient = 3.30 and Harris wind spectrum with wind velocity = $10.0m/s$.

The ocean surface current velocity $U(t)$ can be modeled by using a first-order Gauss-Markov process [114]

$$\dot{U}(t) + \mu U(t) = \omega(t), \tag{5.79}$$

$$U_{\min} \leq U(t) \leq U_{\max}, \tag{5.80}$$

where $\omega(t)$ is Gaussian white noise, $\mu \geq 0$ is a constant, we choose $U_{\min} = 1.6ms^{-1}$, $U_{\max} = 2.4ms^{-1}$ are minimum and maximum magnitude of the current velocity respectively and $\mu = 0$. The full current load is applied from $z = 0$ to $300m$, and thereafter linearly decline to $0.1U$ at $z = 1000m$ to obtain a depth dependent ocean current profile $U(z,t)$. The hyperbolic tangent function smoothing modification with $\varepsilon_d = 1 \times 10^{-3}$ for the signum terms, $\overline{f}_s = 4 \times 10^6 N$, $\overline{f}_L = 1500N$ and a rate limiter with time constant $\tau_c = 0.2$ has been applied to the following proposed controls.

Surface Vessel Control: The surface vessel subjected to disturbance f_s is simulated under the action of backstepping control (5.20) with $u_{rs} = \tanh(z_2(t)/\varepsilon_d)\overline{f}_s$, control gains $k_1 = 10.0$ and $k_2 = 5.0 \times 10^6$. The position, control and disturbance on the surface vessel are shown in Fig. 5.10, where it can be observed that the backstepping control is able to position the vessel near its desired position at the origin.

Crane-Cable-Payload Subsystem Without Controls: Under the action of the vessel control, the dynamics of the cable is simulated without control and the spatial time representation is shown in Fig. 5.11. It can be seen that at $t = 200s$, the subsea payload has deviated more than $30m$ from the origin under the action of the distributed disturbance on the cable and the disturbance force acting on the payload due to the current.

SBLF Positioning Controls: The positioning controls (5.44) and (5.54) developed using SBLF are simulated with crane desired position $b_{0d} = 0m$, constraints $k_{0c} = 30m$, $A_0 = 10m$, control gains $\phi_0 = \phi_2 = \phi_3 = \phi 5 = 0.5$, $\phi_1 = \phi_4 = 5.0$, $u_{rblf} = \tanh(z_6/\varepsilon_d)\bar{f}_L$, subsea payload desired position $b_{Ld} = 10m$ and constraints $k_{Lc} = 50m$, $A_L = 30m$. The spatial time representation is shown in Fig. 5.12 and the position, control and tension at the top (crane) and bottom (subsea payload) boundaries are shown in Figs. 5.13 and 5.14 respectively. The designed control is able to keep the crane at the desired position and the subsea payload position converge from the origin to the desired position when the system is subjected to the environmental disturbances.

Stabilizing Boundary Control: The boundary controls (5.66) and (5.67) are simulated with $u_{rbc} = \tanh\left((\dot{y}(L,t) + \frac{3}{4}\gamma(L)y'(L,t))/\varepsilon_d\right)\overline{f}_L$, $k_0 = k_L = 1\times10^9$ and $\gamma = 1\times10^{-3}$. The spatial time representation for the boundary control is shown in Fig. 5.15 and the position, control and tension at the top (crane) and bottom (subsea payload) boundaries are shown in Figs. 5.16 and 5.17 respectively. From the simulations, it is observed that the proposed boundary controls can stabilize the boundary at the origin under the influence of the disturbances.

5.5 Conclusion

In this chapter, the model of the coupled vessel, crane, cable and payload with nonuniform parameters has been presented. Positioning controls have been derived for the coupled system with uniform parameters using Barrier Lyapunov Functions. Through Lyapunov

analysis, it was shown that the coupled crane, payload flexible system is stable under the control action, the physical limits from operations planning and safety specifications are not transgressed and positioning of crane and payload is achieved. A stabilizing boundary control is proposed for the coupled system with nonuniform parameters. Rigorous Lyapunov stability analysis was carried out and uniform boundedness of the system was shown under the proposed control. Finally, the performance of the proposed controls have been illustrated through numerical simulations.

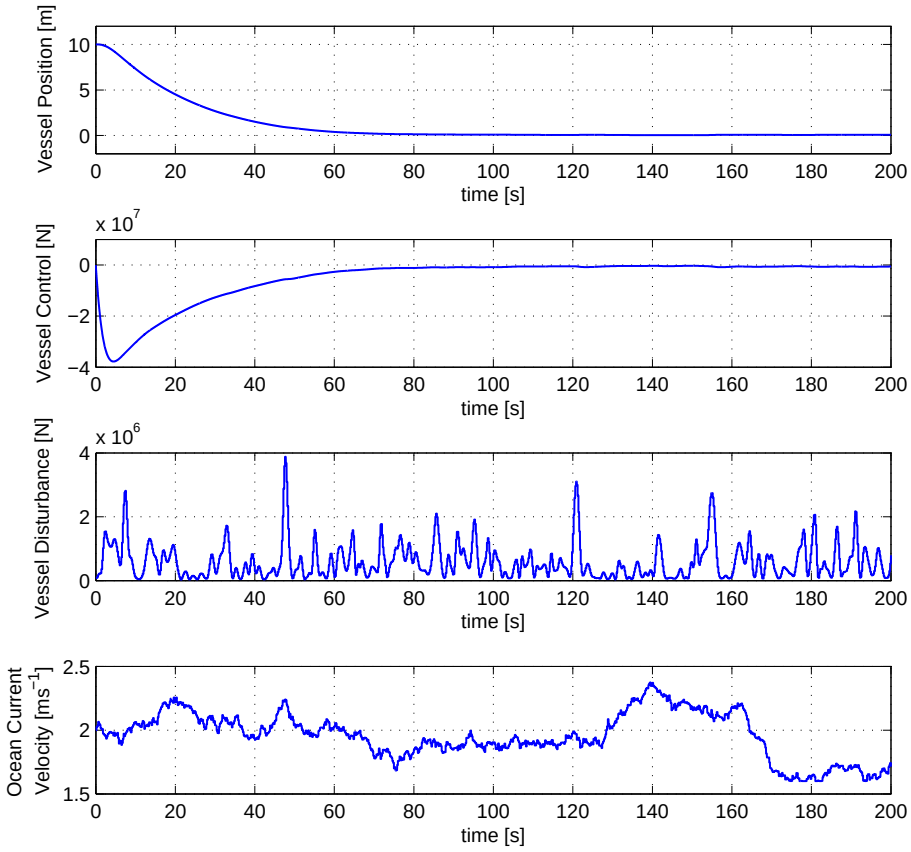

Fig. 5.10: (Top) surface vessel position with desired position at the origin, (center) vessel control thrust and (bottom) disturbance acting on the vessel

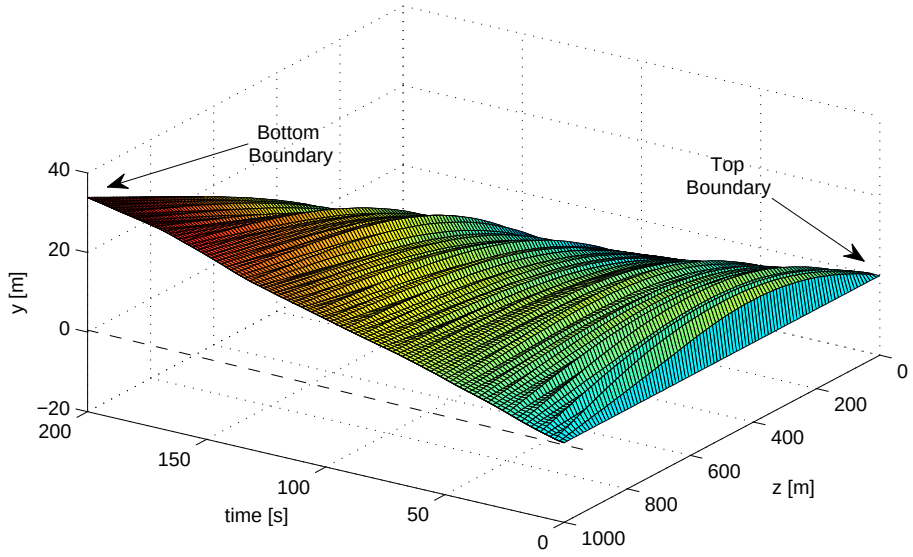

Fig. 5.11: Spatial-time representation of cable motions without control. The top boundary is at the crane and the bottom boundary at the subsea payload.

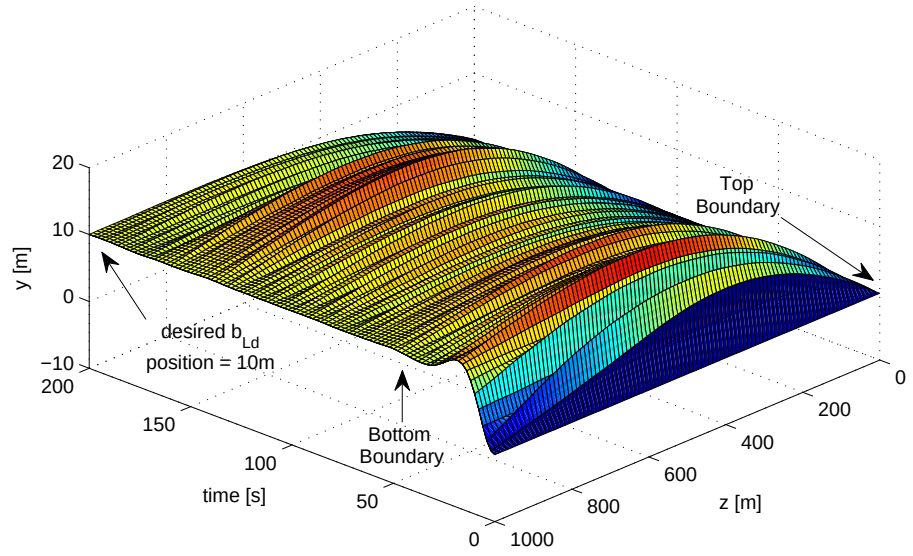

Fig. 5.12: Spatial-time representation of cable motions with positioning control. The top boundary is at the crane and the bottom boundary is at the subsea payload, maintained at desired position $b_L = 10m$.

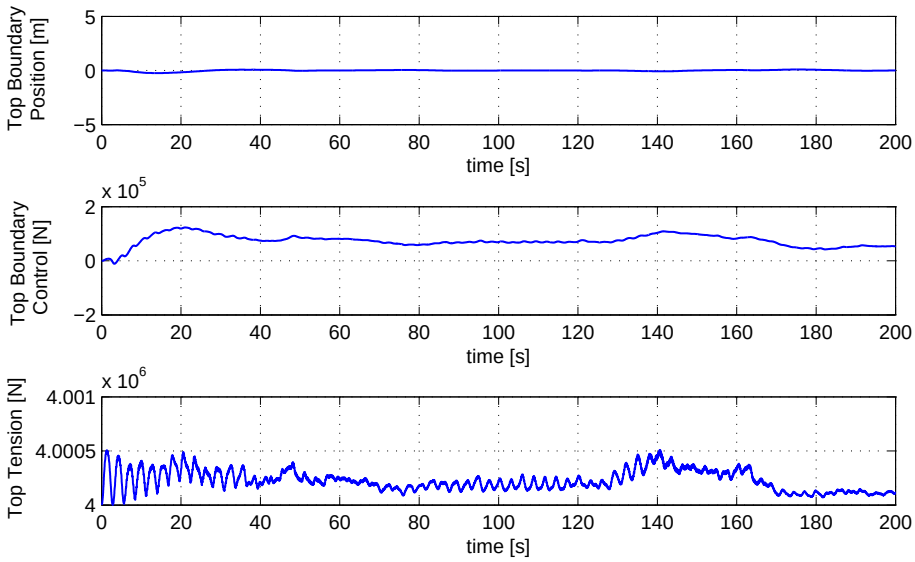

Fig. 5.13: (Top) position of the crane with desired position at origin, (center) control force on the crane and (bottom) tension at crane with position control (5.44).

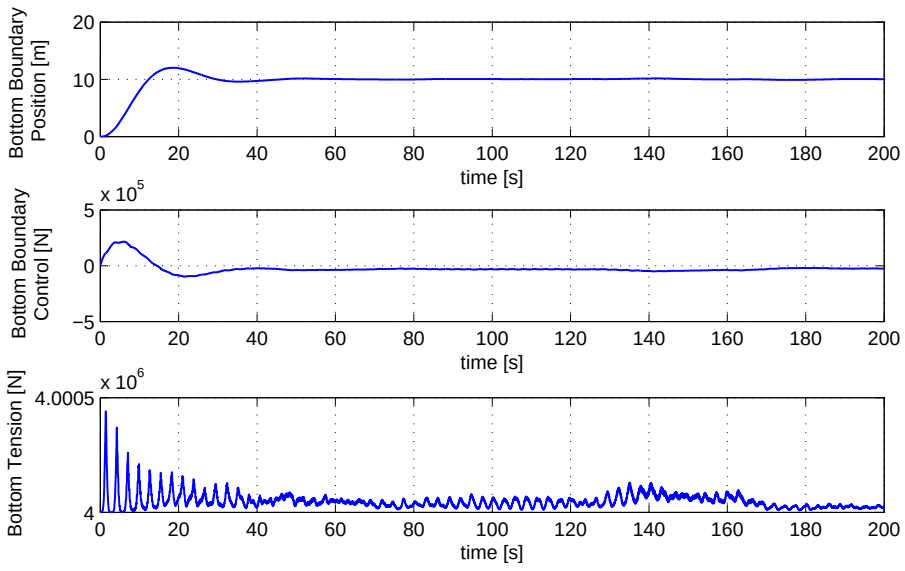

Fig. 5.14: (Top) position of the payload with desired position at $B_{LD} = 10m$, (center) control force and (bottom) cable tension at subsea payload under positioning control (5.54).

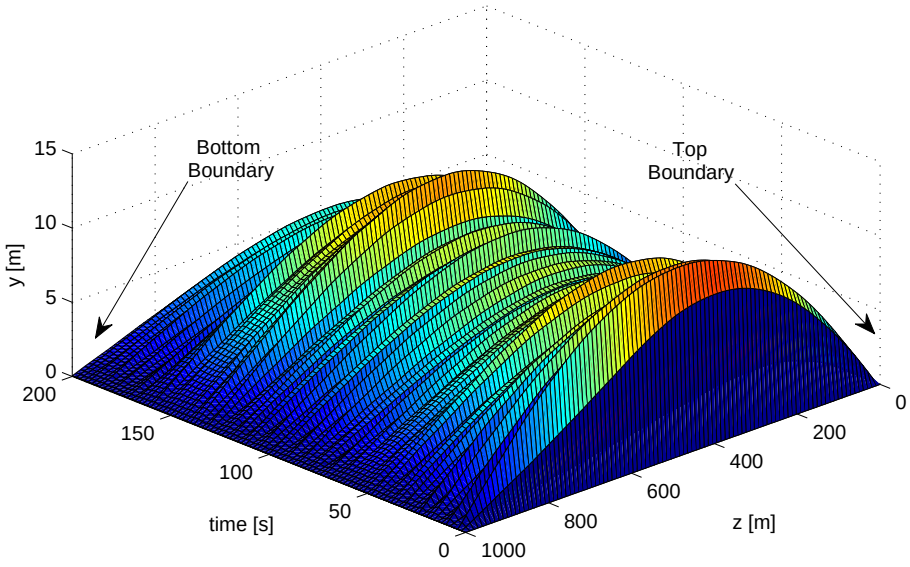

Fig. 5.15: Spatial-time representation of the cable motions control under stabilizing boundary control (5.66) and (5.67).

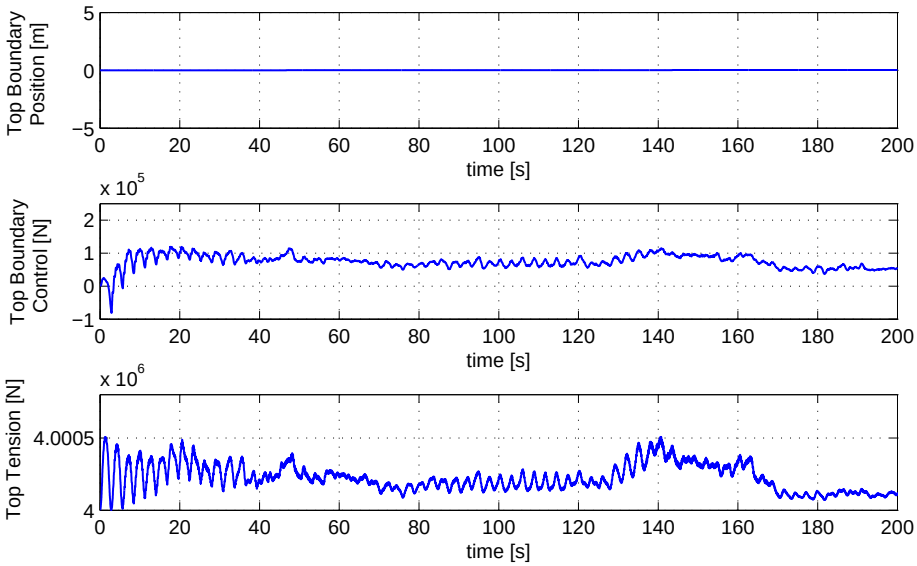

Fig. 5.16: (Top) position of the crane, (center) control force on the crane and (bottom) tension at crane with stabilizing boundary control (5.66).

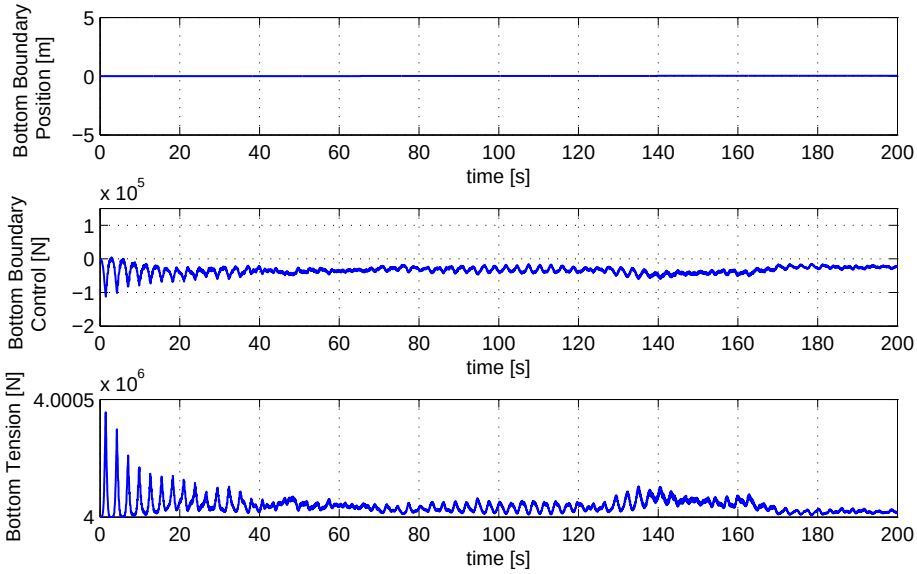

Fig. 5.17: (Top) position of the payload, (center) control force on the payload and (bottom) tension at payload with stabilizing boundary control (5.67).

Chapter 6

Flexible Marine Riser

In this chapter, we consider active control of a marine riser which is modeled as a tensioned beam, persistently perturbed by the environment. As shown in Fig. 6.1, a marine riser is the connection between a platform on the water surface and the subsea system on the sea floor. The riser is subjected to a time-varying distributed load due to the ocean current, resulting in undesirable transverse vibration. The vibration causes stresses in the slender body, which may result in fatigue problems from cyclic loads, damages due to wear and tear, propagation of cracks which requires inspections and costly repairs, and as a worst case, environmental pollution due to leakage from damaged areas. Another important consideration is the angle limit for the upper and lower end joints. The American Petroleum Institute requires that the mean lower and upper joint angles should be kept within two degrees while drilling and the maximum non-drilling angles should be limited to four degrees. Due to the motion of the surface vessel or the transverse vibrations of the riser, the upper or lower angle limit might be exceeded, resulting in damages to the riser end joints. For drilling and work-over operations, one objective is to minimize the bending stresses along the riser and the riser angle magnitudes at the platform and well head [15]. Hence, vibration reduction to reduce bending stresses and the control of the riser angle magnitude is desirable for preventing damage and improving lifespan.

Similar to the cable model considered in the last chapter, the dynamics of the flexible riser is modeled by a set of PDE up to fourth-order partial derivative. We design the boundary control based on the PDE directly to avoid the problems associated with the truncated-model-based design. The control is being applied at the beam boundary through the introduction of a torque actuator at the upper riser package shown in Fig. 6.2. The objective is to reduce the riser angle deflection at the top joint and simultaneously reduce the vibrations of the riser. The control input to the actuator is designed via Lyapunov's synthesis and the required measurements for feedback are the inclination and its rate of change at the upper riser boundary. Although tensioned risers are being considered in this chapter specifically, the analysis and control design can be extended and applied, without loss of generality, for vibration control for a class of tensioned beams exposed to undesirable distributed transverse loads. Other examples of practical application in the marine environment include free hanging underwater pipelines, drill strings and umbilicals.

The remainder of this chapter is organized as follows: In Section 6.1, the dynamic equation (PDE) of the flexible structure and boundary conditions are obtained, where the input torque is modeled into the boundary condition. Following that in Section 6.1.3, the boundary control design is presented via Lyapunov synthesis, where it is shown that uniform boundedness of the closed-loop system can be guaranteed under the distributed perturbations, and exponential stability can be achieved under free vibration condition. Section 6.3 presents the numerical method, AMM, for solving for the governing PDE, required for simulations through mode shapes and generalized coordinates. Simulation studies are carried out in Section 6.5 to demonstrate the effectiveness of the control.

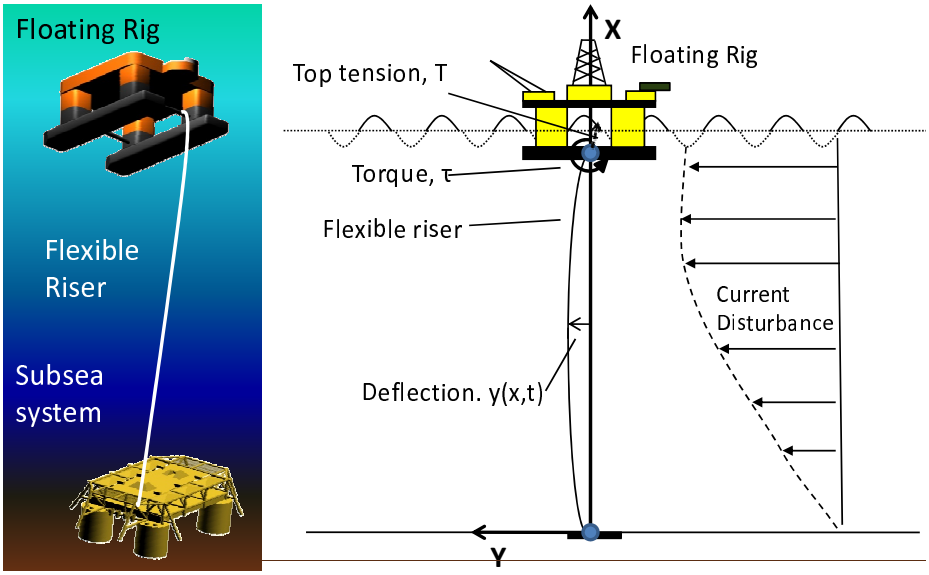

Fig. 6.1: (Left) the marine riser. (right) schematic and assigned frame of reference.

6.1 Problem Formulation

6.1.1 Derivation of the Governing Equation

The reference frame for the riser is shown in Fig. 6.1 with the origin set at the seabed. Due to the symmetry of the cross section for the riser, we can derive the equations of motions for the flexible riser independently for each principal vertical plane. As such, only the planar dynamics of the riser system is considered in the following analysis. The dynamics of the riser system is idealized as a tensioned slender beam for small angles of deflection. The lateral displacement of a point along its length is represented by $y(z,t)$, a function of space $z \in [0, L]$ and time $t \in [0, \infty)$.

In this chapter, we assume that the platform is directly above the subsea well head with no horizontal offset. The riser is filled with seawater and is neutrally buoyant. Horizontal offset and platform motions are not considered as these effects can be included through displacement influence functions or shifting functions by following the guidelines in [115,

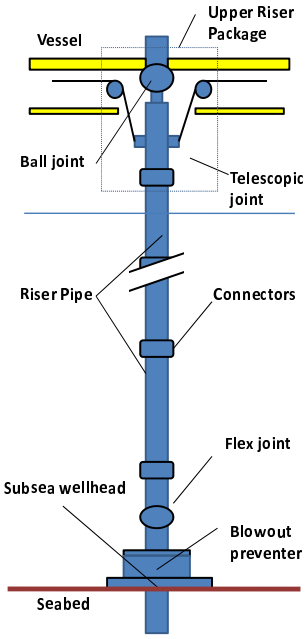

Fig. 6.2: Marine riser upper package and components.

116].

The kinetic energy of the riser system E_k can be represented as

$$E_k = \frac{1}{2} m_z \int_0^L \left[\frac{\partial y(z,t)}{\partial t} \right]^2 dz, \tag{6.1}$$

where $m_z > 0$ is the uniform mass per unit length of the riser. The potential energy for the flexible riser due to the bending strain [42, 117], can be obtained from

$$E_p = \frac{1}{2} EI \int_0^L \left[\frac{\partial^2 y(z,t)}{\partial z^2} \right]^2 dz, \tag{6.2}$$

where EI is the flexural rigidity of the riser. A torque actuator is introduced at the upper riser package to produce a concentrated moment $\tau(t)$ for vibration reduction. To determine the virtual work of the concentrated moment [115], we observe that it does work through the rotation of $y'(z,t)$, at $z = L$, its point of application. The work done by the applied

torque can be written as

$$W_m = \tau(t)\frac{\partial y(L,t)}{\partial z}, \tag{6.3}$$

and the total work done on the system, W, is given by

$$\begin{aligned} W &= W_t + W_f + W_d + W_m \\ &= \int_0^L \left\{ -\frac{1}{2}T\left[\frac{\partial y(z,t)}{\partial z}\right]^2 + \left[f(z,t) - c\frac{\partial y(z,t)}{\partial t}\right] y(z,t) \right\} dz + \tau(t)\frac{\partial y(L,t)}{\partial z}. \end{aligned} \tag{6.4}$$

where W_t is the work done by the internal tension $T(z,t)$ in elongating the riser, W_f is the work done by the distributed transverse load due to the hydrodynamic effects of the current $f(z,t)$ and W_d is the work done by linear structural damping with the structural damping coefficient, $c > 0$.

6.1.2 Variation Principle and Hamilton's Approach

The extended Hamilton's principle [118] is represented by

$$\int_{t_0}^{t_f} \delta(E_k - E_p + W)dt = 0, \tag{6.5}$$

where $t_0 < t < t_f$ is the operating interval and $\delta(\cdot)$ denotes the variation operator, may be physically interpreted as nature trying to equalize the kinetic and potential energies of a system. Substituting Eqs. (6.1), (6.2) and (6.4) into Eq. (6.5), applying the variation operator with $\delta y(z,t) = 0$ at $t = t_1$ and $t = t_2$ and integrating by parts, we obtain

$$\begin{aligned} &-\int_{t_1}^{t_2}\int_0^L \left[m_z\frac{\partial^2 y}{\partial t^2} + \frac{\partial^2}{\partial z^2}\left(EI\frac{\partial^2 y}{\partial z^2}\right) - \frac{\partial}{\partial z}\left(T\frac{\partial y}{\partial z}\right) - f + c\frac{\partial y}{\partial t} \right] \delta y dz dt \\ &-\int_{t_1}^{t_2} \left[EI\frac{\partial^2 y}{\partial z^2}\delta\left(\frac{\partial y}{\partial z}\right)\Big|_0^L - \tau(t)\delta\frac{\partial y(L,t)}{\partial z} \right] dt + \int_{t_1}^{t_2} \left[\frac{\partial}{\partial z}\left(EI\frac{\partial^2 y}{\partial z^2}\right) - T\frac{\partial y}{\partial z} \right] \delta y\Big|_0^L dt = 0. \end{aligned} \tag{6.6}$$

As $\delta y(z,t)$ is assumed to be an nonzero arbitrary variation in $0 < z < L$, the expression under the double integral in Eq. (6.6) is set equal to zero. Hence, we obtain the equation of motion as

$$EI\frac{\partial^4 y(z,t)}{\partial z^4} - T\frac{\partial^2 y(z,t)}{\partial z^2} + m_z\frac{\partial^2 y(z,t)}{\partial t^2} + c\frac{\partial y(z,t)}{\partial t} - f(z,t) = 0, \tag{6.7}$$

$\forall (z,t) \in (0,L) \times [0,\infty)$. Setting the terms with single integrals in Eq. (6.6) equal to zero, we obtain the boundary conditions

$$y(0,t) = 0, \tag{6.8}$$
$$EI\frac{\partial^2 y(0,t)}{\partial z^2} = 0, \tag{6.9}$$
$$y(L,t) = 0, \tag{6.10}$$
$$EI\frac{\partial^2 y(L,t)}{\partial z^2} - \tau(t) = 0, \tag{6.11}$$

where Eqs. (6.8) and (6.9) represent a simple support at $z = 0$, Eqs. (6.10) and (6.11) represent that there is zero deflection and a torque being applied at $z = L$ respectively.

Remark 6.1. *In the above derivations, we have shown that the input torque $\tau(t)$ at the upper riser end can be modeled as a boundary condition* (6.11) *in relation to the dynamics of the system. The flex joint at the wellhead is commonly modeled as a ball joint during analysis [119]. The governing equation* (6.7) *for the flexible marine riser, a forth order PDE with axial tension, structural damping and external disturbances terms, remains in the same form as considered in [7, 120].*

6.1.3 Effects of Time-Varying Current

The effects of a time-varying surface current $U(t)$ on a riser can be modeled as a vortex excitation force [71, 99]. The distributed load on a 3D riser structure, $f(z,t)$ can be expressed as a combination of the in-line drag force $f_D(z,t)$, consisting of a mean drag and

an oscillating drag about the mean modeled as

$$f_D(z,t) = \frac{1}{2}\rho_s C_D(z) U(z,t)^2 D + A_D \cos(4\pi f_v t + \beta), \tag{6.12}$$

and an oscillating lift $f_L(z,t)$, perpendicular to $f_D(z,t)$, about a mean deflected profile,

$$f_L(z,t) = \frac{1}{2}\rho_s C_L(z) U(z,t)^2 D \cos(2\pi f_v t + \alpha), \tag{6.13}$$

where z is an axis perpendicular to plane XOY show in Fig. 6.1, $C_D(z)$ and $C_L(z)$ are the time and spatially varying drag and lift coefficient respectively, f_v is the shedding frequency, ρ_s is the sea water density, α and β are phase angles, and A_D is the amplitude of the oscillatory part of the drag force, typically 20% of the first term in $f_D(z,t)$ [71]. The non-dimensional vortex shedding frequency can be expressed as

$$f_v = \frac{S_t U}{D}, \tag{6.14}$$

where S_t is the Strouhal number and D is the pipe outer diameter.

In this chapter, we consider the deflection of the riser in only one direction. Hence, the distributed excitation force is considered as the drag force Eq. (6.12), $f(z,t) = f_D(z,t)$. The current profile $U(z,t)$, similar to that shown in Fig. 6.1, is a function which relates the depth to the ocean surface current velocity $U(t)$. The transverse VIV from the lift component is not considered in this chapter but the proposed method can be similarly applied without any loss of generality if only the lift component is considered.

Assumption 6.1. *For the distributed disturbance $f(z,t)$, we assume that there exists a constant $\bar{f} \in R^+$, such that $||f(z,t)|| \leq \bar{f}$, $\forall (z,t) \in [0,L] \times [0,\infty)$. This is a reasonable assumption as the effects of the time-varying current, $f(z,t)$, are exogenous, have finite energy and hence are bounded, i.e. $f(z,t) \in \mathcal{L}_\infty([0,L])$.*

Remark 6.2. *For control design in Section 6.2, only the assertion that there exist an upper*

bound on the disturbance in Assumption 1, $||f(z,t)|| < \bar{f}$, is necessary. The knowledge of the exact value for $f(z,t)$ is not required $\forall(z,t) \in [0,L] \times [0,\infty)$. As such, different VIV models up to various levels of fidelity, such as those found in [99–103], can be applied without affecting the control design or analysis.

Remark 6.3. *The VIV problem can be separated into the drag and the lift components, perpendicular to each other. The vector sum results in a force with oscillating magnitude and direction, thereby producing of figure of "8" response in the riser. Under Assumption 6.1, it is possible that control applied to these two cases in separate axis may be sufficient for vibration reduction of the VIV problem. The combination of drag and oscillating lift will be treated in future analysis using a 3D riser model.*

Remark 6.4. *In the following sections, the notations $y'(z,t) = \partial y(z,t)/\partial z$, $y''(z,t) = \partial^2 y(z,t)/\partial z^2$ and $\dot{y}(z,t) = \partial y(z,t)/\partial t$, etc. are used and dependencies of terms are omitted where obvious for conciseness.*

6.2 Control Design

The control objective is to minimize the upper riser angle $y'(L,t)$, and simultaneously reduce the vibrations of the riser $y(z,t)$, subjected to the time-varying distributed transverse load from the ocean current $f(z,t)$. In this section, we use Lyapunov's synthesis to construct a boundary control law $\tau(t)$ for the above objective, and to rigourously show the closed-loop stability of the distributed system. Now, we present some Lemmas and Properties that will be used in subsequent developments.

Lemma 6.1. *[66, 104]: For bounded initial conditions, if there exists a C^1 continuous and positive definite Lyapunov function $V(x)$ satisfying $\kappa_1(\|x\|) \leq V(x) \leq \kappa_2(\|t\|)$, such that $\dot{V}(x) \leq -\lambda V(x) + c$, where κ_1, $\kappa_2 : R^n \to R$ are class K functions and c is a positive constant, then the solution $x = 0$ is uniformly bounded.*

Lemma 6.2. *Let $y_1(z,t)$, $y_2(z,t) \in R$ with $z \in [0,L]$ and $t \in [0,\infty)$, the following inequalities hold:*

$$y_1 y_2 \leq |y_1 y_2| \leq y_1^2 + y_2^2, \tag{6.15}$$

$$2y_1 y_2 \leq 2|y_1 y_2| \leq y_1^2 + y_2^2, \quad \forall y_1, y_2 \in \mathcal{R}. \tag{6.16}$$

From lemma 6.2, we can obtain the inequality [105],

$$|y_1 y_2| = \left| \left(\frac{1}{\sqrt{\delta}} y_1 \right) \left(\sqrt{\delta} y_2 \right) \right| \leq \frac{1}{\delta} y_1^2 + \delta y_2^2, \quad \forall y_1, y_2 \in \mathcal{R} \text{ and } \delta > 0. \tag{6.17}$$

Lemma 6.3. *[106, 107]: Let $y(z,t) \in R$ be a function defined on $z \in [0,L]$ and $t \in [0,\infty)$ that satisfies the boundary condition*

$$y(0,t) = 0, \quad \forall t \in [0,\infty), \tag{6.18}$$

then the following inequalities hold:

$$\int_0^L y^2 dz \leq L^2 \int_0^L [y']^2 dz, \tag{6.19}$$

$$y^2 \leq L \int_0^L [y']^2 dz, \quad \forall z \in [0,L]. \tag{6.20}$$

Property 6.1. *[107]: If the kinetic energy of the system* (6.7) *through* (6.11)*, given by Eq.* (6.1) *is bounded $\forall (z,t) \in [0,L] \times [0,\infty)$, then $\dot{y}'(z,t)$ and $\ddot{y}''(z,t)$ are bounded $\forall (z,t) \in [0,L] \times [0,\infty)$.*

Property 6.2. *[107]: If the potential energy of the system* (6.7) *through* (6.11)*, given by Eq.* (6.2) *is bounded $\forall (z,t) \in [0,L] \times [0,\infty)$, then $y''(z,t)$, $y'''(z,t)$ and $y''''(z,t)$ are bounded $\forall (z,t) \in [0,L] \times [0,\infty)$.*

6.2.1 Boundary Control

Consider the Lyapunov function candidate,

$$V(t) = E_b(t) + E_c(t) + \frac{1}{2}(k_2 + \beta EIk_1)[y'(L,t)]^2, \tag{6.21}$$

where k_1, $k_2 > 0$ are control parameters, $E_b(t)$ and a small crossing term $E_c(t)$ are defined as

$$E_b = \frac{1}{2}m_z\int_0^L \dot{y}^2 dz + \frac{1}{2}EI\int_0^L [y'']^2 dz + \frac{1}{2}T\int_0^L [y']^2 dz, \tag{6.22}$$

$$E_c = \beta m_z \int_0^L y\dot{y} dz, \tag{6.23}$$

and $\beta > 0$ is a small positive weighting constant.

Lemma 6.4. *The function* (6.21)*, can be upper and lower bounded as*

$$0 \leq \lambda_1(E_b + [y'(L,t)]^2) \leq V(t) \leq \lambda_2(E_b + [y'(L,t)]^2), \tag{6.24}$$

where λ_1 and λ_2 are positive constants

Proof: Using Eqs. (6.15) and (6.19) on Eq. (6.23), we obtain

$$|E_c| \leq \beta m_z \int_0^L (\dot{y}^2 + y^2) dz \tag{6.25}$$

$$\leq \beta m_z \int_0^L \dot{y}^2 dz + \beta m_z L^2 \int_0^L [y']^2 dz \tag{6.26}$$

$$\leq 2\beta m_z \frac{\max(1, L^2)}{\min(m_z, T, EI)} E_b \tag{6.27}$$

$$\leq \xi E_b, \tag{6.28}$$

where

$$\xi = 2\beta m_z \frac{\max(1, L^2)}{\min(m_z, T, EI)}. \tag{6.29}$$

Selecting β according to the following sufficient condition,

$$\beta \leq \frac{\min(m_z, T, EI)}{2m_z \max(1, L^2)}, \tag{6.30}$$

we have

$$-\xi E_b \leq E_c \leq \xi E_b, \tag{6.31}$$

$$0 \leq \xi_1 E_b \leq E_b + E_c \leq \xi_2 E_b, \tag{6.32}$$

where for some positive constants $\xi_1 = 1 - \xi$ and $\xi_2 = 1 + \xi$,

$$\xi_1 = 1 - 2\beta m_z \frac{\max(1, L^2)}{\min(m_z, T, EI)} > 0, \tag{6.33}$$

$$\xi_2 = 1 + 2\beta m_z \frac{\max(1, L^2)}{\min(m_z, T, EI)} > 1. \tag{6.34}$$

Given the Lyapunov functional candidate in (6.21), we obtain

$$0 \leq \lambda_1 (E_b + [y'(L,t)]^2) \leq V(t) \leq \lambda_2 (E_b + [y'(L,t)]^2), \tag{6.35}$$

where $\lambda_1 = \min[\xi_1, 0.5(k_2 + \beta EIk_1)]$ and $\lambda_2 = \max[\xi_2, 0.5(k_2 + \beta EIk_1)]$.

Lemma 6.5. *The time derivative of the Lyapunov function in* (6.21) *can be upper bounded with*

$$\dot{V}(t) \leq -\lambda_3 (E_b + [y'(L,t)]^2) + \epsilon, \tag{6.36}$$

where $\lambda_3 > 0$.

Proof: Taking time derivative of $V(t)$, we obtain

$$\dot{V}(t) = \dot{E}_b + \dot{E}_c + (k_2 + \beta EIk_1)\dot{y}'(L,t)y'(L,t). \tag{6.37}$$

The first term of Eq. (6.37) yields

$$\begin{aligned}
\dot{E}_b &= \int_0^L m_z \dot{y}\ddot{y} + EIy''\dot{y}'' + Ty'\dot{y}' dz \\
&= \int_0^L (-c\dot{y} - EIy'''' + Ty'' + f)\dot{y} + EIy''\dot{y}'' + Ty'\dot{y}' dz \\
&= [EIy''\dot{y}' - EIy'''\dot{y} + Ty'\dot{y}]_0^L + \int_0^L \left[(-c\dot{y} - EIy'''' + Ty'' + f)\dot{y} + EIy''''\dot{y} - Ty''\dot{y}\right] dz \\
&= [EIy''\dot{y}' - EIy'''\dot{y} + Ty'\dot{y}]_0^L + \int_0^L \left[-c\dot{y}^2 + f\dot{y}\right] dz. \qquad (6.38)
\end{aligned}$$

From Eq. (6.7) and performing integration by parts, we obtain

$$\begin{aligned}
m_z\ddot{y} &= -c\dot{y} - EIy'''' + Ty'' + f, \qquad (6.39) \\
EI\int_0^L y''\dot{y}'' dz &= EI[y''\dot{y}']_0^L - EI[y'''\dot{y}]_0^L + EI\int_0^L y''''\dot{y} dz, \qquad (6.40) \\
T\int_0^L y'\dot{y}' dz &= T[y'\dot{y}]_0^L - T\int_0^L y''\dot{y} dz. \qquad (6.41)
\end{aligned}$$

Substituting Eqs. (6.39) to (6.41) and boundary conditions (6.8) to (6.11) into Eq. (6.38), we arrive at

$$\begin{aligned}
\dot{E}_b &= [EIy''(L,t)\dot{y}'(L,t)] + \int_0^L \left[-c\dot{y}^2 + f\dot{y}\right] dz \\
&= \tau\dot{y}'(L,t) + \int_0^L \left[-c\dot{y}^2 + f\dot{y}\right] dz \\
&= \tau\dot{y}'(L,t) - c\int_0^L \dot{y}^2 dz + \int_0^L f\dot{y} dz, \qquad (6.42)
\end{aligned}$$

where $\dot{y}(0,t) = \dot{y}(L,t) = 0$ due to the boundary conditions. Using the inequality (6.17), we obtain

$$\begin{aligned}
\dot{E}_b &\leq \tau\dot{y}'(L,t) - c\int_0^L \dot{y}^2 dz + \int_0^L \frac{1}{\delta_1} f^2 dz + \int_0^L \delta_1 \dot{y}^2 dz \\
&\leq \tau\dot{y}'(L,t) - (c - \delta_1)\int_0^L \dot{y}^2 dz + \frac{1}{\delta_1}\int_0^L f^2 dz, \qquad (6.43)
\end{aligned}$$

where $\delta_1 > 0$ is a positive constant. Taking the time derivative of the crossing term (6.23), we have

$$\begin{aligned}
\dot{E}_c &= \beta m_z \int_0^L (\dot{y}^2 + y\ddot{y}) dz \\
&= \beta \int_0^L \left[m_z \dot{y}^2 + y(-c\dot{y} - EIy'''' + Ty'' + f) \right] dz \\
&= \beta \int_0^L \left[-EIyy'''' - cy\dot{y} + fy + Tyy'' + m_z \dot{y}^2 \right] dz. \qquad (6.44)
\end{aligned}$$

The first term of Eq. (6.44) simplifies via integration by parts and boundary conditions to

$$\begin{aligned}
-\beta \int_0^L EIyy'''' dz &= -\beta EI[yy''' - y'y'']_0^L - \beta EI \int_0^L [y'']^2 dz \\
&= \beta EIy'(L,t)\tau - \beta EI \int_0^L [y'']^2 dz. \qquad (6.45)
\end{aligned}$$

The second term using Eq. (6.17), gives

$$-\beta c \int_0^L y\dot{y} dz \leq \beta \frac{c}{\delta_2} \int_0^L \dot{y}^2 dz + \beta c \delta_2 L^2 \int_0^L [y']^2 dz, \qquad (6.46)$$

where $\delta_2 > 0$. The third term with Eq. (6.17) gives

$$\beta \int_0^L yf dz \leq \frac{\beta}{\delta_3} \int_0^L f^2 dz + \beta \delta_3 L^2 \int_0^L [y']^2 dz, \qquad (6.47)$$

where $\delta_3 > 0$, and the fourth term yields through integration by parts,

$$\begin{aligned}
\beta T \int_0^L yy'' dz &= \beta T[yy']_0^L - \beta T \int_0^L y'y' dz \\
&= -\beta T \int_0^L [y']^2 dz. \qquad (6.48)
\end{aligned}$$

From Eqs. (6.43) and (6.45) to (6.48), we arrive at the inequalities

$$\dot{E}_b \leq \tau \dot{y}'(L,t) - (c-\delta_1)\int_0^L \dot{y}^2 dz + \frac{1}{\delta_1}\int_0^L f^2 dz, \tag{6.49}$$

$$\begin{aligned}\dot{E}_c \leq\ & \beta EI y'(L,t)\tau - \beta EI\int_0^L [y'']^2 dz + \beta\frac{c}{\delta_2}\int_0^L \dot{y}^2 dz + \beta c\delta_2 L^2\int_0^L [y'']^2 dz \\ & + \frac{\beta}{\delta_3}\int_0^L f^2 dz + \beta\delta_3 L^2\int_0^L [y'']^2 dz - \beta T\int_0^L [y']^2 dz + \beta\int_0^L m_z\dot{y}^2 dz. \end{aligned}\tag{6.50}$$

Substituting Eqs. (6.49) and (6.50) into Eq. (6.37), we arrive at

$$\begin{aligned}\dot{V} &= \dot{E}_b + \dot{E}_c + (k_2+\beta EIk_1)\dot{y}'(L,t)y'(L,t) \qquad (6.51)\\ &\leq \left(\dot{y}'(L,t)+\beta EIy'(L,t)\right)\tau - (c-\beta m_z-\delta_1-\beta\frac{c}{\delta_2})\int_0^L \dot{y}^2 dz + \left(\frac{1}{\delta_1}+\frac{\beta}{\delta_3}\right)\int_0^L f^2 dz \\ &\quad -\beta EI\int_0^L [y'']^2 dz - \beta\left(T - c\delta_2 L^2 - \delta_3 L^2\right)\int_0^L [y']^2 dz + (k_2+\beta EIk_1)\dot{y}'(L,t)y'(L,t)\end{aligned}$$

Consider the following boundary control law

$$\tau = -\left[k_1\dot{y}'(L,t) + k_2 y'(L,t)\right], \tag{6.52}$$

and substituting the control law (6.52) into Eq. (6.51) under Assumption 6.1, we obtain

$$\begin{aligned}\dot{V} &\leq -\left(\dot{y}'(L,t)+\beta EIy'(L,t)\right)\left[k_1\dot{y}'(L,t)+k_2y'(L,t)\right] + (k_2+\beta EIk_1)\dot{y}'(L,t)y'(L,t) \\ &\quad -(c-\beta m_z-\delta_1-\beta\frac{c}{\delta_2})\int_0^L \dot{y}^2 dz - \beta EI\int_0^L [y'']^2 dz + \left(\frac{1}{\delta_1}+\frac{\beta}{\delta_3}\right)\int_0^L f^2 dz \\ &\quad -\beta\left(T-c\delta_2L^2-\delta_3L^2\right)\int_0^L [y']^2 dz \\ &\leq -k_1[\dot{y}'(L,t)]^2 - k_2\beta EI[y'(L,t)]^2 - (c-\beta m_z-\delta_1-\beta\frac{c}{\delta_2})\int_0^L \dot{y}^2 dz \\ &\quad -\beta EI\int_0^L [y'']^2 dz - \beta\left(T-c\delta_2L^2-\delta_3L^2\right)\int_0^L [y']^2 dz + \left(\frac{1}{\delta_1}+\frac{\beta}{\delta_3}\right)\int_0^L f^2 dz \\ &\leq -\lambda_3(E_b + [y'(L,t)]^2) + \epsilon, \qquad (6.53)\end{aligned}$$

where

$$\begin{aligned}
\lambda_3 &= min\left(\frac{\epsilon_1}{m_z}, \beta, \frac{\epsilon_2}{T}, k_2\beta EI\right) > 0, \\
\epsilon &= \left(\frac{1}{\delta_1} + \frac{\beta}{\delta_3}\right) \max_{t=[0,\infty)} \int_0^L f^2 dz < \infty, \\
\epsilon_1 &= c - \beta m_z - \delta_1 - \beta\frac{c}{\delta_2} > 0, \\
\epsilon_2 &= T - c\delta_2 L^2 - \delta_3 L^2 > 0.
\end{aligned}$$

From Eqs. (6.24) and (6.53), we have

$$\dot{V}(t) \leq -\lambda V(t) + \epsilon, \tag{6.54}$$

where $\lambda = \lambda_3/\lambda_2$. After obtaining Eq. (6.54), we are ready to present the following theorem, which contain the results for the boundary control of the flexible riser.

Theorem 6.1. *Consider the system described by Eq.* (6.7) *and boundary conditions* (6.8) *to* (6.11)*, under Assumption 6.1, and the control law* (6.52)*. Given that the initial conditions are bounded, and that the required state information* $y'(L,t)$ *and* $\dot{y}'(L,t)$ *are available, the closed loop system is uniformly bounded.*

Proof: From Eq. (6.54) and Lemma 6.1, it is straightforward to show the deflection $y(z,t)$ is uniformly bounded. For completeness, the details of the proof are provided here. Multiplying Eq. (6.54) by $e^{\lambda t}$, we obtain

$$\frac{\partial}{\partial t}(Ve^{\lambda t}) \leq \epsilon e^{\lambda t}. \tag{6.55}$$

Integration of the above and applying Lemma 6.1 yields

$$V(t) \leq \left(V(0) - \frac{\epsilon}{\lambda}\right)e^{\lambda t} + \frac{\epsilon}{\lambda} \leq V(0) + \frac{\epsilon}{\lambda} \in \mathcal{L}_\infty, \tag{6.56}$$

Utilizing Eqs. (6.20), (6.22) and (6.24), we have

$$\frac{1}{2L}Ty^2(z,t) \leq \frac{1}{2}T\int_0^L [y'(z,t)]^2 dz \leq E_b(t) \leq \frac{1}{\lambda_1}V(t) \in \mathcal{L}_\infty. \tag{6.57}$$

Hence, we have $y(z,t) \in \mathcal{L}_\infty$. From Eqs. (6.24) and (6.53), we can state the $E_b(t)$ and $y'(L,t)$ are bounded $\forall t \in [0,\infty)$. Since $E_b(t)$ is bounded, $\dot{y}(z,t)$, $y'(z,t)$ and $y''(z,t)$ are bounded $\forall (z,t) \in [0,L]\times[0,\infty)$. From Eq. (6.1), the kinetic energy of the system is bounded and using Property 6.1, $\dot{y}'(z,t)$ is bounded $\forall (z,t) \in [0,L] \times [0,\infty)$. At this point, we have shown that all the signals in the control law (6.52) are bounded. From the boundedness of the potential energy (6.2), we can use Property 6.2 to conclude that $y''''(z,t)$ is bounded. Finally, using Assumption 6.1, Eqs. (6.7) through (6.11), and the above statements, we can conclude that $\ddot{y}(z,t)$ is bounded $\forall (z,t) \in [0,L] \times [0,\infty)$.

Corollary 6.1. *For the system described by governing equation* (6.7)*, and boundary conditions* (6.8) *to* (6.11)*, if the free vibration case is considered, i.e.* $f(z,t) = 0$*, the boundary control* (6.52) *ensures that the riser displacement is exponentially stabilized as follows*

$$|y(z,t)| \leq \sqrt{\frac{2\lambda_2 L}{T\lambda_1}\exp(-\frac{\lambda_3}{\lambda_2}t)}, \quad \forall z \in [0,L], \tag{6.58}$$

where λ*,* λ_1*,* λ_2 *are positive constants.*

Proof: From Eq. (6.53), under the free vibration condition, we obtain the time derivation of the Lyapunov function candidate (6.21) as

$$\dot{V} \leq -\lambda_3(E_b + [y'(L,t)]^2), \tag{6.59}$$

where

$$\begin{aligned}\lambda_3 &= min\left(\frac{\epsilon_1}{m_z}, \beta, \frac{\epsilon_2}{T}, k_2\beta EI\right) > 0,\\ \epsilon_1 &= c - \beta m_z - \delta_1 - \beta\frac{c}{\delta_2} > 0,\\ \epsilon_2 &= T - c\delta_2 L^2 - \delta_3 L^2 > 0.\end{aligned}$$

From Eqs. (6.24) and (6.59), we obtain the upper bound as

$$\dot{V}(t) \leq -\frac{\lambda_3}{\lambda_2}V(t), \tag{6.60}$$

which has a solution of

$$\begin{aligned}V(t) &\leq V(0)\exp\left(-\frac{\lambda_3}{\lambda_2}t\right)\\ &\leq \lambda_2[E_b(0) + y'(L,0)^2]\exp\left(-\frac{\lambda_3}{\lambda_2}t\right).\end{aligned} \tag{6.61}$$

Similarly, utilizing Eqs. (6.20), (6.22) and (6.24), we have

$$\frac{1}{2L}Ty^2(z,t) \leq \frac{1}{2}T\int_0^L [y'(z,t)]^2 dz \leq E_b(t) \leq \frac{1}{\lambda_1}V(t), \tag{6.62}$$

$\forall (z,t) \in [0,L]\times[0,\infty)$ and Eq. (6.58) follows from combining Eqs. (6.61) and (6.62). The bounds for $y'(z,t)$, $y''(z,t)$, $y''''(z,t)$, $\dot{y}(z,t)$, $\dot{y}'(z,t)$ and $\ddot{y}(z,t)$ can be similarly shown as in Theorem 6.1. This concludes the proof.

Remark 6.5. *The proposed control is simple in structure and implementable as $y'(L,t)$, the top riser angle, can be measured directly using inclinometers and $\dot{y}'(L,t)$ can be obtained by time differentiating the measurement of the top riser angle. The problem of the observer spill over effect is avoided as all the required states are measurable or observed directly.*

Remark 6.6. *As the boundary control design is based on the governing PDE* (6.7) *without the use of a truncated model, the problem of control spill over is also avoided.*

Remark 6.7. *The control is independent of system parameters and thus possesses stability robustness to uncertainties in the system parameters.*

Remark 6.8. *The boundary control proposed is modeled, designed and applied at the boundary of the riser. As the control is not distributed, there is no explicit vibration control law. Under the actuation of the proposed boundary control, it has been demonstrated through rigorous stability analysis that the riser distributed state* $y(z,t) \forall z \in [0, L], t \in (0, \infty)$ *are uniformly bounded when subjected to a distributed disturbance and exponentially stable in the absence of environmental disturbance. From the simulations, we observe that the vibration amplitude of the riser is reduced by the proposed boundary control."*

6.3 Method of Numerical Solution

To verify the effectiveness of the proposed approach, the developed boundary control (6.52) is applied to the closed loop system (6.7) with boundary conditions (6.8) to (6.11). As the governing equation for the flexible system derived in this study does not have an easily obtainable solution, numerical methods are required for solving the PDE for simulation purposes. Different approximate methods such as FEM, AMM, finite difference, and Galerkin methods can be used to discretize the system for simulations. AMM is selected in this chapter for its ability to produce accurate, low order simulations that are easy and fast to compute numerically.

6.3.1 Natural Vibration Modes and Orthogonality Conditions

The natural modes of vibration can be obtained by setting external forces in Eq. (6.7) to zero and solving the homogenous equation

$$EI\frac{\partial^4 y}{\partial z^4} - T\frac{\partial^2 y}{\partial z^2} + m_z\frac{\partial^2 y}{\partial t^2} + c\frac{\partial y}{\partial t} = 0. \tag{6.63}$$

From the method of separating variables [121], and using the AMM with constrained modes, the solution $y(z,t)$ is assumed to take the form

$$y(z,t) = \sum_{i=1}^{\infty} \phi_i(z) q_i(t), \tag{6.64}$$

where $\phi_i(z)$ are the mode shape functions or eigenfunctions and $q_i(t)$ are the generalized coordinates. The natural frequencies of the riser can be expressed as

$$\omega_i^2 = \frac{1}{m_z}\left(\frac{i\pi}{L}\right)^2 \left[EI\left(\frac{i\pi}{L}\right)^2 + T\right], \tag{6.65}$$

where ω_i is the natural frequency of the i-mode. Rearranging (6.63) into two systems of differential equation with one dependant on z and the other purely time varying, and noting that each mode shape function $\phi_i(z)$ is the solution of the boundary value problem for the differential equation dependant on z, multiplying ϕ_j and integrating from $z = 0$ to $z = L$, we have

$$EI\int_0^L \phi_i'''' \phi_j dz - T\int_0^L \phi_i'' \phi_j dz - \int_0^L m_z \omega_i^2 \phi_i \phi_j dz = 0, \tag{6.66}$$

As $\phi_i(z)$ and $\phi_j(z)$ should satisfy the boundary conditions with associated natural frequencies ω_i and ω_j, and integrating (6.66) by parts, we obtain the orthogonality condition,

$$\int_0^L \phi_i \phi_j dz = \begin{cases} 0, & \text{i} \neq \text{j} \ ; \\ 1, & \text{i} = \text{j}. \end{cases} \tag{6.67}$$

The mode shape functions are expressed as

$$\phi_i(z) = \frac{\sqrt{2L}}{L}\left(\sin s_{2i} z - \frac{\sin s_{2i} L}{\sinh s_{1i} L}\sinh s_{1i} z\right). \tag{6.68}$$

where

$$s_{1i} = \left\{ \frac{1}{2EI} \left[T + \left(T^2 + 4EIm_z\omega_i^2 \right)^{\frac{1}{2}} \right] \right\}^{\frac{1}{2}}, \tag{6.69}$$

$$s_{2i} = \left\{ \frac{1}{2EI} \left[-T + \left(T^2 + 4EIm_z\omega_i^2 \right)^{\frac{1}{2}} \right] \right\}^{\frac{1}{2}}. \tag{6.70}$$

6.3.2 Forced Vibration Response

As the moment does not correspond to a generic translation, it must be handled indirectly using the method of virtual work. We can model the system as a simply supported structure with a moment at the boundary [115]. From Eq. (6.6), using pinned boundary conditions with a torque generated at $z = L$ leads to

$$\int_0^L m_z \ddot{y}\delta y dz + \int_0^L (EIy'''' - Ty'')\delta y dz + \int_0^L c\dot{y}\delta y dz = \int_0^L f\delta y dz - \tau\delta y'(L,t). \tag{6.71}$$

Substituting Eq. (6.64) into Eq. (6.71), and using Eq. (6.66), we obtain

$$\begin{aligned} &m_z \sum_{i=1}^{\infty}\sum_{j=1}^{\infty} \ddot{q}_i \int_0^L \phi_i\phi_j dz + m_z\omega_i^2 \sum_{i=1}^{\infty}\sum_{j=1}^{\infty} q_i \int_0^L \phi_i\phi_j dz \\ &+c\sum_{i=1}^{\infty}\sum_{j=1}^{\infty} \dot{q}_i \int_0^L \phi_i\phi_j dz = \sum_{j=1}^{\infty}\int_0^L f\phi_j dz - \sum_{j=1}^{\infty}\tau\phi_j'(L). \end{aligned} \tag{6.72}$$

In view of orthogonality condition (6.67), every term in the summation vanishes except when $i = j$. Hence Eq. (6.72) reduces to

$$\sum_{i=1}^{\infty} \left[m_z\ddot{q}_i(t) + c\dot{q}_i(t) + m_z\omega_i^2 q_i(t) \right] = \sum_{i=1}^{\infty}\int_0^L f(z,t)\phi_i(z)dz - \sum_{i=1}^{\infty}\tau(t)\phi_i'(L). \tag{6.73}$$

From Eq. (6.64), we know that each $q_i(t)$ corresponds to a DOF of the system. It is also well known that the first several modes corresponds to lower frequencies are dominant in describing the system dynamics. The infinite series in Eq. (6.64) can be truncated into a

finite one as follows

$$y(z,t) = \sum_{i=1}^{N} \phi_i(z) q_i(t), \tag{6.74}$$

where N is the number of modes taken into consideration. Hence, we arrive at ordinary differential equation (ODE) of the AMM model,

$$\sum_{i=1}^{N} \left[m_z \ddot{q}_i(t) + c\dot{q}_i(t) + m_z \omega_i^2 q_i(t) \right] = \sum_{i=1}^{N} \int_0^L f(z,t)\phi_i(z)dz - \sum_{i=1}^{N} \tau(t)\phi_i'(L). \tag{6.75}$$

The solution $y(z,t)$ can then be obtained by solving for the generalized coordinates, $q_i(t)$ in Eq. (6.75) and substituting mode shapes, $\phi_i(z)$ from Eq. (6.68) into Eq. (6.74).

6.4 Simulation

The closed loop system (6.7) is simulated to investigate the performance of control law (6.52) with system parameters given in Table 1. The system is simulated using the AMM model (6.75) developed in the previous section where the first four modes, $N = 4$ are considered. A fourth-order Runge-Kutta-Merson program with adaptive step size [78] is used to numerically solve the ODE for the generalized coordinates.

The riser, initially at rest, is excited by a distributed transverse load. Large vibrational stresses are normally associated with a resonance that exists when the frequency of the imposed force is tuned to one of the natural frequencies [6]. Hence, the ocean surface current velocity $U(t)$ is modeled as a mean flow with worst case sinusoidal components to simulate the riser with a mean deflected profile. The sinusoids have frequencies of $\omega_i = \{0.867,\ 1.827,\ 2.946,\ 4.282\}$, for $i = 1$ to 4, corresponding to the four natural modes of vibration of the riser. The current $U(t)$ can be expressed as

$$U(t) = \bar{U} + U_m \sum_{i=1}^{N} \sin(\omega_i t), \quad i = 1, 2, \ldots, N, \tag{6.76}$$

where $\bar{U} = 2ms^{-1}$ is the mean flow current and $U_m = 0.2ms^{-1}$ is the amplitude of the oscillating flow. The surface current generated by Eq. (6.76) is shown in Fig. 6.3. The full current load is applied from $z = 1000m$ to $700m$ and thereafter linearly decline to zero at the ocean floor, $z = 0$, to obtain a depth dependent ocean current profile $U(z,t)$.

The vortex excitation $f(z,t)$ is simulated using Eq (6.12) with $C_D = 1.361$ [101] and $\beta = 0$. From (6.14), a reasonable vale of $S_t = 0.2$ is adopted for subcritical flow [71], resulting in a vortex shedding frequency of $f_v = 2.625$. The control parameters are set as $k_1 = k_2 = 1 \times 10^9$.

The controlled and uncontrolled upper and lower riser angles are shown in Fig. 6.4 and 6.5 respectively. It is observed that there are significant improvements in the top riser angle bringing the magnitude near zero when the control is applied. There is peak angle reduction in the bottom angle although the actuator is not located at that position.

Transverse vibration magnitude of the riser is examined at $z = 400m$ and $750m$. The results for controlled and uncontrolled responses are shown in Fig. 6.6 and 6.7. It can be observed that the peak vibration magnitudes are reduced at both locations. The riser profiles for controlled and uncontrolled responses under excitation were overlaid for different time instances and the displacement range are shown in Fig. 6.8. The riser angle and deflection magnitudes are reduced when the control is active with control input shown in Fig. 6.9.

The ocean current disturbance was set to zero at $t = 100s$ to simulate a free vibrating case similar to that carried out in [50]. In Fig. 6.10, it is shown that the riser deflection at $z = 750m$ approaches the equilibrium exponentially with the control law activated. With $\bar{U} = 0$, the control produces a profile shown in Fig 6.11.

6.5 Conclusion

In this chapter, the model of a flexible marine riser with a torque actuator at the upper riser package has been derived. Boundary control has been introduced to reduce the upper riser angle magnitude and the transverse vibration of a riser subjected to a distributed load. Closed-loop stability has been proven directly from the PDE of the system and the problems of traditional truncated-model-based design have been avoided. The control is implementable as the required signals for the control law are generated using measurements which can be obtained from the upper riser boundary. When the disturbance is persistent as in the case of the marine environment, the magnitude of deflection has been shown to be reduced under the control action. The riser has also been shown to be exponentially stabilized in the absence of external disturbance. From the numerical simulations, we observe that there is significant improvement in the upper riser angle magnitude and the vibration reduction of the riser has been achieved.

Tab. 6.1: Numerical values of the riser parameters

Parameters of the physical system	Value
Flexural Rigidity (EI)	$4.0 \times 10^9\ N/m^2$
Length of Riser (L)	$1000\ m$
Mass per unit length (m_z)	$15\ kg/m$
Outer Diameter (D)	$152.4 \times 10^{-3}\ m$
Sea water density (ρ_s)	$1024\ kg/m^3$
Structural damping (c)	5.0 [−]
Tension (T)	$1.11 \times 10^6\ N$

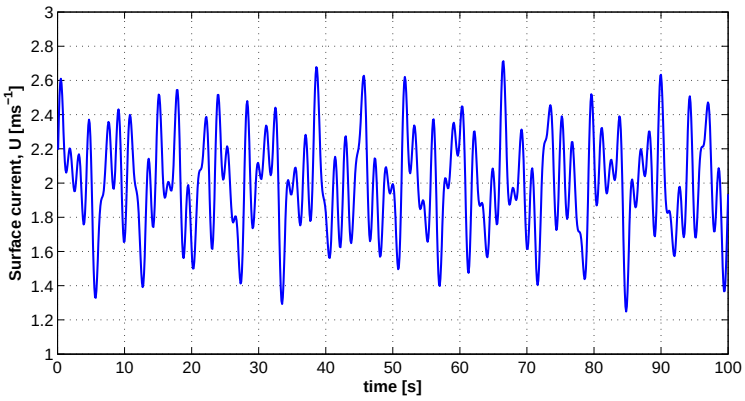

Fig. 6.3: Ocean current velocity modeled as a mean current with worst case sinusoids.

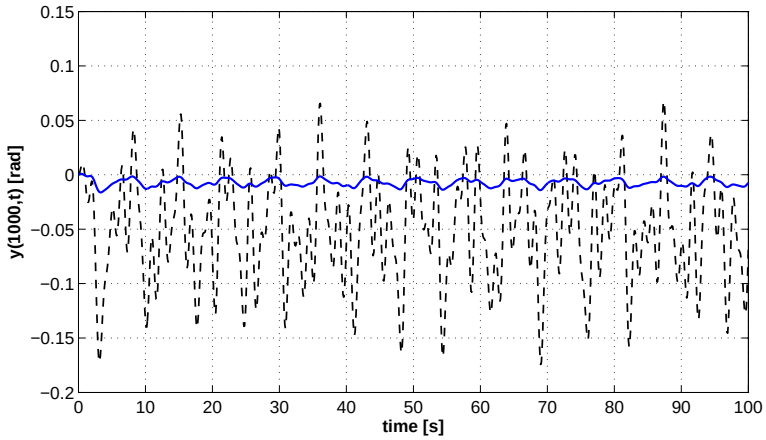

Fig. 6.4: Riser top angle $y'(1000, t)$ with control (solid) and without control (dashed).

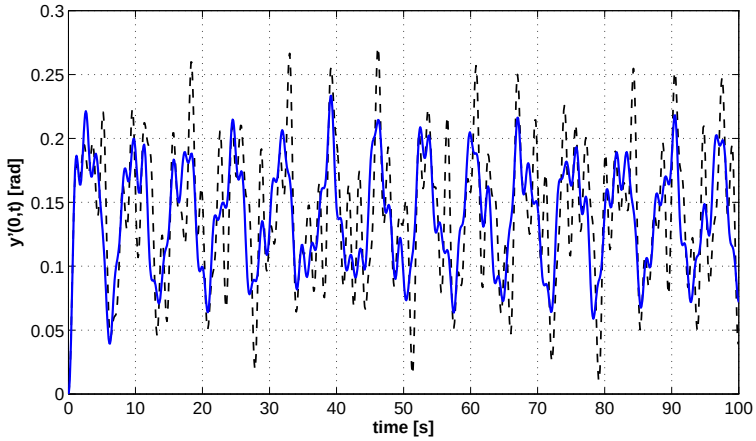

Fig. 6.5: Riser bottom angle $y'(0, t)$ with control (solid) and without control (dashed).

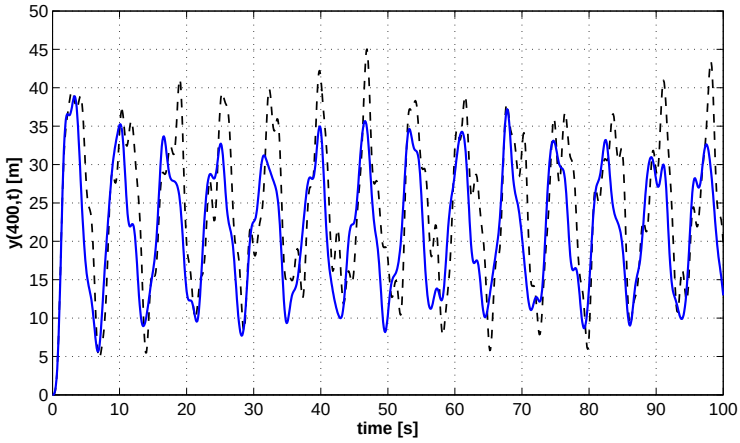

Fig. 6.6: Riser displacement at z = 400m, with control (solid) and without control (dashed).

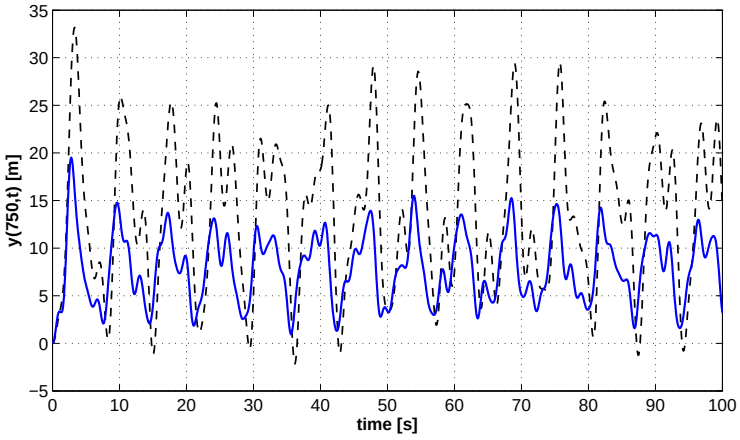

Fig. 6.7: Riser displacement at z = 750m, with control (solid) and without control (dashed).

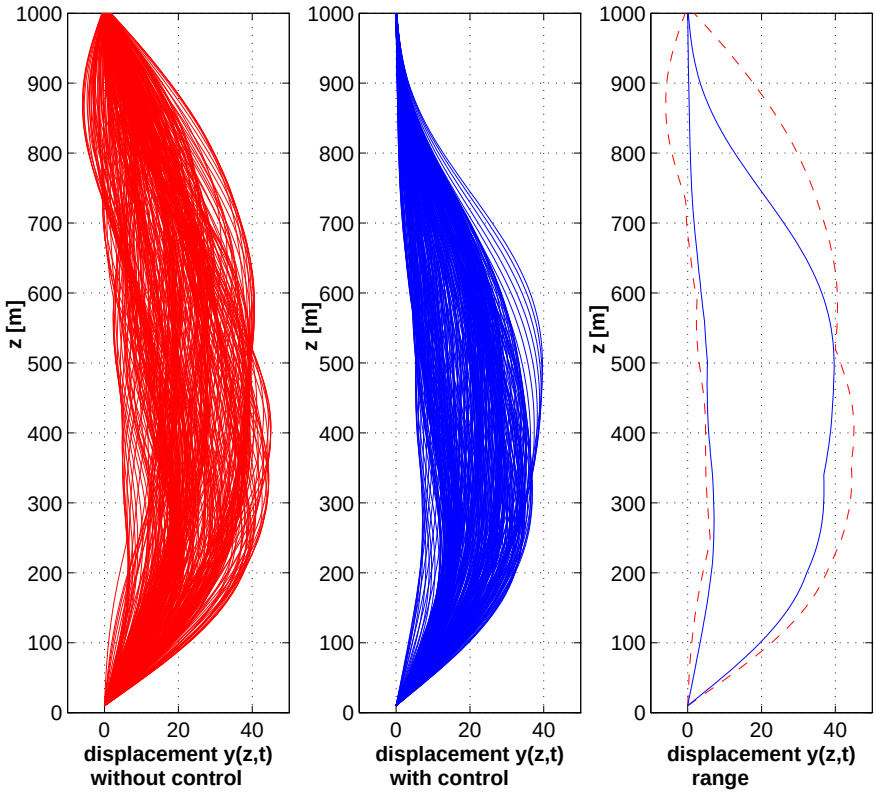

Fig. 6.8: Overlay of riser profiles with control, without control and displacement range.

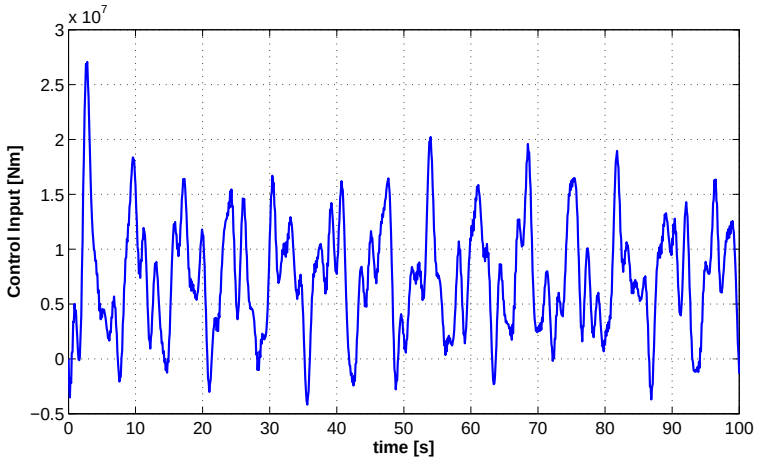

Fig. 6.9: Control input at the boundary.

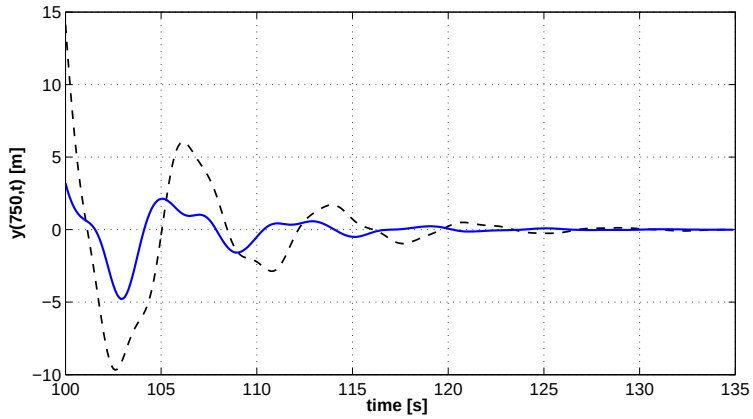

Fig. 6.10: Displacement at z= 750 without disturbance, with control (solid) and without control (dashed).

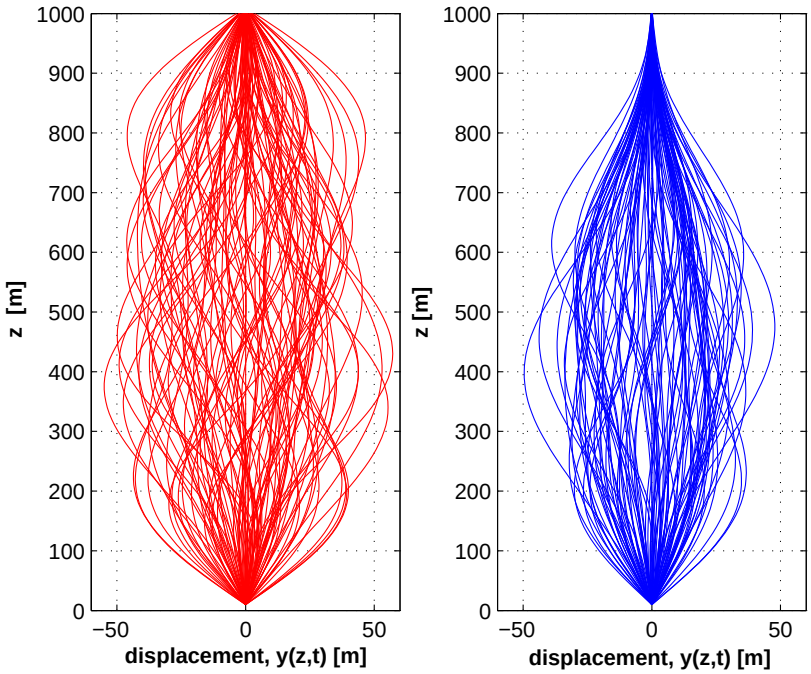

Fig. 6.11: Overlay of riser profiles without control (left) and with control (right) under distributed load $f(z,t)$ when $\bar{U} = 0$

Chapter 7

Conclusions

7.1 Conclusions

This thesis has focused on the control aspects for subsea installation and flexible structures in the marine environment. The key results are as follows:

- **Splash Zone Transition Control**

  We explored the model based adaptive control to augment the PID control when some knowledge of the parameters or structure of the hydrodynamics disturbances affecting the system is known. In the case where the knowledge of the parameters or structure of the disturbances affecting the system is not known, we proposed the use of a non-model based approach, i.e. adaptive NN method to learn and control the system. The system dynamics for the transition from air to water has been investigated and the detailed vertical hydrodynamic loads on the payload as a combination of terms from the pressure effects, slamming and viscous forces including the Froude-Kriloff forces, hydrostatic pressure and viscous drag has been presented. The main contributions are: (i) full state feedback model-based and non-model-based robust adaptive controls have been developed, (ii) rigorous stability analysis has been carried to demonstrate

the closed loop stability of the system. Computer simulations have been carried out to show the effectiveness of the proposed control techniques.

- **Dynamic Positioning of Payload**

  In the dynamic control of offshore structures for installation, an important concern is how to deal with unknown perturbations to the nominal model, in the form of parametric and functional uncertainties, unmodelled dynamics, and disturbances from the environment. Our approach to overcome this problem for the installation of subsea structures is to adopt an intelligent control strategy in the form of approximation-based techniques to compensate for functional uncertainties in the dyanmic model and unknown disturbances from the environment. Stable adaptive neural based positioning control has been designed for installation of subsea structure with attached thrusters in the presence of time-varying environmental disturbances and parametric uncertainties. The main contributions are: (i) the full state and output feedback adaptive neural control design to generate surge, sway and yaw control commands for subsea positioning in presence of parametric uncertainties and disturbances, (ii) the rigorous stability analysis via backstepping and Lyapunov synthesis to demonstrate the semiglobal uniform boundedness of the tracking error, and (iii) the investigation on the effects of a time varying current on the proposed control in comparison with different controls which do not compensate for the current explicitly or generally assume ocean currents to be a constant. Simulation results have demonstrated that the adaptive neural control is robust and effective in reducing the tracking error for the subsea installation operation.

- **Subsea Installation Control with Coupled System**

  The model of the coupled vessel, crane, cable and payload with uniform and nonuniform parameters has been presented. The contributions in the study of the coupled system are (i) the coupled modeling of the vessel, crane, flexible cable and subsea payload where nonuniformity, parametric uncertainties and distributed disturbances

are admissible in the PDE model of the cable. The cable under consideration need not be uniform and the tension can be a function of both transverse gradient and axial coordinate, (ii) the design of positioning controls using Symmetric Barrier Lyapunov Functions (SBLF) and stability analysis of the coupled system. Through Lyapunov synthesis, we ensured that the coupled system is stable, the physical safety limits are not transgressed and simultaneous positioning of the crane and payload is achieved, and (iii) design of the stabilizing boundary controls via Lyapunov synthesis when nonuniformity in the flexible cable is considered. Through rigorous stability analysis, uniform boundedness of the coupled system is demonstrated when excited by the distributed environment load. The performance of the proposed controls have been illustrated through numerical simulations.

- **Flexible Marine Riser**

  Active control of flexible marine riser angle and the reduction of forced vibration under a time-varying distributed load have been considered using boundary control approach. This is the first application of boundary control to a marine riser, for riser angle and forced vibration reduction, through a torque actuator at the upper riser end. The contributions are (i) the modeling of a torque actuator at the upper riser package for the control of a transversely vibrating marine riser subjected to an unknown time-varying distributed load due to the ocean current, (ii) design of a boundary control law to minimize the upper riser angle and simultaneously reduce the vibration of the riser, (iii) rigorous stability analysis of the designed control via Lyapunov synthesis which shows that uniform boundedness of the riser deflection can be guaranteed when excited by the transverse load, and exponential stability can be achieved under free vibration condition, and (iv) numerical simulations on a riser subjected to a mean current with worst case oscillating components which excites the riser natural modes, to verify the applicability and performance.

7.2 Recommendations for Further Research

- Control of longitudinal vibrations and tension: During the lowering operation on long lines, there can be very significant dynamic effects on the lift cable and load. The excitation caused by the motions of the surface vessel can be amplified with large oscillations and high dynamic tensile loads in the lifting line which may result in breaking of the lifting cable. Motions in the heave direction may be only lightly damped, and the virtual (or added) mass of the load can be very significant [2]. Boundary control on axially moving systems has been investigated in [55–59]. In the marine environment, the control is challenging due to the unpredictable exogenous disturbances such as fluctuating currents and transmission of motions from the surface vessel through the lift cable. Passive or active heave compensator can be incorporated following [122]. Coupled with the ship motions, heave control in the longitudinal direction to reduce the high dynamic tensile loads is desirable for safe and reliable operations.

- Control of coupled axial and transverse vibrations: To make the model more complete, the axial and transverse vibrations can be coupled in the dynamic analysis. Due to the coupled effects, the control design and direct prove for the Lyapunov stability is not straightforward. One main challenge arises in the design of a suitable cross term which satisfies the condition of radially unboundedness and subsequent Lyapunov stability.

Appendix A

Appendices for Chapter 5

A1. Proof for Lemma 5.5:

From Eq. (5.30), Lemma 5.3 and using Young's inequality, we obtain

$$\begin{aligned} |V_b(t)| &\leq \int_0^L \rho\beta\{\dot{w}^2(z,t) + w^2(z,t)\}dz \\ &\leq \int_0^L \rho\beta\{\dot{w}^2(z,t) + L^2[w'(z,t)]^2\}dz \\ &\leq \frac{2\rho\beta\max\{1,L^2\}}{L\min\{\rho,\ P,\}}V_a(t) \end{aligned} \tag{A.1}$$

which can be rewritten as

$$-\frac{2\rho\beta\max\{1,L^2\}}{\min\{\rho,\ P\}}V_a(t) \leq V_b(t) \leq \frac{2\rho\beta\max\{1,L^2\}}{\min\{\rho,\ P\}}V_a(t) \tag{A.2}$$

Thus, V_b is bounded as

$$\lambda_1 V_a(t) \leq V_b(t) \leq \lambda_2 V_a(t) \tag{A.3}$$

where

$$\lambda_1 = 1 - \frac{2\rho\beta \max\{1, L^2\}}{\min\{\rho,\ P\}} V_b(t) > 0 \tag{A.4}$$

$$\lambda_2 = 1 + \frac{2\rho\beta \max\{1, L^2\}}{\min\{\rho,\ P\}} V_b(t) > 1 \tag{A.5}$$

provided the inequality (5.31) is satisfied.

A2. Proof for Lemma 5.6:

Taking time derivative of $V_a(t)$ in (5.29), performing integration by parts with boundary conditions (5.26), using Lemma 6.2 with $\delta_1 > 0$ and disturbance (5.25), we have

$$\begin{aligned} \dot{V}_a(t) &= \int_0^L \left\{\rho\dot{w}(z,t)\ddot{w}(z,t) + Pw'(z,t)\dot{w}(z,t)\right\} dz \\ &\leq \int_0^L \left\{-d_c\dot{w}^2(z,t) + \dot{w}(z,t)f^*(z,t)\right\} dz \\ &\leq \int_0^L \left\{-(d_c - \delta_1)\dot{w}^2(z,t) + \frac{1}{\delta_1} f^{*2}(z,t)\right\} dz \end{aligned} \tag{A.6}$$

Taking the time derivative of $V_b(t)$ in (5.30) as above with Lemma 5.3 and constants $\delta_2,\ \delta_3 > 0$ yields

$$\begin{aligned} \dot{V}_b(t) &= \int_0^L \rho\beta w\ddot{w} + \rho\beta\dot{w}^2 dz \\ &= \beta \int_0^L -d_c w\dot{w} + Pww'' + wf^* + \rho\dot{w}^2 dz \\ &\leq \beta \int_0^L \left(\rho + \frac{d_c}{\delta_2}\right)\dot{w}^2 - (P - d_c\delta_2 L^2 - \delta_3 L^2)[w']^2 + \frac{1}{\delta_3} f^{*2} dz \end{aligned} \tag{A.7}$$

Combining Eqs. (A.6) and (A.7),

$$\begin{aligned} V_p(t) &\leq \int_0^L -\beta(P - d_c\delta_2 L^2 - \delta_3 L^2)[w']^2 - \left[d_c - \delta_1 - \beta\left(\rho + \frac{d_c}{\delta_2}\right)\right]\dot{w}^2 \\ &\quad + \left(\frac{1}{\delta_1} + \frac{\beta}{\delta_3}\right) f^*(z,t) dz \\ &\leq -\lambda_3 V_a(t) + \epsilon_p \end{aligned} \tag{A.8}$$

where λ_3 and ϵ_p are given in (5.34) and (5.35) respectively.

A3. Proof for Lemma 5.7:

From Eq. (5.62) and Young's inequality

$$|V_d(t)| \leq \int_0^L \rho(z)\gamma(z)\{\dot{y}^2(z,t) + [y'(z,t)]^2\}dz \tag{A.9}$$

Comparing (A.9) with (5.62), we obtain

$$|V_d(t)| \leq \int_0^L \rho(z)\gamma(z)\{\dot{y}^2(z,t) + [y'(z,t)]^2\}dz \tag{A.10}$$

$$\leq \frac{2\overline{\rho}\int_0^L \gamma(z)dz}{L\min\{\underline{\rho},\ \underline{T},\underline{\theta}\}}V_c(t) \tag{A.11}$$

which can be rewritten as

$$-\frac{2\overline{\rho}\int_0^L \gamma(z)dz}{L\min\{\underline{\rho},\ \underline{T},\underline{\theta}\}}V_c(t) \leq V_d(t) \leq \frac{2\overline{\rho}\int_0^L \gamma(z)dz}{L\min\{\underline{\rho},\ \underline{T},\underline{\theta}\}}V_c(t) \tag{A.12}$$

Thus, V_d is bounded as

$$\lambda_4 V_c(t) \leq V_d(t) \leq \lambda_5 V_c(t) \tag{A.13}$$

where

$$\lambda_4 = 1 - \frac{2\overline{\rho}\int_0^L \gamma(z)dz}{L\min\{\underline{\rho},\ \underline{T},\underline{\theta}\}}V_d(t) > 0 \tag{A.14}$$

$$\lambda_5 = 1 + \frac{2\overline{\rho}\int_0^L \gamma(z)dz}{L\min\{\underline{\rho},\ \underline{T},\underline{\theta}\}}V_d(t) > 1 \tag{A.15}$$

provided condition (5.64) is satisfied.

A4. Proof for Lemma 5.8:

Taking time derivative of $V_c(t)$, performing integration by parts, using Lemma 6.2 with

$\delta_4 > 0$ and substituting the governing equation of the cable (5.4), we have

$$\begin{aligned}
\dot{V}_c(t) &= \int_0^L \left\{\rho\dot{y}\ddot{y} + T_0 y'\dot{y}' + \theta[y']^3\dot{y}'\right\} dz \\
&= \int_0^L \left\{\dot{y}\left[T_0' y' + (2\theta y'' + \theta' y')[y']^2 + (T_0 + \theta[y']^2)y''\right]\right. \\
&\quad \left. + +(T_0 + \theta[y']^2)y'\dot{y}' - d_c\dot{y}^2 + \dot{y}f\right\} dz \\
&= \int_0^L \left\{\frac{\partial[T\dot{y}y']}{\partial z} - d_c\dot{y}^2 + \dot{y}f\right\} dz \\
&\leq T(L,t)\dot{y}(L,t)y'(L,t) - T(0,t)\dot{y}(0,t)y'(0,t) \\
&\quad -(d_c - \delta_4)\int_0^L \dot{y}^2 dz + \frac{1}{\delta_4}\int_0^L f^2 dz
\end{aligned} \tag{A.16}$$

Similar treatment of $V_d(t)$ as $V_c(t)$ above, with $\delta_5 > 0$, yields

$$\begin{aligned}
\dot{V}_d(t) &= \frac{1}{L}\int_0^L \gamma z\left\{y'\rho\ddot{y} + \rho\dot{y}\dot{y}'\right\} dz \\
&= \frac{1}{L}\int_0^L \gamma z\left\{\frac{1}{2}\frac{\partial\{T_0[y']^2\}}{\partial z} + \frac{1}{2}T_0'[y']^2 + \frac{3}{4}\frac{\partial\{\theta[y']^4\}}{\partial z}\right. \\
&\quad \left. + \frac{1}{4}\theta'[y']^4 + \frac{1}{2}(\rho - d_c)\frac{\partial[\dot{y}]^2}{\partial z} + y'f\right\} dz \\
&\leq \frac{1}{2}\gamma(L)T_0(L)[y'(L,t)]^2 - \frac{1}{2L}\int_0^L \left(\frac{\partial\{\gamma z\}}{\partial z}T_0 - \gamma z T_0'\right)[y']^2 dz \\
&\quad + \frac{3}{4}\gamma(L)\theta(L)[y'(L,t)]^4 - \frac{1}{4L}\int_0^L \left(3\frac{\partial\{\gamma z\}}{\partial z}\theta - \gamma z\theta'\right)[y']^4 dx \\
&\quad + \frac{1}{2}\gamma(L)\rho(L)\dot{y}^2(L,t) - \frac{1}{2L}\int_0^L \frac{\partial\{\gamma\rho z\}}{\partial z}[\dot{y}]^2 dz + \frac{\delta_5}{L}\int_0^L \gamma^2 z^2[y']^2 dx + \frac{1}{\delta_5 L}\int_0^L f^2 dz
\end{aligned} \tag{A.17}$$

For clarity, we separate $V_e(t)$ into $V_{e0}(t)$ and V_{eL} at $z = 0$ and $z = L$ respectively for the boundary control design. Taking the time derivative of $V_{e0}(t)$ along Eq. (5.7) yields

$$\dot{V}_{e0} = \dot{y}(0,t)\left[u_0(t) - T(0,t)y'(0,t) - d_0(t)\dot{b}_0(t) - M_0\ddot{y}_s\right]$$

Substituting the boundary control of the crane (5.66) at $z = 0$ into Eq. (A.18), we obtain

$$\begin{aligned}\dot{V}_{e0} &= \dot{y}(0.t)\left[-k_0\dot{y}(0,t)+T(0,t)y'(0,t)\right]\\ &= -k_0\dot{y}^2(0,t)+T(0,t)y'(0,t)\dot{y}(0.t)\end{aligned} \tag{A.18}$$

For control deign of the cable-payload boundary via attached thrusters at $z=L$, we take the time derivative of $V_{eL}(t)$ along Eq. (5.8),

$$\begin{aligned}\dot{V}_{eL}(t) &= M_L\Big[\dot{y}(L,t)+\frac{3}{4}\gamma(L)y'(L,t)\Big]\Big[\ddot{y}(L,t)+\frac{3}{4}\gamma(L)\dot{y}'(L,t)\Big]\\ &= \Big[\dot{y}(L,t)+\frac{3}{4}\gamma(L)y'(L,t)\Big]\Big[u_L(t)+T(L,t)y'(L,t)-d_L(t)\dot{b}_L(t)\\ &\quad +f_L(t)+\frac{3}{4}M_L\gamma(L)\dot{y}'(L,t)\Big]\end{aligned} \tag{A.19}$$

Substituting the designed boundary control (5.67) at $z=L$, we have

$$\begin{aligned}\dot{V}_{eL}(t) &= \Big[\dot{y}(L,t)+\frac{3}{4}\gamma(L)y'(L,t)\Big]\Big[-k_L\Big[\dot{y}(L,t)+\frac{3}{4}\gamma(L)y'(L,t)\Big]-T(L,t)y'(L,t)\\ &\quad -\mathrm{sgn}\Big[\dot{y}(L,t)+\frac{3}{4}\gamma(L)y'(L,t)\Big]\overline{f}_L+f_L(t)\Big]\\ &\le -k_L\Big[\dot{y}(L,t)+\frac{3}{4}\gamma(L)y'(L,t)\Big]^2-T(L,t)y'(L,t)\dot{y}(L,t)-\frac{3}{4}\gamma(L)T(L,t)[y'(L,t)]^2\end{aligned} \tag{A.20}$$

Combining Eqs. (A.16), (A.17), (A.20) and (A.18),

$$\begin{aligned}\dot{V}(t) \le\ & \frac{1}{2}\gamma(L)T_0(L)[y'(L,t)]^2+\frac{3}{4}\gamma(L)\theta(L)[y'(L,t)]^4+\frac{1}{2}\gamma(L)\rho(L)\dot{y}^2(L,t)\\ & -\frac{1}{2L}\int_0^L\left(\frac{\partial\{\gamma z\}}{\partial z}T_0-\gamma zT_0'-2\delta_5\gamma^2z^2\right)[y']^2dz\\ & -\frac{1}{4L}\int_0^L\left(3\frac{\partial\{\gamma z\}}{\partial z}\theta-\gamma z\theta'\right)[y']^4dx\\ & -\frac{1}{2L}\int_0^L\left(\frac{\partial\{\gamma\rho z\}}{\partial z}+2Ld_c-2L\delta_4\right)[\dot{y}]^2dz+\left(\frac{1}{\delta_4}+\frac{1}{\delta_5L}\right)\int_0^Lf^2dz\\ & -k_0\dot{y}^2(0,t)-k_L\Big[\dot{y}(L,t)+\frac{3}{8}\gamma(L)y'(L,t)\Big]^2-\frac{3}{4}T(L,t)\gamma(L)[y'(L,t)]^2\end{aligned}$$

Using $\theta(L)[y'(L,t)]^2 = T(L,t) - T_0(L)$,

$$\begin{aligned} V(t) \;\leq\; & -\frac{1}{4}\gamma(L)T_0(L)[y'(L,t)]^2 + \frac{1}{2}\gamma(L)\rho(L)\dot{y}^2(L,t) \\ & -k_L\Big[\dot{y}(L,t) + \frac{3}{4}\gamma(L)y'(L,t)\Big]^2 - \frac{1}{4L}\int_0^L \left(3\frac{\partial\{\gamma z\}}{\partial z}\theta - \gamma z\theta'\right)[y']^4 dx \\ & -\frac{1}{2L}\int_0^L \left(\frac{\partial\{\gamma z\}}{\partial z}T_0 - \gamma z T_0' - 2\delta_5\gamma^2 z^2\right)[y']^2 dz + \left(\frac{1}{\delta_4} + \frac{1}{\delta_5 L}\right)\int_0^L f^2 dz \\ & -\frac{1}{2L}\int_0^L \left(\frac{\partial\{\gamma\rho z\}}{\partial z} + 2Ld_c - 2L\delta_4\right)[\dot{y}]^2 dz - k_0\dot{y}^2(0,t) \end{aligned} \tag{A.21}$$

From the first three terms in (A.21), we have

$$\begin{aligned} & -\frac{1}{4}\gamma(L)T_0(L)[y'(L,t)]^2 + \frac{1}{2}\gamma(L)\rho(L)\dot{y}^2(L,t) - \frac{1}{2}k_L\Big[\dot{y}(L,t) + \frac{3}{4}\gamma(L)y'(L,t)\Big]^2 \\ \leq\; & -\Big[k_L\frac{9}{32}\gamma(L)^2 + \frac{1}{4}\gamma(L)T_0(L)\Big]\Big[y'(L,t)\Big]^2 - \frac{1}{2}\Big[k_L - \gamma(L)\rho(L)\Big]\dot{y}^2(L,t) \\ & +k_L\frac{9}{16}\gamma(L)^2[y'(L,t)]^2 + \frac{k_L}{2}[\dot{y}(L,t)]^2 \\ \leq\; & -\Big[-k_L\frac{9}{32}\gamma(L)^2 + \frac{1}{4}\gamma(L)T_0(L)\Big]\Big[y'(L,t)\Big]^2 - \frac{1}{2}\Big[\frac{k_L}{2} - \gamma(L)\rho(L)\Big]\dot{y}^2(L,t) \end{aligned} \tag{A.22}$$

From Eq. (A.21), (A.22) and (5.60), we can show that

$$\dot{V}(t) \;\leq\; -\lambda_6[V_c(t) + V_e(t)] + \varepsilon \tag{A.23}$$

where

$$\begin{aligned} \lambda_6 \;=\; & \min\Bigg\{\int_0^L \left(\frac{\partial\{\gamma(z)\rho(z)z\}}{L\rho(z)\partial z} + \frac{2d_c}{\rho(z)} - \frac{2\delta_4}{\rho(z)}\right)dz \\ & \int_0^L \frac{1}{LT_0(z)}\left(\frac{\partial\{\gamma z\}}{\partial z}T_0 - \gamma z T_0' - 2\delta_5\gamma^2 z^2\right)dz, \qquad (A.24) \\ & \int_0^L \frac{1}{2L\theta(z)}\left(3\frac{\partial\{\gamma z\}}{\partial z}\theta - \gamma z\theta'\right)dz,\ \frac{2k_0}{M_0},\ \frac{2k_L}{M_L} \Bigg\} > 0 \qquad (A.25) \\ \varepsilon \;=\; & \left(\frac{1}{\delta_4} + \frac{1}{\delta_5 L}\right)\max_{t=[0,\infty)}\int_0^L f^2 dz \leq \infty \qquad (A.26) \end{aligned}$$

with admissible values of control gain k_L bounded as

$$2\gamma(L)\rho(L) < k_L < \frac{8}{9}\frac{T_0(L)}{\gamma(L)} \tag{A.27}$$

Bibliography

[1] K. P. Tee, S. S. Ge, and E. H. Tay, "Adaptive Control of Electrostatic Microactuators With Bidirectional Drive," *IEEE Transactions on Control Systems Technology*, vol. 17, no. 2, pp. 340–352, 2009.

[2] S. Rowe, B. Mackenzie, and R. Snell, "Deepwater installation of subsea hardware," *Proc. of the 10th Offshore Symp.*, vol. 26, 2001.

[3] O. Engineer, "Wideband wins the day at Orman Lange," *Offshore Engineer*, vol. Dec, pp. 32–34, 2005.

[4] B. C. Gerwick, *Construction of marine And offshore structures*. CRC Press, 2007.

[5] Y. H. Chen and F. M. Lin, "General drag-force linerization for nonlinear analysis of marine risers," *Ocean Engineering*, vol. 16, pp. 265–280, 1989.

[6] A. Bokaian, "Natural frequencies of beams under tensile axial loads," *Journal Sound and Vibration*, vol. 142 (3), pp. 481–489, 1990.

[7] L. N. Virgin and R. H. Plaut, "Effect of axial loads on forced vibration of beams," *Journal Sound and Vibration*, vol. 168 (9), pp. 395–405, 1993.

[8] R. D. Young, J. R. Fowler, E. A. Fisher, and R. R. Luke, "Dynamic analysis as an aid to the design of marine risers," *ASME, Journal of Pressure Vessel Tech.*, vol. 100, pp. 200–205, 1978.

[9] M. H. Patel and A. S. Jesudasen, "Theory and model tests for the dynamic response of free hanging risers," *Journal Sound and Vibration*, vol. 112(1), pp. 149–166, 1987.

[10] S. Kaewunruen, J. Chiravatchradj, and S. Chucheepsakul, "Nonlinear free vibrations of marine risers/pipes transport fluid," *Ocean Engineering*, vol. 32, pp. 417–440, 2005.

[11] F. Hover, S. Miller, and M. Triantafyllou, "Vortex-induced vibration of marine cables: experiments using force feedback," *Journal of fluids and structures*, vol. 11, no. 3, pp. 307–326, 1997.

[12] F. Hover, H. Tvedt, and M. Triantafyllou, "Vortex-induced vibrations of a cylinder with tripping wires," *Journal of Fluid Mechanics*, vol. 448, pp. 175–195, 2001.

[13] A. Techet, F. Hover, and M. Triantafyllou, "Vortical patterns behind a tapered cylinder oscillating transversely to a uniform flow," *Journal of Fluid Mechanics*, vol. 363, pp. 79–96, 1998.

[14] F. Hover and M. Triantafyllou, "Linear dynamics of curved tensioned elastic beams," *Journal of Sound and Vibration*, vol. 228, no. 4, pp. 923–930, 1999.

[15] A. J. Sorensen, B. Leira, J. P. Strand, and C. M. Larsen, "Optimal setpoint chasing in dynamic positioning of deep-water drilling and intervention vessels," *International Journal Robust Nonlinear Control*, vol. 11, pp. 1187–1205, 2001.

[16] H. Suzuki, Q.Tao, and K.Yoshida, "Automatic installation of underwater elastic structures under unknown currents," *Proc. of the Intl. Symp. on Underwater Technology*, vol. 14, pp. 274–281, 1998.

[17] K. Watanabe, H. Suzuki, Q.Tao, and K.Yoshida, "Basis research on underwater docking of flexible structures," *Robotics and Automation, IEEE Intl. Conf. on*, pp. 458–463, 1998.

[18] F. Hover, "Experiments in dynamic positioning of a towed pipe," in *OCEANS'93.'Engineering in Harmony with Ocean'. In proc. of*, 1993.

[19] G. Cybenko, "Approximation by superpositions of a sigmoidal function," *Mathematics of Control, Signals, and Systems (MCSS)*, vol. 2, no. 4, pp. 303–314, 1989.

[20] T. Khanna, "Foundations of Neural Networks.," 1990.

[21] K. Funahashi, "On the approximate realization of continuous mappings by neural networks," *Neural networks*, vol. 2, no. 3, pp. 183–192, 1989.

[22] K. Hornik, M. Stinchcombe, and H. White, "Multilayer feedforward networks are universal approximators," *Neural Networks*, vol. 2, pp. 359–366, 1989.

[23] V. Cherkassky, D. Gehring, and F. Mulier, "Comparison of adaptive methods for function estimation from samples," *IEEE Transactions on Neural Networks*, vol. 7, no. 4, pp. 969–984, 1996.

[24] C. Wang and S. S. Ge, "Adaptive backstepping control of uncertain Lorenz system," *International Journal of Bifurcation and Chaos*, vol. 11, no. 4, pp. 1115–1119, 2001.

[25] P. E. Moraal and J. W. Grizzle, "Observer design for nonlinear systems with discrete-time measurements," *IEEE Transactions on Automatic Control*, vol. 40, no. 3, pp. 395–404, March, 1995.

[26] A. Dabroom and H. Khalil, "Output feedback sampled-data control of nonlinear systems using high-gain observers," *IEEE Transactions on Automatic Control*, vol. 46, no. 11, pp. 1712–1725, 2001.

[27] S. S. Ge, T. H. Lee, and C. J. Harris, *Adaptive Neural Network Control of Robotic Manipulators*. London: World Scientific, 1998.

[28] F. L. Lewis, S. Jagannathan, and A. Yesildirek, *Neural Network Control of Robot Manipulators and Nonlinear Systems*. London : Taylor & Francis, 1999.

[29] A. T. Vemuri and M. M. Polycarpou, "Neural-network-based robust fault diagnosis in robotic systems," *IEEE Transactions on neural networks*, vol. 8, no. 6, pp. 1410–1420, 1997.

[30] A. Vemuri, M. Polycarpou, and S. Diakourtis, "Neural network based fault detection in robotic manipulators," *IEEE Transactions on Robotics and Automation*, vol. 14, no. 2, pp. 342–348, 1998.

[31] F. C. Chen and C. C. Liu, "Adaptively controlling nonlinear continuous-time systems using multilayer neural networks," *IEEE Transactions Automatic Control*, vol. 39, no. 6, pp. 1206–1310, June, 1994.

[32] S. S. Ge, T. H. Lee, and S. X. Ren, "Adaptive friction compensation of servo mechanisms," *International Journal of System Science*, vol. 32, no. 4, pp. 523–532, 2001.

[33] K. K. Tan, S. N. Huang, and T. H. Lee, "Adaptive backstepping control for a class of nonlinear systems using neural network approximations," *International Journal of Robust and Nonlinear Contr.*, vol. 14, pp. 643–664, 2004.

[34] K. S. Narendra and K. Parthasarathy, "Identification and control of dynamic systems using neural networks," *IEEE Transactions on Neural Network*, vol. 1, no. 1, pp. 4–27, 1990.

[35] A. U. Levin and K. S. Narendra, "Control of nonlinear dynamical systems using neural networks-part ii: observability, identification, and control," *IEEE Transactions on Neural Networks*, vol. 7, no. 1, pp. 30–42, 1996.

[36] S. S. Ge, C. C. Hang, and T. Zhang, "Nonlinear adaptive control using neural network and its application to CSTR systems," *Journal of Process Contr.*, vol. 9, pp. 313–323, 1998.

[37] T. Zhang, S. S. Ge, and C. C. Hang, "Design and performance analysis of a direct adaptive controller for nonlinear systems," *Automatica*, vol. 35, pp. 1809–1817, 1999.

[38] K. P. Tee and S. S. Ge, "Control of fully actuated ocean surface vessels using a class of feedforward approximators," *IEEE Transactions on Control Systems Technologies*, vol. 14, pp. 750–756, 2006.

[39] K. Takagi and H. Nishimura, "Control of a jib-type crane mounted on a flexible structure," *IEEE Transactions on Control Systems Technology*, vol. 11, no. 1, pp. 32–42, 2003.

[40] T. Nagashio and T. Kida, "Robust Control of Flexible Mechanical Systems by Utilizing Symmetry and Its Application to Large Space Structures," *IEEE Transactions on Control Systems Technology*, vol. 17, no. 3, pp. 671 – 680, 2009.

[41] X. Wang and D. Chen, "Output tracking control of a one-link flexible manipulator via causal inversion," *IEEE Transactions on Control Systems Technology*, vol. 14, no. 1, pp. 141–148, 2006.

[42] R. H. J. Cannon and E. Schmitz, "Initial experiments on the end-point control of a flexible one-link robot," *Intl. Journal Robotic Research*, vol. 3(3), pp. 62–75, 1984.

[43] B. Siciliano and W. J. Book, "A singular perturbation approach to control of lightweight flexible manipulators," *Intl. Journal Robotics Reseach*, vol. 7(4), pp. 79–90, 1988.

[44] M. W. Vandegrift, F. L. Lewis, and S. Q. Zhu, "Flexible-link robot arm control by a feedback linearization/singular perturbation approach," *Journal of robotic systems*, vol. 11, no. 7, pp. 591–603, 1994.

[45] M. J. Balas, "Active control of flexible systems," *Journal of Optimization Theory and Applications*, vol. 25, pp. 415–436, 1978.

[46] L. Meirovitch and H. Baruh, "On the problem of observation spillover in self-adjoint distributed systems," *Journal of Optimization Theory and Applications*, vol. 30 no.2, pp. 269–291, 1983.

[47] G. Zhu, S. S. Ge, and T. H. Lee, "Variable structure regulation of a flexible arm with a translational base," *Proc. Conf. on Decision and Control*, vol. 36, pp. 1361–1366, 1997.

[48] S. S. Ge, T. H. Lee, G. Zhu, and F. Hong, "Variable structure control of a distributed parameter flexible beam," *Journal Robotic Systems*, vol. 18, pp. 17–27, 2001.

[49] I. Karafyllis, P. D. Christofides, and P. Daoutidis, "Dynamics of a reaction-diffusion system with Brusselator kinetics under feedback control," *Physical Review Series E*, vol. 59, pp. 372–380, 1999.

[50] M. Fard and S. I. Sagatun, "Exponential stabilization of a transversely vibrating beam by boundary control via lyapunov's direct method," *Journal of Dynamic Systems, Measurement, and Control*, vol. 123, pp. 195–200, 2001.

[51] A. Armaou and M. A. Demetriou, "Optimal actuator/sensor placement for linear parabolic PDEs using spatial H2 norm," *Chemical Engineering Science*, vol. 61, no. 22, pp. 7351–7367, 2006.

[52] S. M. Shahruz and L. G. Krishna, "Boundary control of a nonlinear string," *Journal Sound and Vibration*, vol. 195, pp. 169–174, 1996.

[53] S. M. Shahruz and C. A. Narashimha, "Suppression of vibration in stretched strings by boundary control," *Journal Sound and Vibration*, vol. 204, pp. 835–840, 1997.

[54] C. F. Baicu, C. D. Rahn, and B. D. Nibali, "Active boundary control of elastic cables: theory and experiment," *Journal Sound and Vibration*, vol. 198 (1), pp. 17–26, 1996.

[55] K. J. Yang, K. S. Hong, and F. Matsuno, "Robust adaptive boundary control of an axially moving string under a spatiotemporally varying tension," *Journal of Sound and Vibration*, vol. 273, no. 4-5, pp. 1007–1029, 2004.

[56] S. Lee and C. Mote Jr, "Vibration control of an axially moving string by boundary control," *Journal of dynamic systems, measurement, and control*, vol. 118, p. 66, 1996.

[57] R. F. Fung and C. C. Tseng, "Boundary control of an axially moving string via lyapunov method," *Journal of Dynamic Systems, Measurement, and Control*, vol. 121, pp. 105–110, 1999.

[58] T. Li, Z. Hou, and J. Li, "Stabilization analysis of a generalized nonlinear axially moving string by boundary velocity feedback," *Automatica*, vol. 44, no. 2, pp. 498–503, 2008.

[59] J. Y. Choi, K. S. Hong, and K. J. Yang, "Exponential stabilization of an axially moving tensioned strip by passive damping and boundary control," *Journal of Vibration and Control*, vol. 10, no. 5, p. 661, 2004.

[60] R. Datko, J. Lagnese, and M. P. Polis, "An example on the effect of time delays in boundary feedback stabilization of wave equations," *SIAM Journal of Control and Optimization*, vol. 24, pp. 152–156, 1986.

[61] A. Braz, "Boundary control of beams using active constrained layer damping," *Transactions of ASME, Journal of Vibration and Acoustics*, vol. 119, pp. 166–172, 1997.

[62] N. Tanaka and H. Iwamoto, "Active boundary control of an euler-bernoulli beam for generating vibration-free state," *Journal Sound and Vibration*, vol. 304, pp. 570–586, 2007.

[63] N. Tanaka and Y. Kikushima, "Active wave control of a flexible beam (Fundamental characteristics of an active-sink system and its verification)," *JSME International Journal, Series C*, vol. 35, no. 2, pp. 236–244, 1992.

[64] N. Tanaka and Y. Kikushima, "A Study of Active Vibration Isolation," *Transactions of the ASME, Journal of Vibration, Acoustics, Stress and Reliability in Design*, vol. 107, pp. 392–397, 1988.

[65] R. M. Sanner and J. E. Slotine, "Gaussian networks for direct adaptive control," *IEEE Transactions Neural Networks*, vol. 3, no. 6, pp. 837–863, 1992.

[66] S. S. Ge and C. Wang, "Adaptive neural network control of uncertain MIMO nonlinear systems," *IEEE Transactions on Neural Network*, vol. 15, no. 3, pp. 674–692, 2004.

[67] S. S. Ge, C. C. Hang, and T. Zhang, "Adaptive neural network control of nonlinear systems by state and output feedback," *IEEE Transactions on Systems, Man and Cybernetics*, vol. 29, no. 6, pp. 818 – 828, 1999.

[68] S. Behtash, "Robust output tracking for nonlinear system," *International Journal of Control*, vol. 51, no. 6, pp. 931–933, 1990.

[69] K. P. Tee, S. S. Ge, and E. H. Tay, "Barrier Lyapunov Functions for the control of output-constrained nonlinear systems," *Automatica*, 2009.

[70] S. S. Ge, C. C. Hang, T. Lee, and T. Zhang, *Stable Adaptive Neural Network Control*. Boston: MA: Kluwer Academic, 2001.

[71] O. M. Faltinsen, *Sea Loads on Ships and Offshore Structures*. NY: Cambridge University Press, 1990.

[72] S. I. Sagatun, "Active control of underwater installation," *IEEE Transactions on Control Systems Technologies*, vol. 10, no. 5, pp. 743–748, September, 2002.

[73] F. G. Nielsen, *Marine Operasjoner*. Report UK-01-86, Trondhiem, Norway,: Faculty of Marine Technology - The Norwegian University of Science and Technology, 2000.

[74] A. M. Annaswamy, F. P. Skantze, and A. P. Loh, "Adaptive control of continuous time systems with convex/concave parameterization," *Automatica*, vol. 34, pp. 33–49, 1998.

[75] K. J. Astrom and B. Wittenmark, *Adaptive Control*. Readizg, Mass: Addison-Wesley, 1989.

[76] J. F. Wilson, *Dynamics of Offshore Structure*. Hoboken, New Jersy: Wiley, 2003.

[77] R. G. Bea, T. Xu, J. Stear, and R. Ramos, "Wave forces on decks of offshore platforms," *Journal of Waterway, Port, Coastal and Ocean Engineering*, vol. 125, no. 3, pp. 136–144, 1999.

[78] S. S. Ge, T. H. Lee, and C. J. Harris, *Adaptive Neural Network Control of Robotic Manipulators*. London: World Scientific, 1998.

[79] M. M. Polycarpou and P. A. Ioannou, "A robust adaptive non-linear control design," *Proc. of the American Control Conference*, vol. 2, pp. 1365–1369, 1993.

[80] P. Ioannou and J. Sun, *Robust Adaptive Control*. Eaglewood Cliffs, New Jersey: Prentice-Hall, 1996.

[81] B. V. E. How, S. S. Ge, and Y. S. Choo, "Load Positioning for Subsea Installation via Approximation Based Adaptive Control," *Control Applications, 2007. CCA 2007. IEEE International Conference on*, pp. 723–728, 2007.

[82] T. I. Fossen, *Marine Control Systems: Guidiance, Navigation, and Ctrl of Ships, Rigs and Underwater Vehicles*. Norway: Marine Cybernetics, 2002.

[83] R. Yittervik, S. A. Reinholdtsen, C. M. Larsen, and G. K. Furnes, "Marine operations in deep water and a variable current flow environment," *3rd Intl. Conf. on Hydroelasticity in Mar. Tech.*, 2003.

[84] J. R. Morison, M. P. O'Brien, J. W. Johnson, and S. A. Schaaf, "The force exerted by surface waves on piles," *Petroleum Transactions, AIME*, vol. 189, pp. 149–54, 1950.

[85] K. S. Narendra and A. M. Annaswamy, *Stable Adaptive Systems*. New York: Prentice Hall, 1989.

[86] L. L. Whitcomb and D. Yoerger, "Development, comparison and preliminary experimental validation of nonlinear dynamic thruster models," *IEEE Journal Oceanic Engineering*, vol. 24, no. 4, 1999.

[87] R. Bachmayer, L. L. Whitcomb, and M. A. Grosenbaugh, "An accurate four-quadrant nonlinear dynamical model for marine thrusters: Theory and experimental validation," *IEEE Journal Oceanic Engineering*, vol. 25, no. 1, pp. 146–59, 2000.

[88] D. A. Smallwood and L. L. Whitcomb, "Model-based dynamic positioning of underwater robotic vehicles:theory and experiment," *IEEE Journal Oceanic Engineering*, vol. 29, no. 1, 2004.

[89] H. K. Khalil, *Nonlinear Systems*. New York: Mecmillan, 1992.

[90] G. Antonelli, F. Caccavale, S. Chiaverini, and G. Fusco, "A novel adaptive control law for underwater vehicles," *IEEE Transactions on Control Systems Technologies*, vol. 11, pp. 221–232, 2003.

[91] M. D. Feezor, F. Y. Sorrell, P. R. Blankinship, and J. G. Bellingham, "Autonomous underwater vehicle homing/docking via electromagnetic guidance," *IEEE Journal Oceanic Engineering*, vol. 26, no. 4, pp. 515–521, 2001.

[92] J. P. Lasalle and S. Lefschetz, *Stability by Lyapunov's Direct Method with Applications*. New York: Academic Press, 1961.

[93] S. Arimoto and F. Miyazaki, "Stability and robustness of PID feedback control for robot manipulators of sensory capability," *Robotics Research, First international Symposium*, vol. 21, pp. 78–83, 1984.

[94] K. Ngo, R. Mahony, and Z. Jiang, "Integrator backstepping using barrier functions for systems with multiple state constraints," in *44th IEEE Conference on Decision and Control, 2005 and 2005 European Control Conference. CDC-ECC'05*, pp. 8306–8312, 2005.

[95] H. S. Sane, D. S. Bernstein, and W. Corning-IntelliSense, "Robust nonlinear control of the electromagnetically controlled oscillator," in *American Control Conference, 2002. Proceedings of the 2002*, vol. 1, 2002.

[96] H. Benaroya, *Mechanical Vibration, Analysis, Uncertainties and Control*. New York: Marcel Dekker, 2004.

[97] E. W. Lee, "Non-linear forced vibration of a stretched string," *British Journal of Applied Physics*, vol. 8, pp. 411–413, 1957.

[98] O. Morgul, B. P. Rao, and F. Conrad, "On the stabilization of a cable with a tip mass," *IEEE Transactions on automatic control*, vol. 39, no. 10, pp. 2140–2145, 1994.

[99] R. Blevins, *Flow-induced Vibration*. Van Nostrand Reinhold Co, 1977.

[100] S. K. Chakrabarti and R. E. Frampton, "Review of riser analysis techniques," *Applied Ocean Resesearch*, vol. 4, pp. 73–90, 1982.

[101] J. Wanderley and C. Levi, "Vortex induced loads on marine risers," *Ocean Engineering*, vol. 32, no. 11-12, pp. 1281–1295, 2005.

[102] C. Yamamoto, J. Meneghini, F. Saltara, R. Fregonesi, and J. Ferrari, "Numerical simulations of vortex-induced vibration on flexible cylinders," *Journal of Fluids and Structures*, vol. 19, no. 4, pp. 467–489, 2004.

[103] J. R. Meneghini, F. Saltara, R. A. Fregonesi, C. T. Yamamoto, E. Casaprima, and J. A. Ferrari, "Numerical simulations of VIV on long flexible cylinders immersed in complex flow fields," *European Journal of Mechanics/B Fluids*, vol. 23, no. 1, pp. 51–63, 2004.

[104] D. M. Dawson, Z. Qu, F. L. Lewis, and J. F. Dorsey, "Robust control for the tracking of robot motion," *International Journal Control*, vol. 52 (3), pp. 581–595, 1990.

[105] C. D. Rahn, *Mechantronic Control of Distributed Noise and Vibration*. Springer, 2001.

[106] G. H. Hardy, J. E. Littlewood, and G. Polya, *Inequalities*. Cambridge University Press, 1959.

[107] M. S. Queiroz, D. M. Dawson, S. P. Nagarkatti, and F. Zhang, *Lyapunov Based Control of Mechanical Systems*. Birkhauser, Boston, 2000.

[108] M. Kristic, I. Kanellakopoulos, and P. Kokotovic, *Nonlinear and Adaptive Control Design*. John Wiley & sons, 1995.

[109] J. Slotine and W. Li, *Applied Nonlinear Control*. Prentice Hall, Englewood Cliffs, NJ, 1991.

[110] Z. Qu, "Robust and adaptive boundary control of a stretched string on amoving transporter," *IEEE Transactions on Automatic Control*, vol. 46, no. 3, pp. 470–476, 2001.

[111] J. J. Slotine and J. A. Coetsee, "Adaptive sliding controller synthesis for non-linear systems," vol. 43, pp. 1631–1653, 1986.

[112] J. X. Xu, H. Hashimoto, J. J. E. Slotine, Y. Arai, and F. Harashima, "Implementation of VSS control to robotic manipulators-smoothing modification," *IEEE Transactions Industrial Electronics*, vol. **36** 3, pp. 321–329, 1989.

[113] A. Ledoux, B. Molin, G. Delhommeau, and F. Remy, "A Lagally formulation of the wave drift force," *Proc 21st International Workshop Water Waves and Floating Bodies*, 2006.

[114] T. I. Fossen, *Marine Control Systems: Guidance, Navigation and Control of Ships, Rigs and Underwater Vehicles*. Norway: Marine Cybernetics AS, 2002.

[115] W. Weaver, S. Timoshenko, and D. Young, *Vibration Problems in Engineering*. New York: Wiley, 1990.

[116] S. M. Lin and S. Y. Lee, "The forced vibration and boundary control of pretwisted timoshenko beams with general time dependent elastic boundary conditions," *Journal Sound and Vibration*, vol. 254 (1), pp. 69–90, 2002.

[117] Y. Sakawa, F. Matsuno, and S. Fukushima, "Modeling and feedback control of a flexible arm," *Journal Robotic Systems*, vol. 2, no. 4, pp. 453–472, 1985.

[118] H. Goldstein, *Classical Mechanics*. Addison-Wesley Press, Inc, 1951.

[119] Y. Cheng, J. K. Vandiver, and G. Moe, "Linear vibration analysis of marine risers using the wkb-based dynamic stiffness method," *Journal Sound and Vibration*, vol. 251(4), pp. 750–760, 2002.

[120] G. K. Furnes, "On marine riser responses in time and depth dependent flows," *Journal of Fluids and Structures*, vol. 14, pp. 257–273, 2000.

[121] E. Kreyszig, *Advanced Engineering Mathematics*. Ohio: John Wiley and Sons, 2006.

[122] F. S. Hover, M. A. Grosenbaugh, and M. S. Triantafyllou, "Neural-network-based robust fault diagnosis in robotic systems," *IEEE Journal of Oceanic Engineering*, vol. 19, no. 3, p. 449, 1994.

Author's Publications

The contents of this thesis are based on the following papers that have been published, accepted, or submitted to peer-reviewed journals and conferences.

Journals:

1. B.V.E. How, S.S. Ge and Y.S. Choo, "Active Control of Flexible Marine Risers", *Journal of Sound and Vibration*, vol. 320, (4)5, 2009, pp. 758-776
2. B.V.E. How, S.S. Ge and Y.S. Choo, "Dynamic Load Positioning for Subsea Installation via Adaptive Neural Control", *IEEE Journal of Oceanic Engineering*, In Press, 2009
3. S.S. Ge, W. He, B.V.E. How and Y.S. Choo, "Boundary Control of a Coupled Nonlinear Flexible Marine Riser", *IEEE Transactions on Control Systems Technology*, In Press, 2010
4. B.V.E. How, S.S. Ge and Y.S. Choo, "Control of Coupled Vessel, Crane, Cable and Payload Dynamics for Subsea Installation Operations", *IEEE Transactions on Control System Technology*, In Press, 2010
5. M. Chen, S. S. Ge and B.V.E. How, "Robust Adaptive Neural Network Control for a Class of Uncertain MIMO Nonlinear Systems with Input Nonlinearities", *IEEE Transactions on Neural Network*, In Press, 2010
6. M. Chen, S.S. Ge, B.V.E. How and Y.S. Choo, "Robust Adaptive Position Mooring Control for Marine Vessels", *IEEE Transactions on Control System Technology*, 2009, Provisionally accepted.
7. R. Cui, S.S. Ge, B.V.E. How and Y.S. Choo, "Leader-Follower Formation Control of Underactuated Autonomous Underwater Vehicles", *Ocean Engineering*, 2009, Submitted

Conferences:

1. B.V.E. How, Y.S. Choo and S.S. Ge, "Dynamic Load Positioning for Installation of Subsea Systems" *in Proceedings of the 2009 International Conference on Subsea Technology, SubseaTech2009*, Jun 2009, St. Petersburg, Russia.

2. R. Cui, S.S. Ge, B.V.E. How and Y. S. Choo, "Leader-Follower Formation Control of Underactuated Autonomous Underwater vehicles (AUV) with Leader's Position Measurement Only" *in Proceedings of the 2009 IEEE International Conference on Robotics and Automation (ICRA09)*, May 2009, Kobe, Japan.

3. B.V.E. How, S.S. Ge, Y.S. Choo and C. Roc'h, "Intelligent Position Mooring Control of Floating Structures", *in Proceedings of the Advanced Maritime Engineering Conference 2008 (AMEC2008)*, Sep 2008, Chiba, Japan, pp. 709-715

4. B.V.E. How, S.S. Ge and Y.S. Choo, "Angle Control and Vibration Reduction of Flexible Marine Risers", *International Conference on Instrumentation, Control and Information Technology (SICE08)*, Aug 2008, Tokyo, Japan, pp. 794-799

5. B.V.E. How, S.S. Ge and Y.S. Choo, "Load Positioning for Subsea Installation via Approximation Based Adaptive Control", *in Proceedings of the IEEE International Conference on Control Applications*, Oct 2007 (CCA07). Singapore, pp. 723-728

6. V. Chandrasekhar, W.K.G. Seah, Y.S. Choo and B.V.E. How, "Localization in underwater sensor networks: survey and challenges" *in Proceedings of the 1st ACM international workshop on Underwater networks 2006*, New York, USA, pp.33-40

7. B.V.E. How, S.S. Ge and Y.S. Choo, "Adaptive Control of Hydrodynamic Loads in Splash Zone", *in Proceedings of the IEEE International Conference on Control Applications*, Oct 2006, (CCA06), Munich Germany, pp. 1843-1848